A Continuous Span Aluminum Girder Concrete Deck Bridge

Final Report

Part 1 of 2:
Field Test Performance and Evaluation

July 1996

Center for Transportation Research and Education

Iowa State University

A CONTINUOUS SPAN ALUMINUM GIRDER CONCRETE DECK BRIDGE

FINAL REPORT
PART I

FIELD TEST PERFORMANCE AND EVALUATION

by

R. E. Abendroth
W. W. Sanders
V. Mahadevan

Bridge Engineering Center
Iowa State University

through the
Center for Transportation Research and Education

with funding by the
Iowa Department of Transportation and the
Federal Highway Administration

July 1996

TABLE OF CONTENTS

TABLE OF CONTENTS (cont'd)

TABLE OF CONTENTS (cont'd)

LIST OF FIGURES

LIST OF FIGURES (cont'd)

LIST OF FIGURES (cont'd)

LIST OF TABLES

NOMENCLATURE

A	=	non-composite cross-sectional area of the girder,
C_w	=	warpage constant,
d_e	=	distance between the center of the outside roadway girder web and the edge of the exterior lane (-1.0 ft $\leq d_e \leq 5.5$ ft),
e	=	a factor that relates LDF_e to LDF_i,
e_g	=	eccentricity of a girder with respect to the slab (distance between the centroid of a girder and the mid-depth of the slab),
E	=	modulus of elasticity,
E_a	=	modulus of elasticity of aluminum (10,400,000 psi),
E_c	=	modulus of elasticity of concrete (4,300 psi),
f'_c	=	28-day concrete compressive strength,
G	=	shear modulus of elasticity,
I	=	non-composite girder moment of inertia,
I_c	=	gross moment of inertia of the slab,
J	=	torsional constant,
K_g	=	girder longitudinal stiffness parameter,
L	=	span length,
LDF_e	=	exterior girder load distribution factor,
LDF_i	=	interior girder load distribution factor,
LDF_j	=	load distribution factor for the jth girder,
M_j	=	bending moment in the jth girder,
M_{max}	=	maximum bending moment caused by a single wheel load P,
M_T	=	maximum bending moment at a particular transverse cross section in the bridge caused by multiple wheel loads P,
n	=	modular ratio (E_a/E_c),
N_b	=	number of girders,
N_ℓ	=	number of traffic lanes,
N_s	=	number of single lines of wheel loads,
P	=	wheel load,
S	=	girder spacing,
t_s	=	slab thickness,
μ_a	=	Poisson's ratio for aluminum (0.30),
μ_c	=	Poisson's ratio for concrete (0.20),
V	=	spacing between near axles (14 ft $\leq V \leq$ 30 ft), and
w_i	=	unit concrete weight (150 pcf).

PREFACE

The final report entitled "A Continuous Span Aluminum Girder Concrete Deck Bridge" is published in two parts: Part I - "Field Test Performance and Evaluation" and Part II - "Fatigue Tests of Aluminum Girders". Part I of the final report addresses the field testing and analysis of those results to establish the behavior of the original Clive Road Bridge that carried highway traffic over Interstate 80 (I-80) in the northwest region of Des Moines, Iowa. The bridge was load tested in 1959, shortly after its construction and in 1993, just prior to its demolition. This part of the final report presents some of the results from both field tests, finite element predictions of the behavior of the aluminum bridge girders, and load distribution studies. Part II of the final report addresses the laboratory fatigue testing and analysis of those results to establish the behavior of aluminum girders that were removed from the original Clive Road Bridge. The fatigue strength of weld details that existed in the original bridge girders and weld details that are common in welded girders and were added to the aluminum girders are presented in Part II of the final report.

ABSTRACT

Aluminum bridge structures are unique structures. They have been used as a viable alternative during time periods when fabricated structural steel had been difficult to obtain. In recent years, there has been increased interest in new bridge materials, including aluminum. Its lightweight and corrosion resistance provides opportunities for its use in special situations. Research that addresses the behavior of full-scale aluminum members needs to be conducted to provide behavioral characteristics that can be incorporated into additional design recommendations for aluminum bridge structures and components.

In 1957, the Iowa State Highway Commission, with financial assistance from the aluminum industry, constructed a 220-ft long, four-span continuous, aluminum girder bridge to carry traffic on Clive Road (86th Street) over Interstate 80 near Des Moines, Iowa. The bridge, which was one of only nine existing aluminum girder bridges in the continental United States, was constructed with four, all-welded, aluminum girders. The girders were fabricated in pairs with welded diaphragms between an exterior and an interior girder. The interior diaphragms between the girder pairs were bolted to girder brackets. A composite, reinforced concrete deck served as the roadway surface. The bridge, which had performed successfully for about 35 years of service, was removed in the fall of 1993 to make way for an interchange at the same location.

Load tests of the bridge were conducted by driving an overloaded truck to preselected locations on the bridge deck and then monitoring the induced strains in the girder flanges and diaphragm webs of the bridge. Deflections were also measured in the northern end span. Fatigue testing of the aluminum girders that were removed from the end spans were conducted by applying constant-amplitude, cyclic loads. These tests established the fatigue strength of an existing, welded, flange-splice detail and added, welded, flange-cover plates and web-stiffener plate details. The results from the experimental tests of this research will provide additional information regarding behavioral characteristics of full-scale, aluminum members and confirm that aluminum has the strength properties needed for highway bridge girders.

This part of the final report focuses on the load tests of the bridge and the analysis of the experimental data to establish the behavior of the aluminum girder bridge and aluminum girders. A review of the inspection history of the bridge is included and shows that except for the need of a possible deck resurfacing, the bridge was in very good condition. A comparison of the experimental girder strain and deflection test results and those results obtained from a finite element analysis of the bridge showed that the theoretical model accurately predicted the bridge response to applied wheel loads. The analytical model was used to determine the effect that changes in the magnitude of design parameters had on the response of the bridge. The results of the load tests and theoretical analyses provided basic information on load distribution and confirmed that the new AASHTO LRFD Bridge Design Specifications provide load distribution criteria that were applicable to the original Clive Road aluminum girder - concrete deck bridge. Even though these specifications currently identify only precast concrete and steel girder bridges, the load distribution criteria appears also to be applicable for I-shaped aluminum girder bridges.

CHAPTER 1. INTRODUCTION

1.1. General Background

Aluminum girder highway bridges are unique structures. Only seven bridges that used aluminum for the major components were built in the United States of America (3). One of these bridges (4,5,13,20) was built in 1957 to carry Clive Road (86th Street) traffic over Interstate 80 (I-80). The bridge was located in Polk County near the northwest side of Des Moines, Iowa. This bridge was constructed during a period of time when structural steel was not readily available.

Initially, the State Highway Department (then known as the Iowa State Highway Commission-ISHC) in Iowa considered composite steel or concrete girder construction for this bridge. However, at the urging of and with partial financial support from the aluminum industry, a continuous four-span, composite, I-shaped, welded, aluminum girder bridge (the only one of the seven aluminum bridges to involve welded construction) was designed and constructed for an HS-20 loading. As a result of industry participation and due to the unique features of the bridge, it was designed and built as the subject of a research project (HR-51) under the direction of the Iowa Highway Research Board (IHRB) (10). As part of another IHRB research study conducted in the late 50's (HR-67), the Clive Road Bridge was one of four interstate bridges that was tested under static and dynamic loading conditions (10). Since this bridge was studied during two research projects, extensive records on the bridge fabrication, construction and behavior are available.

The bridge had performed successfully during its 35 years of service, as evidenced by a review of the inspection reports that were periodically written throughout the life of the bridge. These reports revealed that the girders in the second and third spans had been struck in 1978 by overheight vehicles. The major notches that occurred in the bottom flanges of the impacted girders had been ground smooth. Also, the inspection reports noted that cracks had developed in four of the

welded joints between the intermediate diaphragms and the girder webs in Span 3 (the third span south of the north abutment). Some of these cracks may have been caused by the major vehicle impacts and/or induced by fatigue loading. Even though many years of useful life remained for this bridge, it was removed during September and October of 1993 as part of an interchange and roadway widening construction project.

Just prior to the start of the bridge demolition, static load tests of the bridge were conducted by researchers at Iowa State University (2,14). These field tests were performed to obtain strain and deflection data that provide needed information on the performance and effectiveness of aluminum as a primary structural material. The girder bending strain results measured during the 1993 field tests, predicted responses obtained from a finite element model of the bridge, and load distribution behavior for this bridge are presented in this report. A historical discussion that addresses the construction and the 1959 field testing of the bridge is given in Ref. 2 and 10. A discussion the potential redesign of the bridge based on current European codes is contained in Ref. 9.

1.2. Need for Study

Design specifications for aluminum girder highway bridges (8) have been available for a number of years. The recent American Association of State Highway and Transportation Officials (AASHTO) Load and Resistance Factor Design (LRFD) Bridge Specifications (1) includes a section for the design of aluminum bridges. However, in many instances, the design criteria for aluminum girder bridges have been taken directly from or modified from those for steel girder bridges (1,17). The load distribution criteria for aluminum girder bridges, which was a design criteria of specific interest to this research, is based on the research that was conducted for steel girder and concrete slab bridges. Specific studies are needed to determine the applicability of the steel girder design criteria

to aluminum girder bridges. In addition, the majority of the information that is available on the fatigue strength of aluminum structures has come from primarily small-scale specimens. Only a limited number of fatigue tests of large-scale specimens have been conducted. These tests did not involve high numbers of load cycles. Therefore, utilization of those results in the development of design criteria for long-term behavior has not been confirmed. The development of design specifications for structural use of aluminum has been hampered by the lack of full-scale test results. The opportunity to obtain data from full-sized aluminum structures does not occur often.

Several years ago, Iowa DOT and Polk County engineers determined that the Clive Road Bridge needed to be redesigned as a full-interchange. The removal of the original bridge provided a unique opportunity to obtain experimental data for both the static load behavior of an aluminum girder bridge and the fatigue strength behavior of full-scale aluminum components. This report focuses on the field-test behavior and its analysis. The results of the fatigue tests will be discussed in Part II of the final report.

1.3. Research Program

The overall research program consists of four parts: inspection, static-load field tests and analyses of the original bridge, and laboratory fatigue-tests of aluminum girder sections. The inspection of the bridge superstructure, particularly the aluminum girders, was done by a team consisting of Iowa State University (ISU) staff, Lehigh University staff, and personnel from Iowa Department of Transportation (Iowa DOT).

The 1993 field tests consisted of loading the bridge with an overloaded truck that was driven to various points on the bridge. The load points complied with the critical AASHTO Bridge Design Specifications (17) loading positions. Instrumentation consisted of electrical resistance strain gages

and direct current displacement transducers. The test results provided data on load distribution and on general static behavior.

Laboratory fatigue tests are currently being conducted on the girders that were removed from the northern end-span. The girder sections have been modified by welding plate attachments that reflect the type of connections that are used in present construction techniques for which additional fatigue data is needed. The beams are also being tested to establish their remaining fatigue life. Other objectives of the research program are to provide information on the effects of 35 years of service of an aluminum girder bridge and to establish load distribution factors for the composite concrete deck-aluminum girder bridge.

1.4. Literature Survey

Between 1946 and 1963 seven aluminum bridges were constructed for highway overpasses and river crossings in the United States of America (3) and one was built in Canada. For these bridges, the girder types used included built-up I-shaped, box, and triangular cross sections. Welding or riveting was used in the fabrication of these structures. Gordon A. Alison (3) conducted a survey that addressed the seven aluminum bridges. From the survey responses, he concluded that the field performance of the aluminum bridges has been excellent.

The first aluminum bridge (20) that was constructed in the USA was designed by Alcoa Aluminum Corporation as a 100-ft span, plate girder railroad bridge for a track that served their smelter facility. This bridge replaced one span of an existing seven span bridge over the Grasse River, near Massena, New York. In 1959, the world's first long-span aluminum highway bridge (a 290-ft long riveted box arch span, with multiple 20-ft long approach spans) was constructed for the Aluminum Company of Canada. During 1957, an aluminum bridge was erected over I-80 in Des

Moines, Iowa. This continuous four-span, welded, I-shaped, aluminum plate girder bridge with a composite concrete deck was designed by Ned L. Ashton. This bridge was removed in 1993 so that a full-interchange could be constructed at the same location. Two aluminum girder bridges were built in 1959 and 1960. These 115-ft wide bridges have a 77-ft span, involving a 31-deg. skew angle. Each aluminum-alloy, riveted plate girder acts compositely with a concrete deck. These bridges carry the Long Island Expressway over the Jericho Turnpike in Jericho, Long Island, New York.

Between 1961 and 1963, three bridges were constructed using a girder cross section that was developed to reduce the quantity of aluminum which was needed to construct a bridge. These girders were fabricated using vertically stiffened, 6061-T6 aluminum alloy sheets that formed multiple triangular-shapes. The girders were connected together with longitudinal extrusions. Two of these four-span bridges were designed by Kaiser Aluminum and Chemical Corporation and were erected over the Sunrise Highway near Amityville, Long Island, New York. The third bridge was a three-span bridge that was built in Sykesville, Maryland. This bridge was designed by the Maryland State Highway Administration and International Aluminum Structures, Incorporated to span over a local road, a river, and a railroad.

As noted earlier, the aluminum girder bridge considered in this study was constructed as part of a Iowa Highway Research Board project and subsequently studied as part of an investigation of the dynamics of highway bridges (10). The study, conducted in 1959, consisted of theoretical and experimental investigations of four interstate highway bridges. The results of the field tests of the Clive Road Bridge were used in comparisons prepared in this study. The 1959 field tests were conducted at speeds from "creeping" to the maximum attainable speed for the test vehicle. Only the test results associated with the "creeping" tests, which simulated static tests, were used in the

comparisons. The truck was placed transversely according to the lane definition in effect during 1959. This placement is slightly different from that specified in current specifications (1,17) and provides slightly lower maximum girder strains for eccentric loading conditions.

Wheel load distribution studies have been conducted by many researchers. Tarhini and Frederick (19) present finite element analyses and modeling techniques of I-girder highway bridges. In their study of wheel load distribution the parameters considered were the size and spacing of girders, presence of cross bracing, concrete slab thickness, span length, composite and noncomposite behavior. The following conclusions were made from their research: Channel type of diaphragms had negligible effects on wheel load distribution; for composite single-span bridges, a large change in the moment of inertia of the bridge deck produced a relatively small change in wheel load distribution; a nonlinear relationship exists between the beam spacings and the wheel load distribution factor; from the finite element analysis, span length was found to be important factor in load distribution; and a formula for wheel load distribution related to span length and girder spacing (suggested as an alternate to the AASHTO expression, S/5.5) was developed using the results of the finite element analysis.

$$\text{Distribution factor} = 0.00013L^2 - 0.021L + 1.25\sqrt{S} - \frac{(S+7)}{10} \qquad (1.1)$$

where, L = bridge span length (ft) and S = girder spacing (ft).

In the research work done by Bishara, Lui, and El-Ali (6) on wheel load distribution, the parameters chosen for their sensitivity studies were the span length, number of girders, number of loaded lanes, skew angle and deck slab width. The researchers did not introduce bridge stiffness parameters such as the bending or torsional stiffness of the girders or the relative bending stiffness of deck slab to that for the steel girders. The span length was varied from 75 to 125 ft, deck slab

total width was varied from 39 to 66 ft, skew angle was varied from 0 to 60 degrees, number of girders was varied from 5 to 8, and the loaded traffic lanes were either two or three. Their parameter studies produced the following conclusions: For interior girders, the bridge span length had a slight effect on the distribution of wheel loads and that the load distribution factor increased almost linearly with span length. For bridges with a skew angle not exceeding 30 degrees, a 5% reduction in the interior girder distribution factor compared to that for a non-skewed condition occurs while for skew angles between 30 and 60 degrees, the reduction attains 28%; changes in the number of girders and the deck width have nonlinear effects on the interior girder wheel load distribution factor; and changes in the span length have a more pronounced effect on the exterior girder wheel load distribution factor compared to the effect caused by changes in the slab width.

Walker (21) used finite-element models for his research on lateral load distribution. He chose bridge parameters to represent a range of steel girder bridge designs. Span lengths were varied from 50 to 400 ft to obtain a wide variation of structural parameters for non-skewed bridges. In this study, he assumed composite action between the longitudinal, I-type girders and the deck. Parameters variations were performed in combinations of girder spacing and slab thickness for several span lengths. He tabulated the load distribution results using a stiffness parameter that was a measure of the relative bending stiffness of the slab to that of the girders. He concluded that for eccentrically placed loads, the influence of the inclusion of transverse trussed diaphragms on wheel load distribution was nearly negligible; however, for centrally placed loading, their effect was more pronounced. Walker commented that S/5.5 rule from the AASHTO Specifications (17) overestimates the bending moments in the girders.

Sanders and Ellebys' (15) work on wheel load distribution in highway bridges lead them to conclude that the AASHTO equation (S/5.5) generally gives realistic values for many typical beam

and slab bridges. These researchers also stated that the important factors that are to be considered while investigating load distribution on major bridge types are: relative flexural stiffness of the girders in longitudinal and transverse directions, relative torsional stiffness of the girders, bridge width and span length. An alternate equation for calculating the load distribution was presented which takes into account various factors such as the number of design traffic lanes, a stiffness parameter which depends upon the type of bridge and its material properties.

For over the sixty years that AASHTO has been publishing standard specifications for bridges, numerous studies related to wheel load distribution have been conducted. These studies were usually limited to a specific type of bridge deck and beam or supporting structure. As the results of these studies became available, provisions that addressed the specific concept that was investigated were added to the bridge design specifications. This approach to specification development resulted in nonuniform criteria and in some cases ambiguous design parameters. In a comprehensive study on wheel load distribution, Sanders (16) emphasized the need for additional studies of load distribution to clarify and consolidate the criteria and to make them more realistic. National Cooperative Highway Research Program (NCHRP) Project 12-26 (22) was undertaken to address the variables that affect load distribution and to develop a comprehensive design specification criteria for wheel load distribution.

Extensive work on load distribution in highway bridges was done by Zokaie, Osterkamp, and Imbsen (22). These researchers conducted detail analyses of bridges that were subjected to a predefined set of loads. Based on their comprehensive study, they provided wheel load distribution expressions that accounted for numerous parameters. The previous formulas for wheel load distribution involved only one or two design parameters. Zokaie et al's. expressions are applicable within a specific range for the design parameters. In general, these formulas predict responses that

are within 5% of the results predicted of a more accurate analysis. In addition, the study resulted in recommendations for the use of computer programs to achieve more accurate results. The recommendations focused on the use of plane-grid analysis, as well as finite-element analysis, where different truck types and their combinations may be considered. The studies and the resulting specification proposal for girder/slab bridges focused on steel and concrete girders with no evaluation of aluminum girders. However, the specifications can recognize the different properties for aluminum, although no verification of the applicability was conducted.

Some of the conclusions formulated with several of the older research studies on wheel load distribution may require some modifications because changes have occurred in the AASHTO Specifications for design traffic lanes and placement of traffic lanes on a bridge to cause maximum bending moments in the bridge girders, since the prior research was conducted.

CHAPTER 2. BRIDGE FIELD TESTING

2.1. Description of the Bridge

The bridge under consideration was a continuous four-span bridge with an overall length of 220 ft and a width of 36 ft. Figure 2.1 shows photos of the bridge and Fig. 2.2 shows an elevation and transverse cross section of the bridge. The roadway width was equal to 30 ft and a 3 ft wide curb existed along both the east and west sides of the bridge. Four, welded, I-shaped, aluminum girders that were fabricated from 5083-H113 aluminum plates were spaced at 9 ft-6 in. on center. The girder spans were 41 ft-3 in., 68 ft-9 in., 68 ft-9 in., and 41 ft-3 in. The girders acted compositely with an 8-in. thick reinforced concrete (RC) slab through the use of shear connectors.

The depth of the interior girders was approximately 38 in. and that of the exterior girders was about 36 in. The flange widths ranged from 12 to 18 in. A total of six different girder cross sections (three for each interior girder and three for each exterior girder) were used along the length of the bridge. For each line of girders, one field-bolted and five shop-welded connections were used to splice the girders at the points where the cross section of a girder changed. These splices transferred both bending moment and shear forces across the joint. The bolted-field splice for the two western most lines of girders occurred in span 2, while the bolted-field splice for the two eastern most line of girders occurred in span 3 (see Fig. 2.2a for the span numbers).

The continuous aluminum girders were connected to each other by welded, I-shaped, aluminum diaphragms that were uniformly spaced at 13 ft-9 in. along the length of the bridge. The plate material for the diaphragms was the same as that for the girders. Six sizes of diaphragms were used in the bridge. The diaphragm connections between the exterior girders and the interior girders were shop welded, while those between the interior girders were field bolted. This type of construction permitted the shop fabrication and field erection of the girders in pairs. Two sections

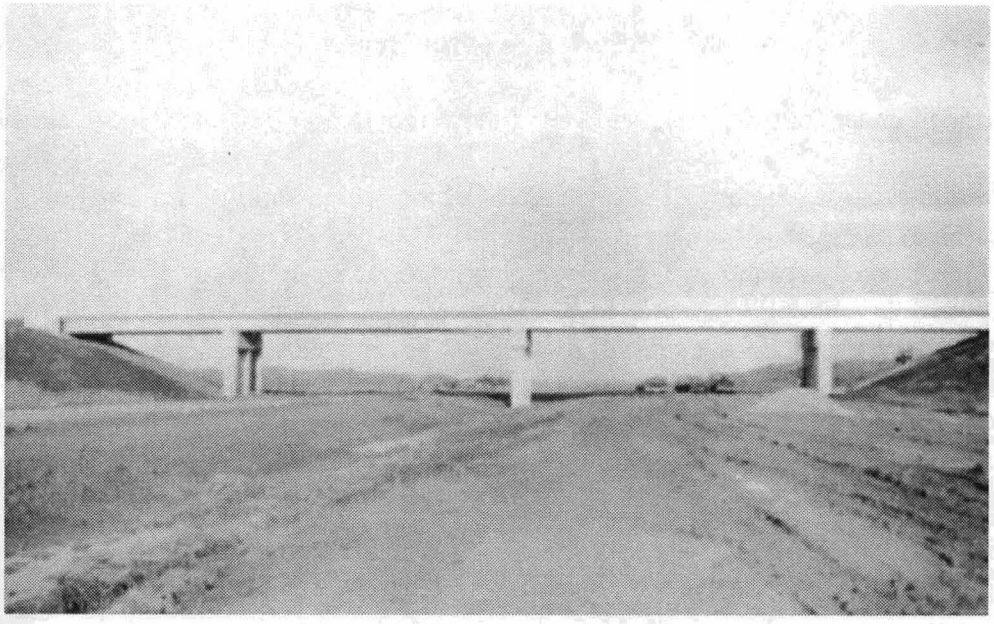

(a)

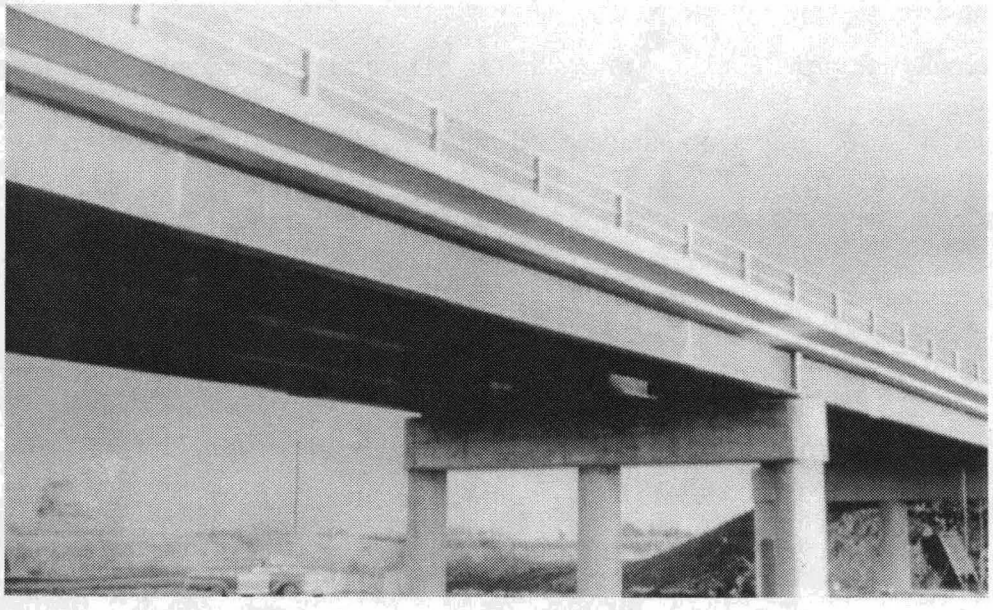

(b)

Figure 2.1 Bridge Photographs: (a) Elevation, (b) Bridge Superstructure
(1958) photographs from IHRB Project HR-51 files of Iowa DOT)

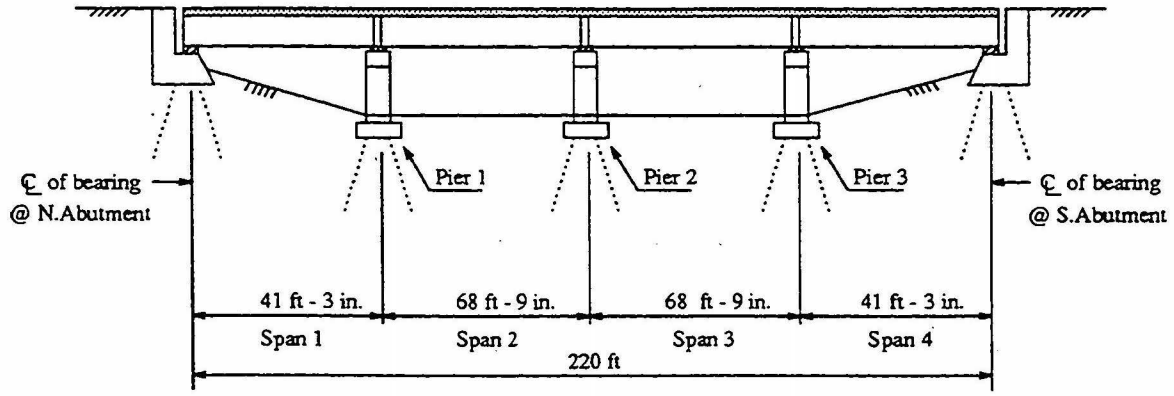

(a)

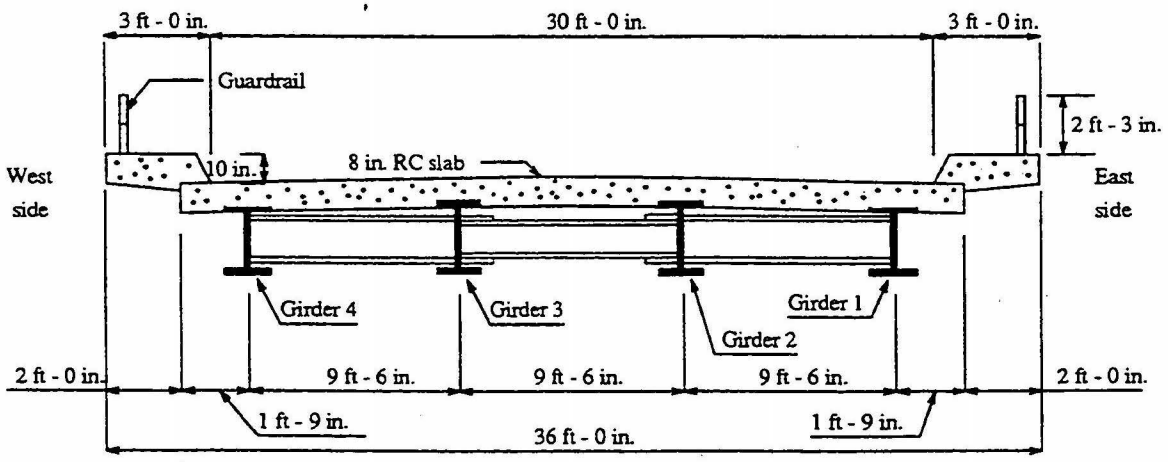

(b)

Figure 2.2. Test bridge: (a) West elevation, (b) Cross section looking north

were 125-ft long and two sections were 95-ft long. The basic aluminum skeleton was erected in four lifts - two weighing about 21,000 lbs and the other two weighing about 16,000 lbs. The relative light weight of the members is one of the significant advantages that aluminum has over structural steel and precast concrete. After erecting the individual girder pairs, the four staggered field splices (one for each girder line) were bolted to form continuous girders.

The aluminum plate material that was provided by the three different aluminum producers showed general consistency in their physical and chemical properties. The average yield strength was 32,200 psi, ultimate tensile strength was 46,900 psi, and an elongation over a 2-in. gage length at failure was 18.8%. Typical chemical properties for the aluminum plates are shown in Table 2.1.

Table 2.1. Typical chemical properties for 5083-H113 aluminum plates

Element	% by Weight	Element	% by Weight
Al	93.40	Zn	0.20
Mg	4.55	Cr	0.18
Mn	0.70	Ti	0.12
Fe	0.30	Cu	0.10
Si	0.30	others	0.15[a]
[a]Total of all other elements			

The welding procedures and welding equipment were in compliance with and the welding operators were qualified in accordance with the welding qualification requirements of the American Society of Mechanical Engineers (ASME) Boiler and Pressure Vessel Code Section IX (Part B). In 1958, the American Welding Society had not published a structural welding code for aluminum; however, one was developed in 1983, with a third edition (18) available shortly, which would be applicable to any reconstruction or rehabilitation. All of the welds were made by the inert-gas, shielded-metal-arc, welding process with a 5183-filler metal and a shielding gas of 75% Helium and 25% Argon that

was dispensed at a flow rate of about 100-120 ft^3/hr. Most of the welding was done at the connection between the web and the flange plates of the girders and diaphragms, where 5/16-in. continuous fillet welds were deposited along each side of the web plate. These welds were made using automatic welding machines with a continuous feed 1/16-in. diameter aluminum welding wire. The welding speed was about 18-22 in./min. The web splices and the flange splices in the girder were made using a semi-automatic process.

The bolted diaphragm connections and bolted girder splices were made using 7/8-in. diameter aluminum bolts that were tightened to 80-85% of the torque obtained from torque tension tests of the bolts. Aluminum washers were used under both the head and nut of the bolts.

Three different height angle-shaped aluminum shear connectors were welded all along the length of each girder top flange to achieve composite behavior between an aluminum girder and the RC slab. A total of 450 shear lugs were used on the four girder lines. The angles, which had square-cut ends, were spaced non-uniformly along each girder with the closest spacing in the regions of the span length where the induced shear forces were the largest. To provide additional horizontal shear strength for the shear connectors, a small rectangular aluminum plate, which bisected the 90° angle between the legs of the angle, was welded to the angle fillet opposite the heal of the angle. To prevent vertical separation between the RC slab and the top flanges of the girders, a rectangular aluminum bar was welded across the angle legs and the bisecting plate.

Prior to casting the concrete for the bridge deck, a protective barrier was added to the aluminum surfaces or parts that would become in contact with the concrete. A zinc-chromate wash primer and primer coats were placed on all of the aluminum contact surfaces, and a coat of an alkali-resistant bituminous paint was applied to the top flange of the girders. Inspection of these surfaces

after demolition of the bridge showed that this protection system was fully effective, since no visible deterioration of the aluminum was detected at these critical interface locations.

After the erection and assembly of the aluminum bridge superstructure and after casting of the concrete for the bridge deck and the curbs, an aluminum pipe and post guardrail system was attached to the curbs along both sides of the bridge. Additional details on the bridge are provided in Ref. 2, 10 and 14.

2.2. Inspection of the Bridge

Throughout the 35 year life of the bridge, a number of field inspections were made. A few fatigue cracks, generally at the welded diaphragm to girder connections, were found. These cracks were monitored and no significant crack propagation had occurred. In many instances, small holes were drilled at a crack tip to act as a crack arrestor. As noted earlier, the only major damage to the bridge occurred when the bottom flange of the east exterior beam above the westbound lane of I-80 was hit by an overheight truck. This girder was partially straightened and some of the flange material at the point of impact had been removed by grinding to eliminate the gouge in the flange.

In the fall of 1993, the first part of the current research project was initiated with a final inspection of the northern interior span of the bridge by Lehigh University and ISU staff. No additional cracks beyond those noted in the last Iowa DOT inspection report were visually detected in the aluminum girders. Over the years, the deck of bridge had gradually deteriorated. A number of transverse hairline concrete cracks and some areas of concrete spalling that exposed the reinforcing steel were detected. The bridge expansion joints at the abutments produced loud noises when traffic crossed these joints. If the bridge were to have continued in service, asphalt resurfacing of the deck would probably have been required. The cracks that were found in the aluminum

superstructure, concrete deck, or concrete substructure would not have necessitated removal, repair, or rehabilitation (beyond deck resurfacing) of the bridge. The bridge was removed only to allow for the construction of a wider and longer bridge for the new interchange.

2.3. Static Load Testing of the Bridge

2.3.1. Test trucks

The bridge was tested in 1959 as part of the HR-67 project (10) and again in 1993 as part of this study. The trucks used in the two studies were substantially of the same configuration, except that the truck used in the current study weighed about 20% more than the truck used in the earlier study. A photograph and the geometric configurations of the test trucks are shown in Figs. 2.3 and 2.4, respectively. Table 2.2 lists the axle spacing between the front axle and front-rear axle and between the two rear axles, S_1 and S_2, respectively; the gage for the front axle and rear axles, G_1 and G_2, respectively; the front axle, front-rear axle, and back-rear axle loads, P_1, P_2, and P_3, respectively; and the gross-weight of the test trucks.

Table 2.2. Truck wheel load parameters

Truck	G_1 (in.)	G_2 (in.)	S_1 (in.)	S_2 (in.)	P_1 (kips)	P_2 (kips)	P_3 (kips)	Gross Wt. (kips)
1959	72	72	176	48	8.79	15.93	15.93	40.65
1993	81	72.25	173.5	51	14.1	17.8	17.7	49.60

2.3.2. Truck positions

For the 1993 field test, loads were placed at different positions along the length of the bridge to cause maximum positive or negative bending moments in the spans or at the piers, respectively. The five longitudinal truck positions shown in Fig. 2.5 were used to produce maximum positive

Figure 2.3 Photograph of 1993 test truck

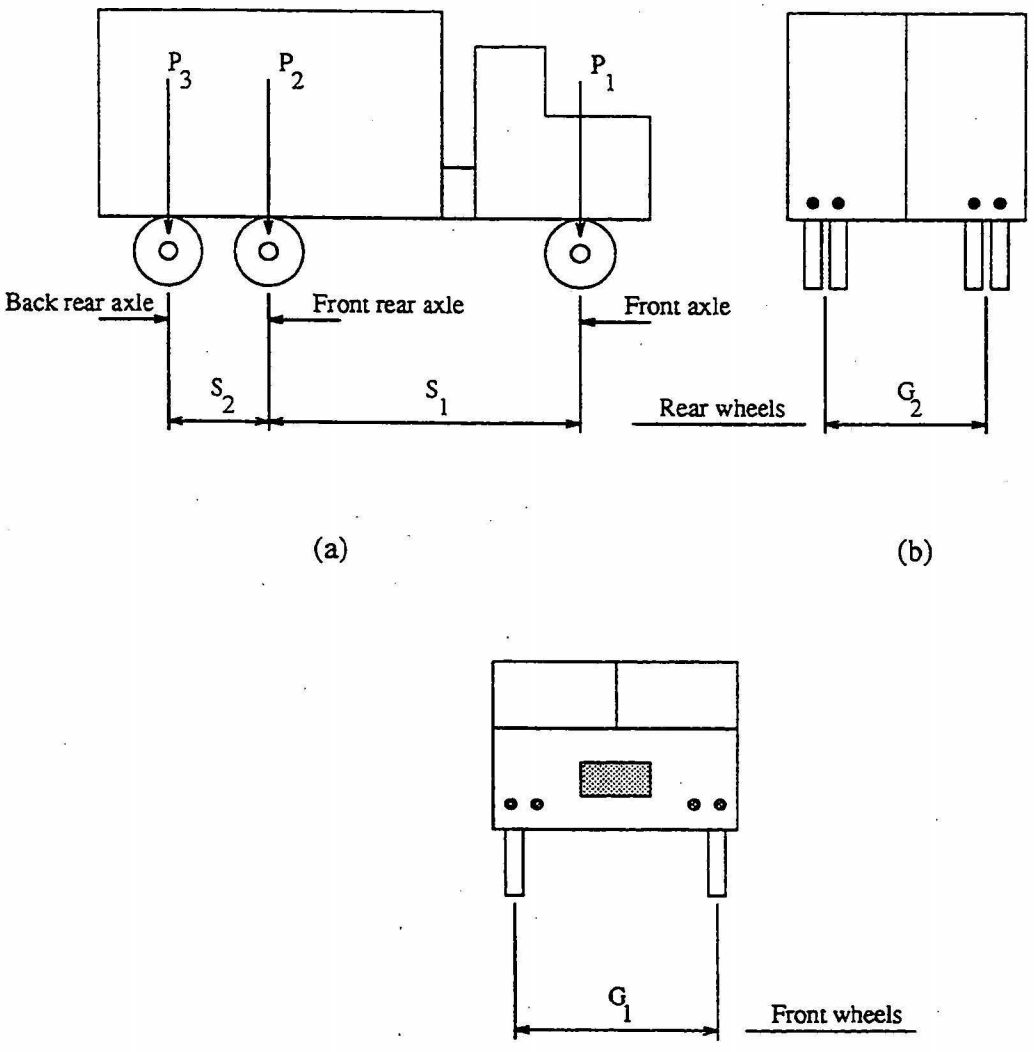

Figure 2.4. Test vehicle: (a) Side view, (b) Rear view, (c) Front view

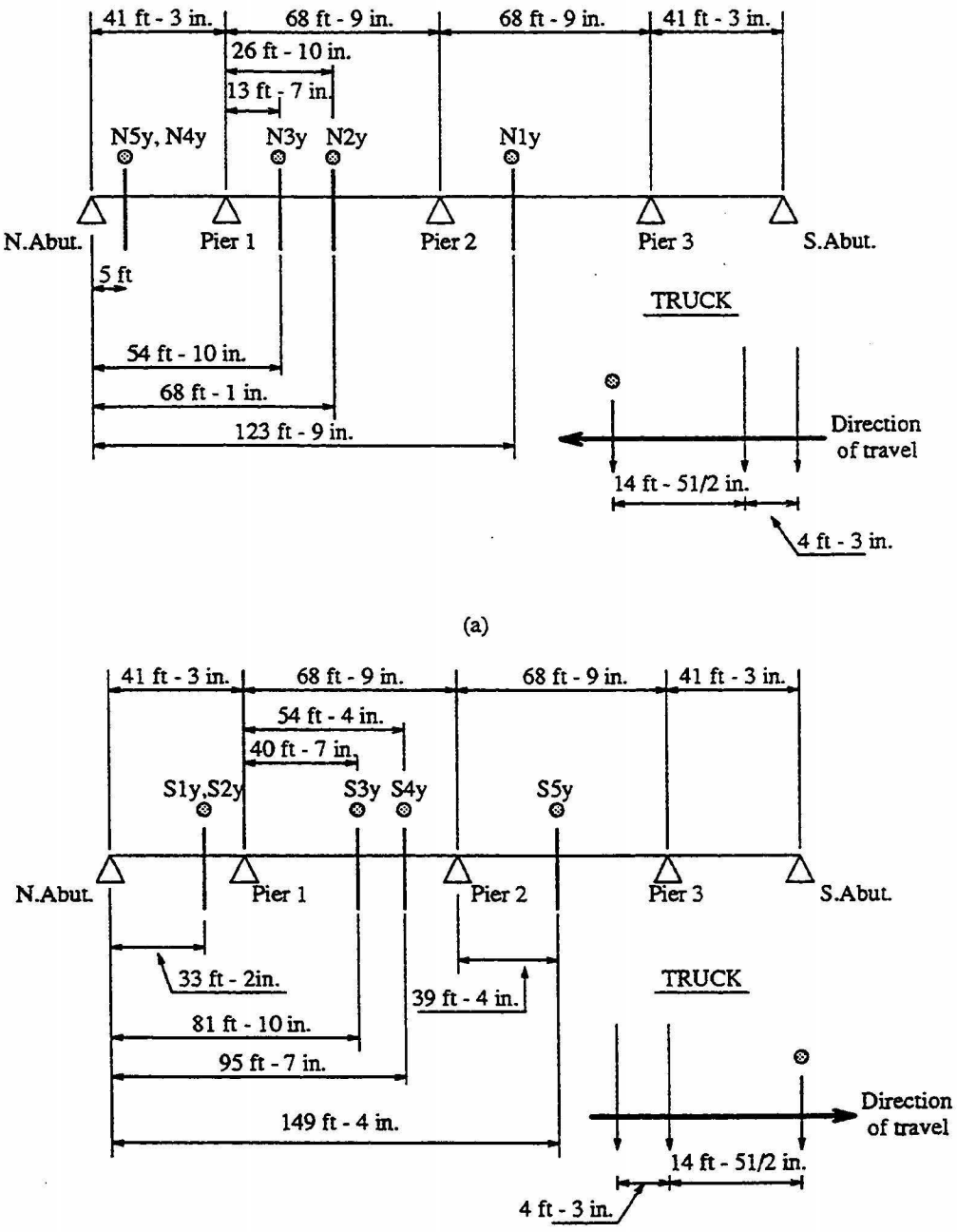

Figure 2.5. Longitudinal truck positions for 1993 tests: (a) Truck northbound, (b) Truck southbound

moments at the 0.45 point of span 1 and maximum negative moments at piers 1 and 2. These positions were established by investigating influence line diagrams for bending moments in continuous beams with a constant flexural rigidity (12). The shaded dot indicated in the figure represents the position of the front axle of the truck. The load positions of the vehicle on the bridge are designated as Nxy or Sxy, where N and S refer to the northbound and southbound directions of travel for the truck, respectively. The first number after the N or S, indicated by the letter "x", represents for the position of the truck along the length of the bridge, with respect to the direction of travel for the truck; while the second number, indicated by the letter "y", represents the position of the truck across the width of the bridge. For both the northern and southern directions of travel, the truck was positioned at six different locations across the width of the bridge.

The design traffic lane positions, noted by the circled numbers in Fig. 2.6, were established in accordance with the 1992 edition of the AASHTO Specifications for Highway Bridges (1). These Specifications state that the standard truck shall be assumed to occupy a 10-ft wide design traffic lane and that the wheel loads shall be placed within, but not closer than 2 ft from the edge of a lane. The number of traffic lanes in a roadway shall be determined by the total whole number of traffic lanes that can be placed within the roadway width. The 12-ft wide lanes in turn are to be placed anywhere transversely across the roadway cross section to produce maximum bending stress, although they may not overlap. For the Clive Road Bridge, two traffic lane arrangements were considered to induce maximum girder stresses.

1. The two traffic lanes are arranged side by side with the outside edge of the first lane coinciding with the edge of the curb. This arrangement produces the maximum eccentricity of the lanes with respect to the centerline of the bridge. When the first wheel load was placed 2 ft from the edge of the curb, the maximum load was distributed to the exterior girder of the bridge.

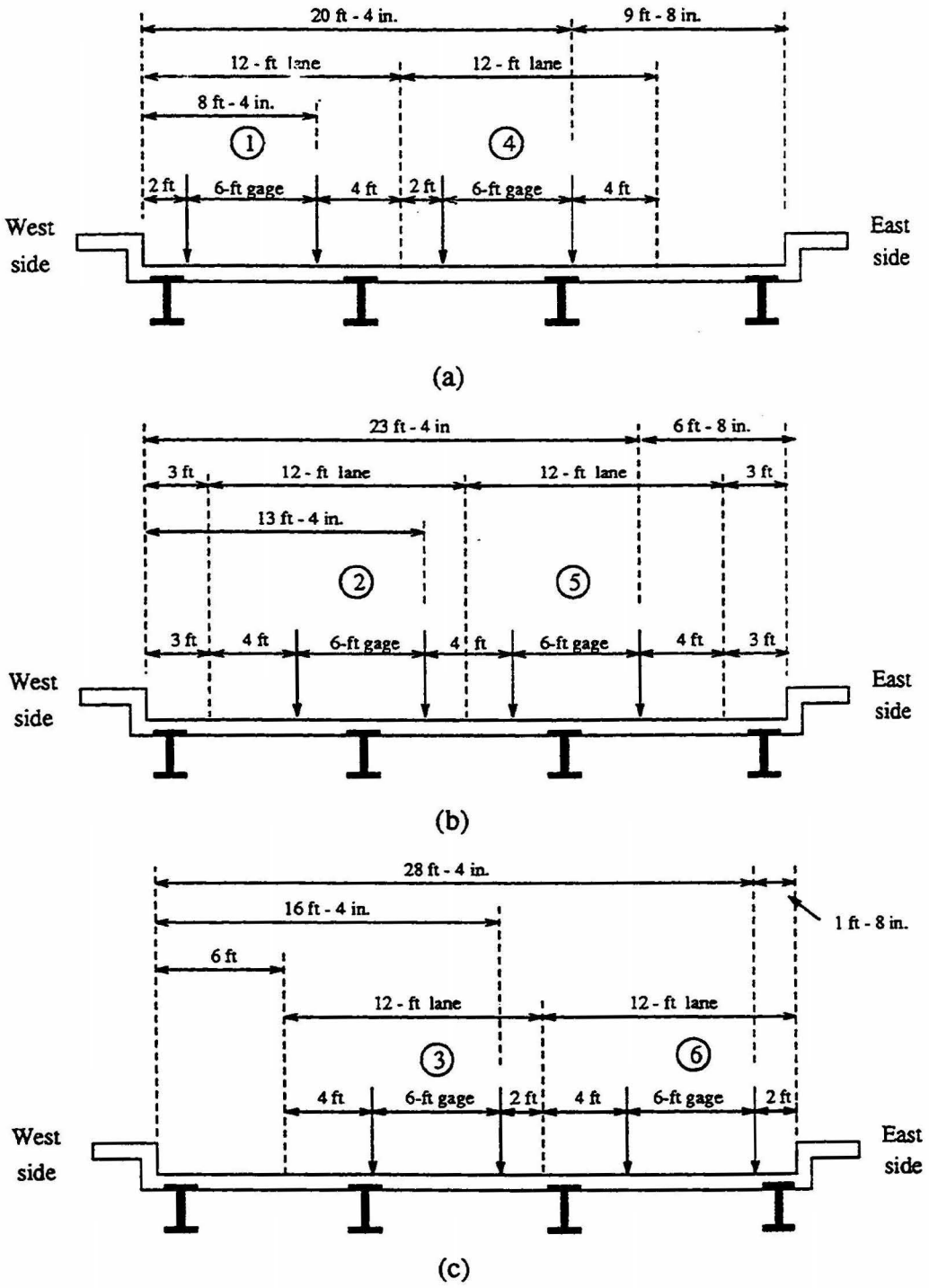

Figure 2.6. Transverse truck positions for 1993 tests: (a) Position 1 and 4, (b) Position 2 and 5, (c) Position 3 and 6

2. The two traffic lanes were positioned on each side of the bridge centerline. Trucks were placed eccentrically in the 12-ft wide lanes, with a wheel load of each truck at 2 ft from the centerline of the bridge. This load arrangement induced the maximum bending moments in the interior girders of the bridge.

The design traffic lane positions, which were numbered consecutively starting at the west side of the bridge, will be referred to as lane lines. For the northbound truck, load positions N1y and N2y (shown in Fig. 2.5) were selected to produce the maximum negative bending moment at pier 2, and positions N3y and N4y were chosen to induce the maximum negative bending moment at pier 1. Load position N5y was selected to cause the maximum positive moment at the 0.45 point of span 1. Following a similar approach for the truck traveling in the southbound direction, load positions S4y and S5y were used to produce the maximum negative moment at pier 2, positions S3y and S2y were selected to induce the maximum negative bending moment at pier 1, and position S1y was chosen to cause the maximum positive bending moment at the 0.45 point of span 1. Therefore, along each load line, five different load positions for the front axle of the truck were identified. Since two of these load positions for each direction of travel were nearly identical, only four load points for each lane line were actually used to position the truck on the bridge. For the southbound direction S2y was eliminated and for the northbound direction N5y was omitted.

According to the final report (10) for the 1959 bridge tests, the static load tests were conducted by slowly driving the test vehicle, at a speed associated with idling the motor, across the length of the bridge. Therefore, the truck was never stopped at a specific point on the bridge deck. The transverse load positions for the 1959 tests are shown in Fig. 2.7. The lanes were uniformly placed across the roadway width, with the lane width equal to the roadway width divided by the number of lanes. For each loading lane on the east side of the bridge, a corresponding loading lane

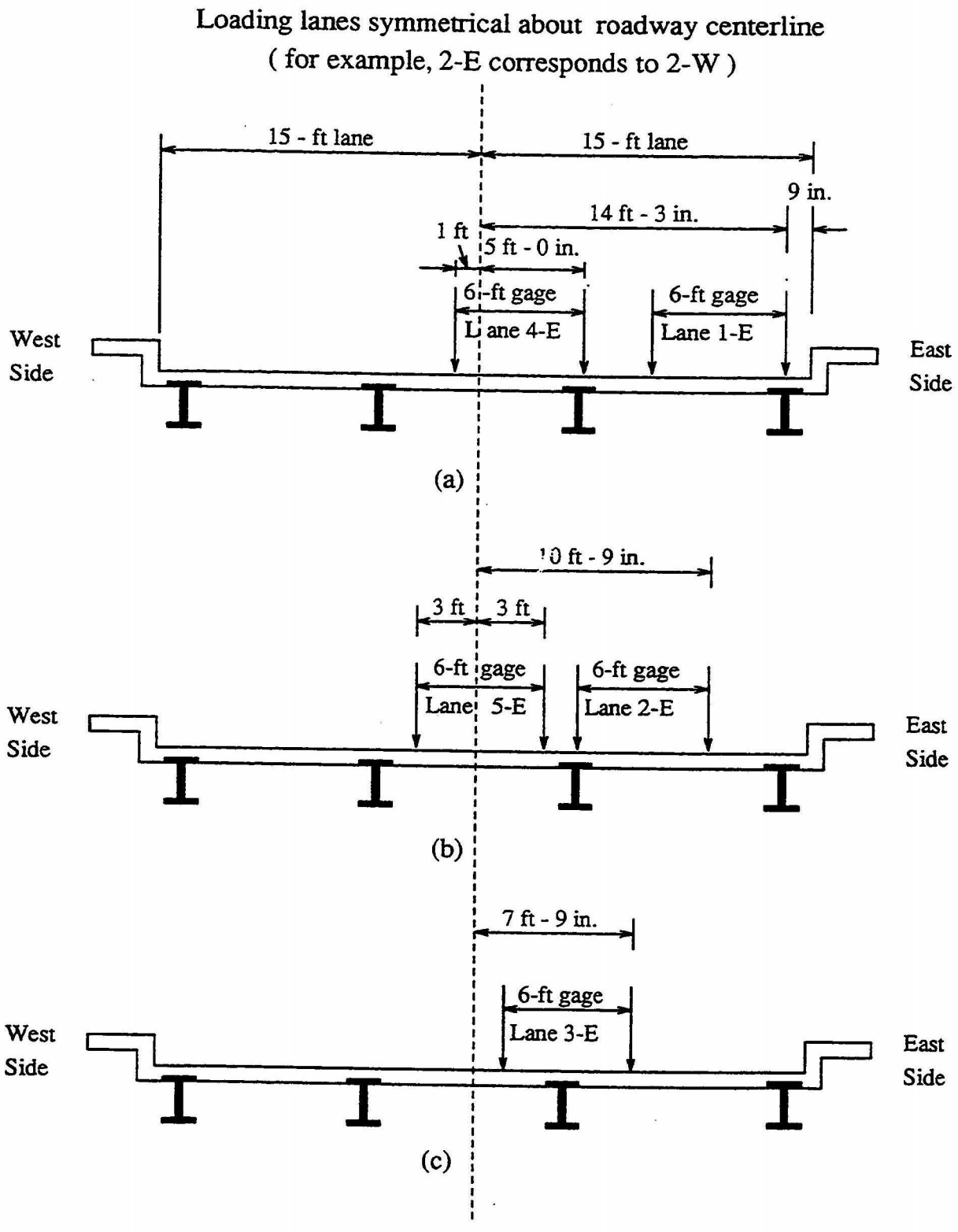

Figure 2.7. Transverse truck positions for 1959 tests: (a) Lanes 1-E and 4-E, (b) Lanes 2-E and 5-E, (c) Lane 3-E

that was symmetrical with respect to centerline of the bridge existed on the west side of the bridge. For example, Lane 2-E and 2-W are symmetric lane load positions.

2.3.3. Instrumentation

To monitor the bridge behavior during the 1993 field tests, electrical resistance strain gages (strain gages) and string-type, direct-current, displacement transducers (DCDTs) were attached to the aluminum girders. For each girder, the longitudinal bending strains were measured at the 0.45 point in span 1 and at 18 in. north of the girder bearing centerline at piers 1 and 2 (Sections A, B, and C, respectively, shown in Fig. 2.8). The offset at piers 1 and 2 was needed to avoid the diaphragms and girder bearing stiffeners at these locations. These three cross sections for girders 1 and 2 (the two eastern most girders) were monitored with four strain gages that were located on the inside face of the top and bottom flanges at a distance of at least two times the flange thickness from the flange tips, as shown in Fig. 2.9. Girders 3 and 4 (the two western most girders) had four strain gages at similar locations for the cross sections at the 0.45 point of span 1 (Section A) and near pier 1 (Section B) and two strain gages (one on each flange) at the cross section near pier 2 (Section C). The two rows of intermediate diaphragms located at the one-third points (Sections D and E) in span 1 had two strain gages that were attached to the web plate. These strain gages were located 2 ft from the ends and 3 in. below the underside of the top flange of the diaphragms as shown in Fig. 2.9b.

The DCDTs were attached to the bottom flange of the four girders at the 0.30, 0.50, and 0.70 points in span 1 (Sections F, G, and H, respectively, shown in Fig. 2.8). To measure potential vertical movement of the girders at their bearings on the north abutment (Section I), the stems of mechanical dial gages were placed against the inside face of the girder bottom flanges. All electrical instrumentation was directly wired to a data acquisition system.

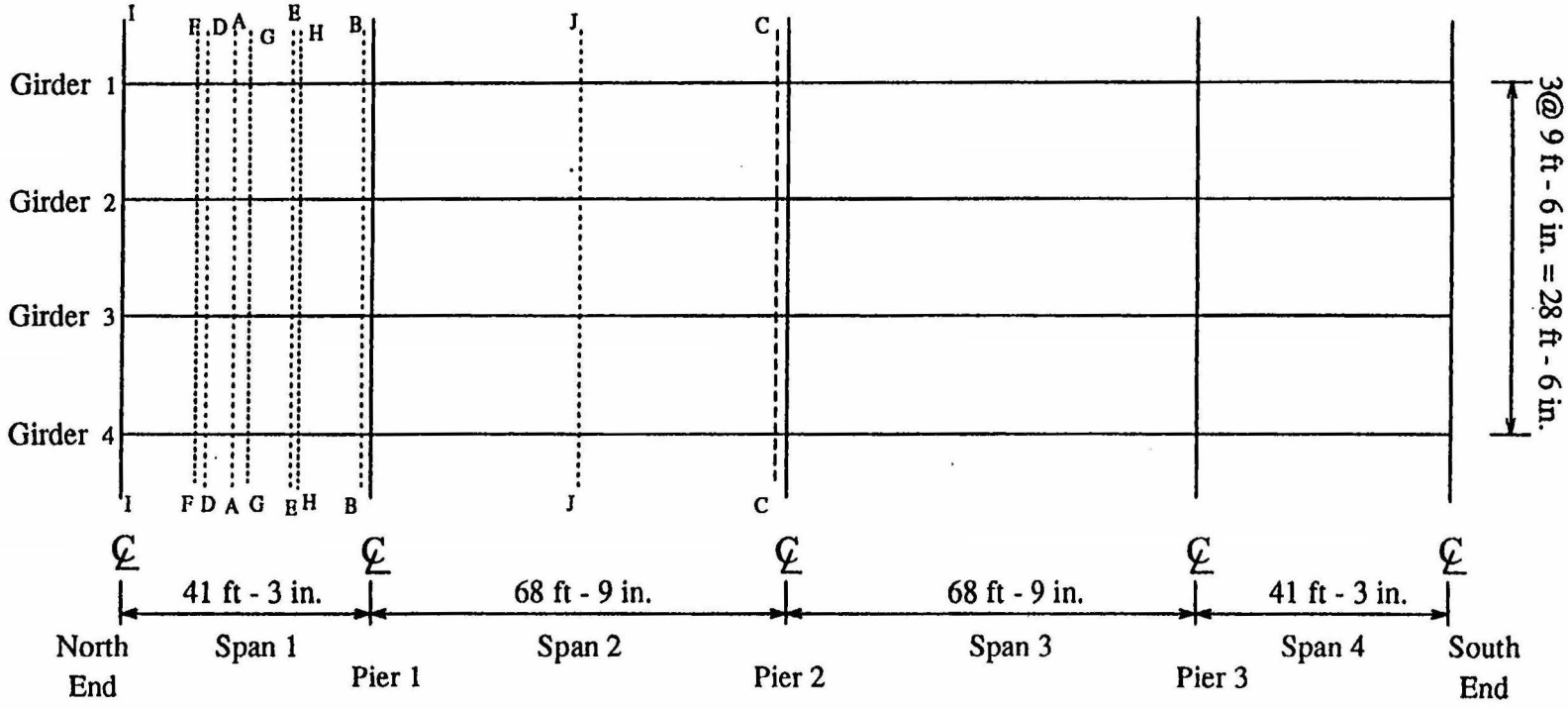

Figure 2.8. Instrumentation locations

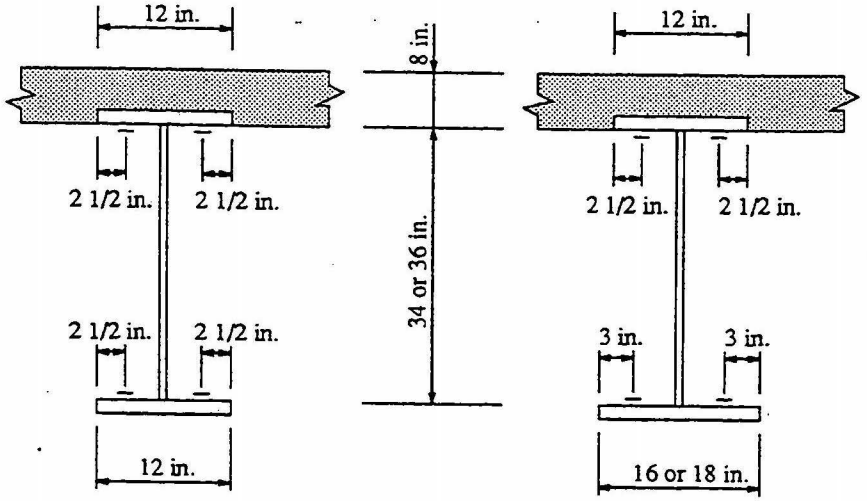

(a)

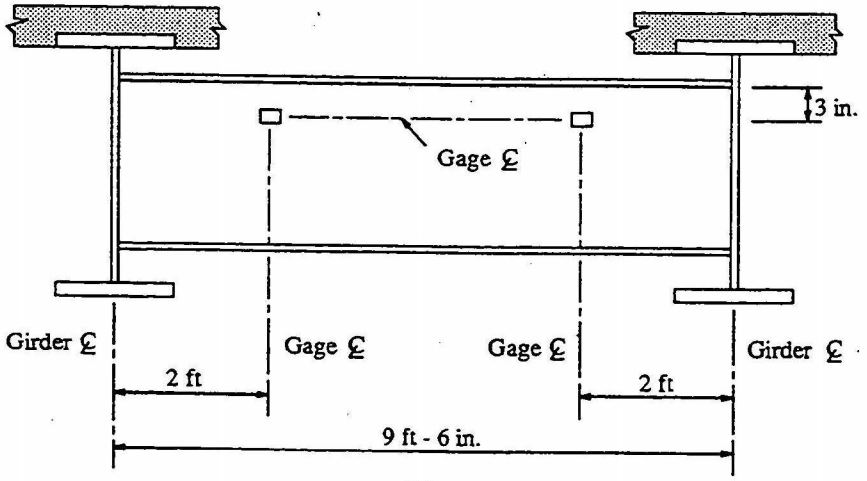

(b)

Figure 2.9. Location of strain gages for 1993 tests: a) Girder cross sections, b) Diaphragm elevation

For the 1959 field tests (10), the strain gages that were attached at the mid-width of the bottom flange on the extreme fiber of each girder at four cross sections along the length of the bridge were used to establish the girder bending moments, as the test vehicle was driven across the bridge. Since the bridge was symmetrical about pier 2, only the northern half of the bridge length was instrumented. Referring to Fig. 2.8, the positive girder bending moments at the 0.40 point in span 1 and at the midspan of span 2 were evaluated using the strain gages at sections A and J, respectively. The negative girder bending moments near piers 1 and 2 were calculated from the strain reading at sections B and C, respectively, which were 20 in. north of each girder bearing point. The girder strains were measured with a direct-writing recorder that produced a continuous record of strain versus time. Pneumatic tubes that were placed across the roadway width at pier 2 and the north abutment were used to determine when the truck crossed these positions. The impulses from these tubes were recorded on the strip record of strains as event markers. A time interval of one second duration was also recorded for calibration purposes.

To calculate girder bending moments at a cross section from a single strain gage record during the 1959 field test, the location of the neutral axis of composite girders at that cross section needed to be established. The neutral axis was experimentally evaluated from bending strains measured by five strain gages that were attached at girder cross sections. Since the bridge was symmetrical with respect to its length and width, only an exterior and an interior girder needed to be instrumented at the four longitudinal cross sections (sections A, B, C, and J).

2.3.4. Test procedures

Before beginning the 1993 field tests, the load positions (corresponding to the notations Nxy and Sxy) across the width and along the length of the bridge were marked on the slab surface. Just prior to driving the test truck onto the bridge for each of the lane lines (circled numbers 1 through

6 in Fig. 2.6), the instrumentation readings were initialized by the data acquisition system. The truck was then driven to the first load location so that the center of the driver side front wheel was directly over the marked position S11. After the strain and deflection readings were taken, the truck was driven to the next position (position S31) along the length of the bridge. This procedure was repeated for all of the load positions along this lane line. Then, the truck was driven in reverse off the bridge across the north abutment so that another set of instrumentation readings could be taken when no wheel loads were on the bridge. After completing each traffic lane passage, the truck was aligned with the next lane line, to begin the next pass across the bridge. The entire process was repeated for each of the six lateral positions across the width of the bridge for both directions of travel.

The 1959 static load field test (10) involved slowly driving the test vehicle at the motor idle speed along the test lanes shown in Fig. 2.7 and recording the bottom flange girder strains at sections A, B, C, and J shown in Fig. 2.8. A total of four passes of the truck along each test lane were performed. The instrumentation provided a continuous time record of the strain at each monitored cross section. The position of the truck wheel loads were calculated by observing the event markers on the strain record that corresponded to when the truck crossed the pneumatic tubes and knowing the length of the strain record that occurred over a one second time interval. The vehicle speed was computed by dividing the distance between the pneumatic tubes by the time period between the two event markers on the continuous strain record.

CHAPTER 3. BRIDGE FIELD TEST EXPERIMENTAL AND ANALYTICAL RESULTS

3.1. Experimental Results of the 1993 Field Test

When the truck was at load positions S12 through S15 and N42 through N45 (longitudinal position and interior lane line positions shown in Figs. 2.5 and 2.6, respectively) in span 1, tensile bending strains at the 0.45 point in span 1 were measured at the inside face of the bottom flange of all four aluminum girders. For these same load positions, the measured bending strains at the 0.45 point in span 1 on the inside face of the top of flange in a particular girder was either an extremely small tensile or compressive strain. Analyzing this strain data by applying a linear strain distribution across the depth of the composite girders, assuming that full-composite behavior was developed between the girders and the RC slab, and recalling that the top flanges of the aluminum girders were embedded within the bridge deck, the neutral axis (defined as the location at which zero bending strains exists) occurred within the slab or just below the bottom of the slab. This general location for the neutral axis was verified by analytically evaluating the first moment of areas of the individual composite girders when elastic behavior occurs. The analytical solution predicted that the neutral axis would be within the slab depth and about 1 in. from the bottom of the slab for both the interior and exterior girders. The neutral axis location for the composite aluminum girders was significantly higher than that for comparable composite steel girders. The lower modulus of elasticity for aluminum as compared to that for structural steel caused the difference in the neutral axis location.

Figure 3.1 shows the average longitudinal strains in the bottom flange of girder 4 (west exterior girder) at the 0.45 point of span 1 when the truck was at Positions S1y, S3y, S4y, and S5y for the southbound direction of travel and at Positions N4y, N3y, N2y, and N1y for the northbound direction of travel shown in Fig. 2.5, when the truck was traveling along lane lines 1, 2, and 3 shown in Fig. 2.6. The strains were obtained from gages A43 and A44 that were attached to the inside face

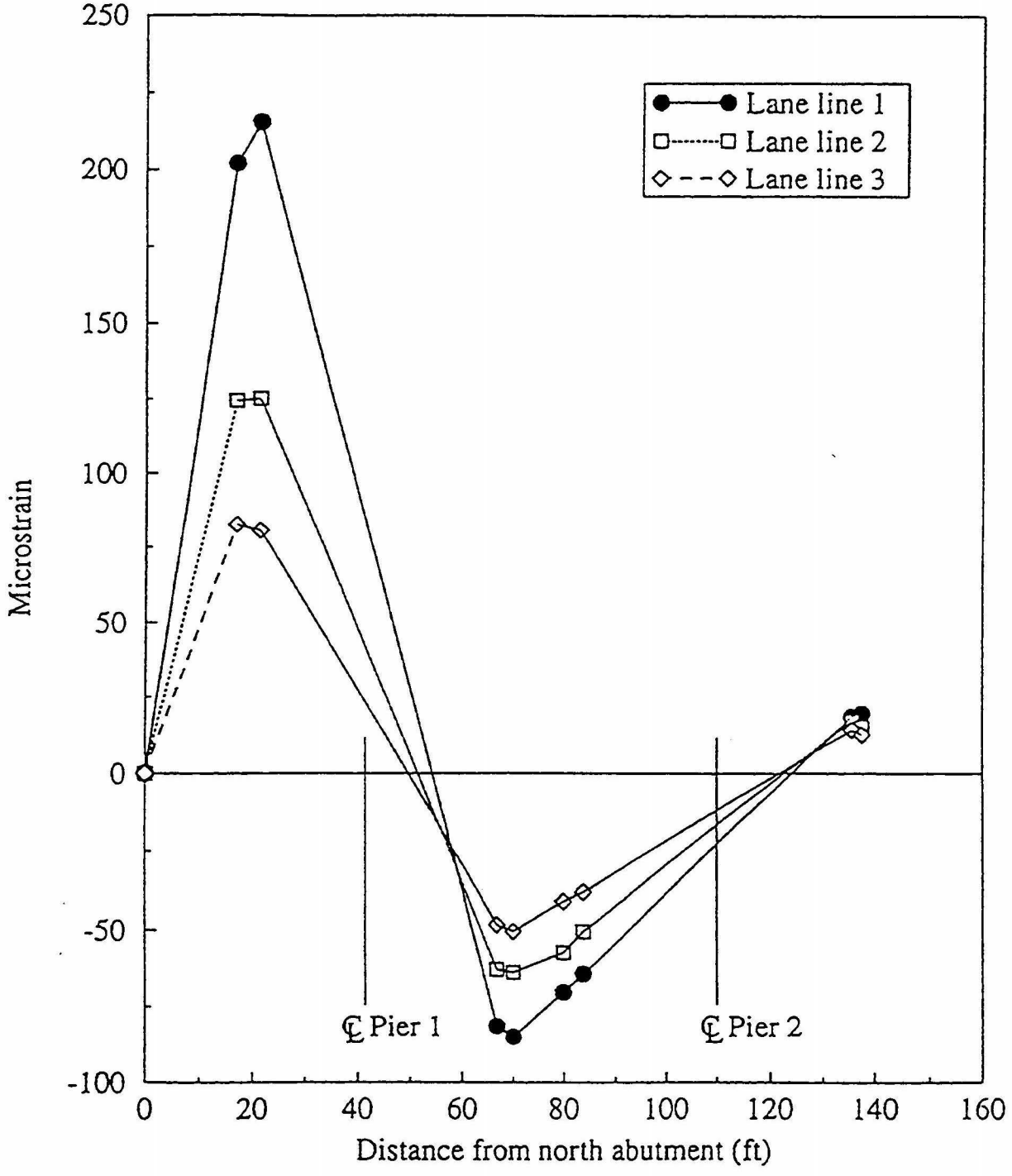

Figure 3.1. Influence lines for the bottom flange average strain in girder 4 at the 0.45 point of span 1

of the bottom flange. The strain gage numbers consisted of a letter followed by two numbers. The letter corresponds to the section location along the bridge length (Fig. 2.8), the first number represents the girder number (Fig. 2.2), and the last number indicates the position on the cross section of the girder where the strain gage was attached (Fig. 2.9a). The horizontal axis in this figure represents the distance from the centerline of the girder bearing at the north abutment to the center of gravity for the test truck. The graph for each lane line loading is essentially a strain influence line for the average strain in the bottom flange at the 0.45 point of span 1 for the test truck, as the vehicle was driven across the bridge. A positive strain indicates a tensile strain, and a negative strain indicates a compressive strain.

As a result of the critical location of the front axle load position along the bridge length, the distance between the front axle and the center of gravity for the truck, and the direction of travel, the strain data shown in Fig. 3.1 appears as data point pairs. Starting from the north abutment and progressing towards the south abutment, the data point pairs correspond to load positions N4y, S1y; N3y, S3y; N2y, S4y; and N1y, S5y. For this and other strain gage locations, minimal differences in the longitudinal girder strains occurred between the northbound and the corresponding southbound load points. Therefore, the bridge response was not dependent on the direction of travel for the truck. Since the results were essentially the same for each direction of travel, only the data associated with the southbound direction of the truck was plotted for the other girder strain influence lines.

Figure 3.2 shows the strain influence lines for the strain in the bottom flange of girder 3 (west interior girder) at the 0.45 point of span 1. To produce this strain data, the average of the strains measured by gages A33 and A34 was used when the southbound truck was positioned with the driver's side front wheel at one of six different alignments across the width of the bridge. These

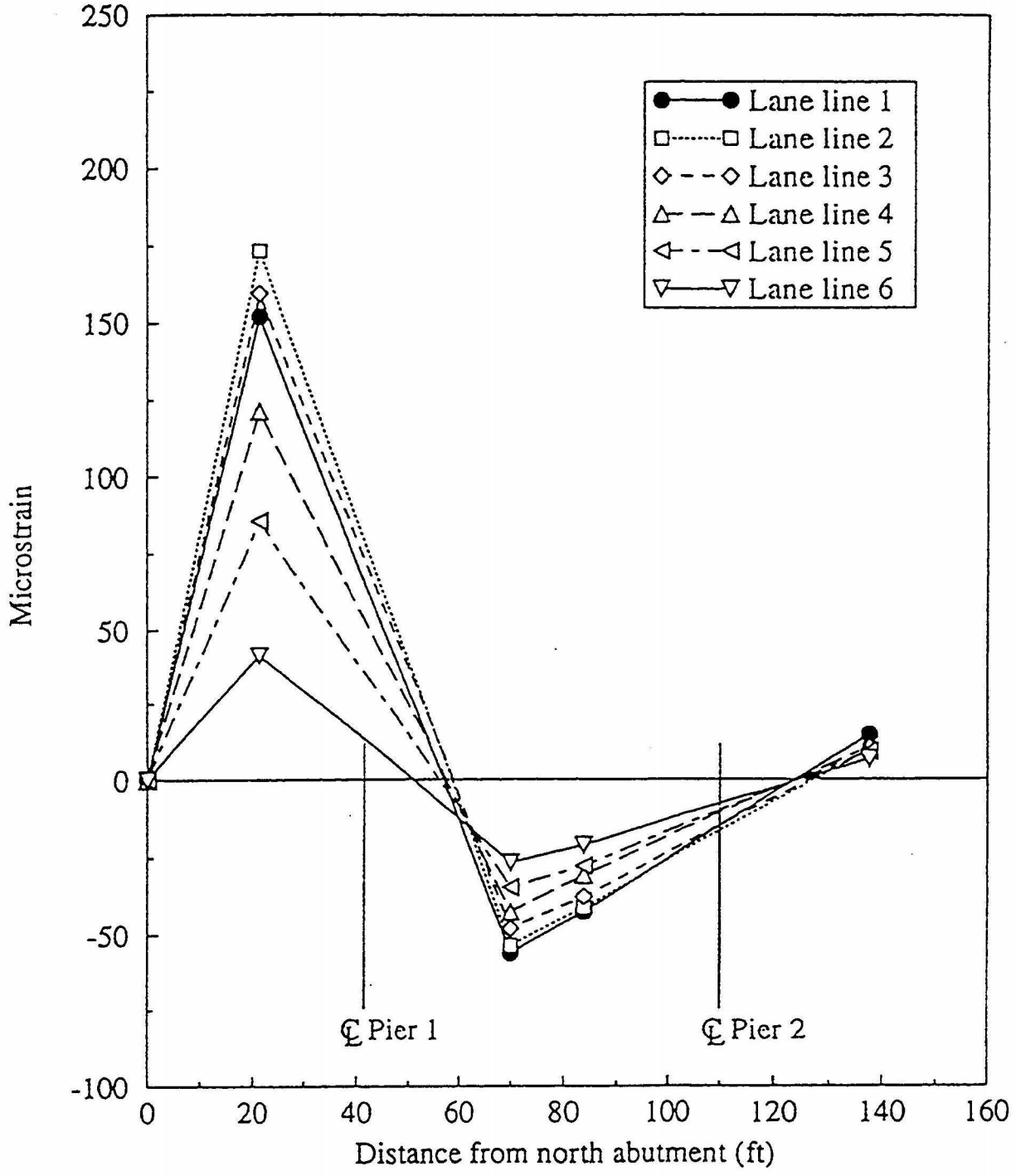

Figure 3.2. Influence lines for the bottom flange average strain in girder 3 at the 0.45 point of span 1

alignments were referred to as lane lines 1 through 6. Starting from the north abutment and progressing towards the south abutment, the data points for each lane line correspond to the load positions S1y, S3y, S4y, and S5y. Figure 3.3 shows the strain influence lines for the strain in the bottom flange of girder 4 (west exterior girder) at 18 in. north of pier 1. The data points shown in this figure correspond with the same longitudinal wheel load positions that were discussed for Fig. 3.2. The maximum girder strains occurred with the lane lines that positioned the wheel loads closest to the particular girder.

Gages A44 and A13 were positioned on the exterior girders (Girders 4 and 1, respectively), in similar locations; therefore, they were symmetrically located with respect to the midwidth of the bridge. A comparison of the girder strain influence lines (not shown herein) involving lane lines 1, 2, and 3 for gage A44 and involving lane lines 6, 5, and 4 for gage A13 revealed that the bridge did not exactly respond in a symmetric manner. Smaller bending strains were observed in girder 1 as compared to those in girder 4. However, a comparison of the patterns for the strain influence lines reflected an overall symmetric response between girders 1 and 4. A comparison of the measured girder bending strains at the other gages that were attached at other symmetric positions on girders 1 and 4 and on girders 2 and 3 revealed not only an overall symmetric response of the bridge to the truck loads, but also quite consistent magnitudes of girder bending strains.

Figure 3.4 shows the average bottom flange girder strains at the 0.45 point in span 1 for each girder, as the truck was located at load positions S11 through S16. Figure 3.5 shows similar girder responses for the average bottom flange girder strains at 18 in. north of pier 1, when the truck was at load positions S31 through S36. For comparative purposes, straight lines were drawn between the adjacent data points in each figure. As expected, the largest bending strains occurred in the girder that was closest to the center of gravity location for the truck. When the truck was positioned

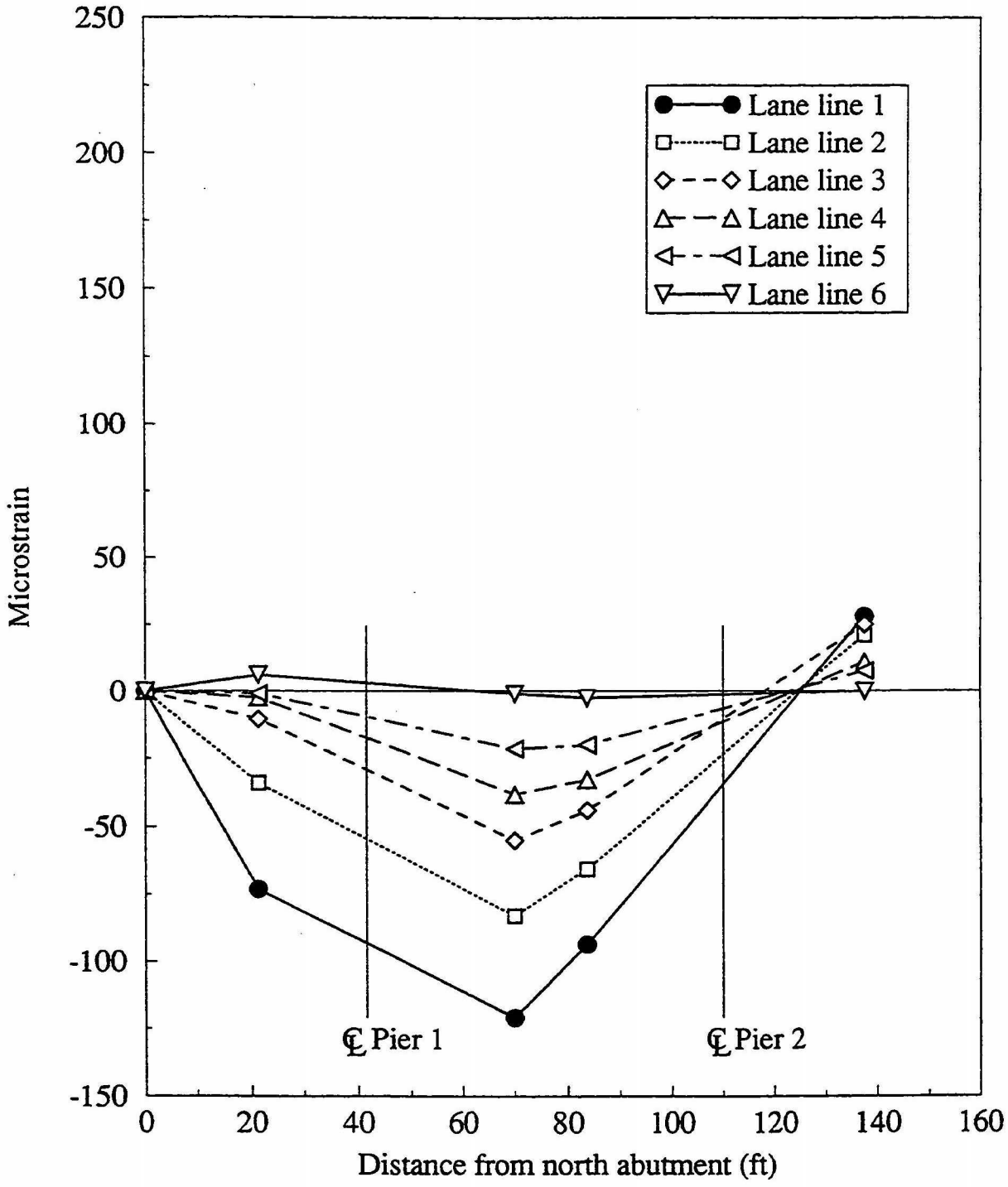

Figure 3.3. Influence lines for the bottom flange average strain in girder 4 near pier 1

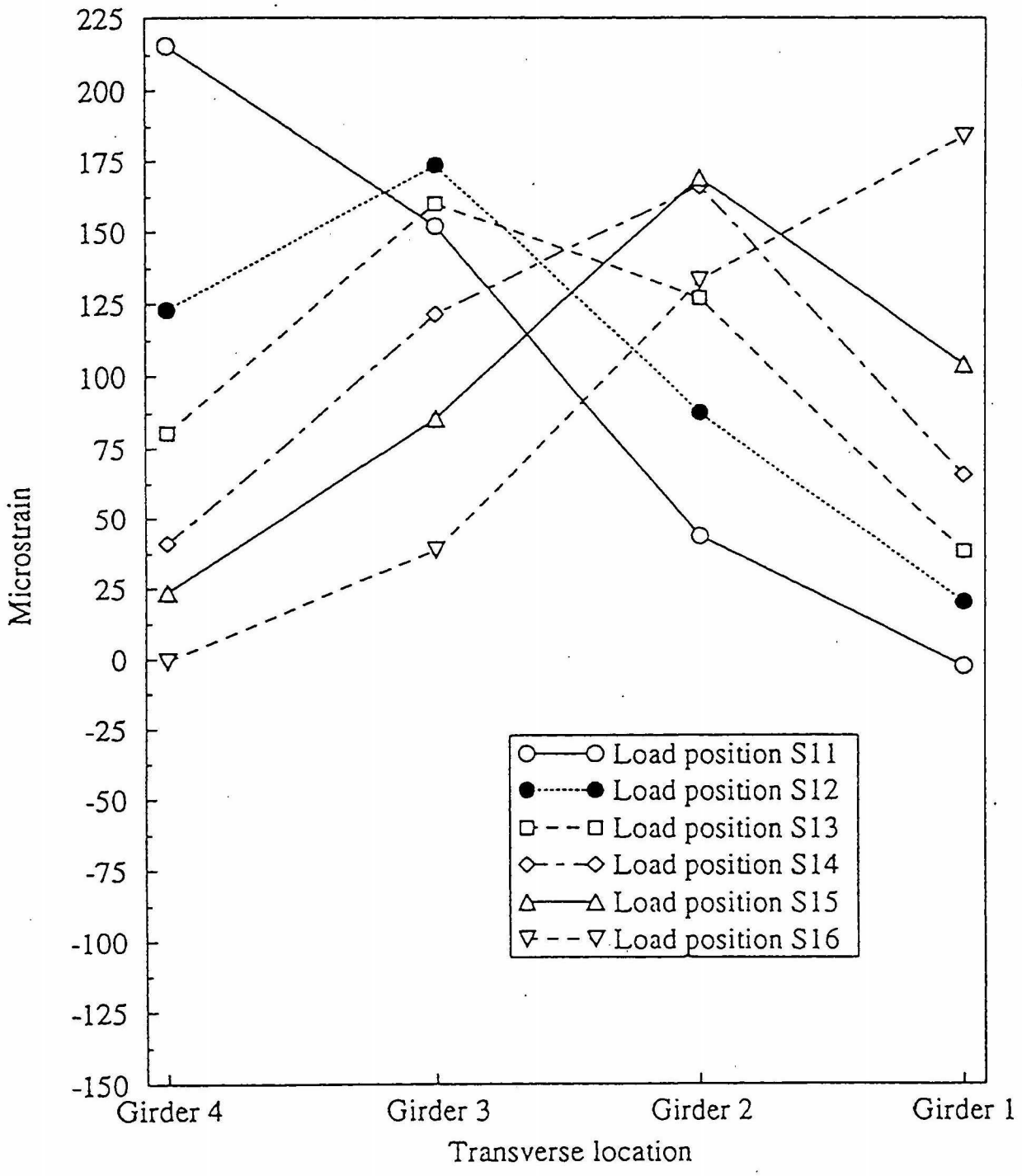

Figure 3.4. Average bottom flange girder strains at the 0.45 point of span 1 for various load positions

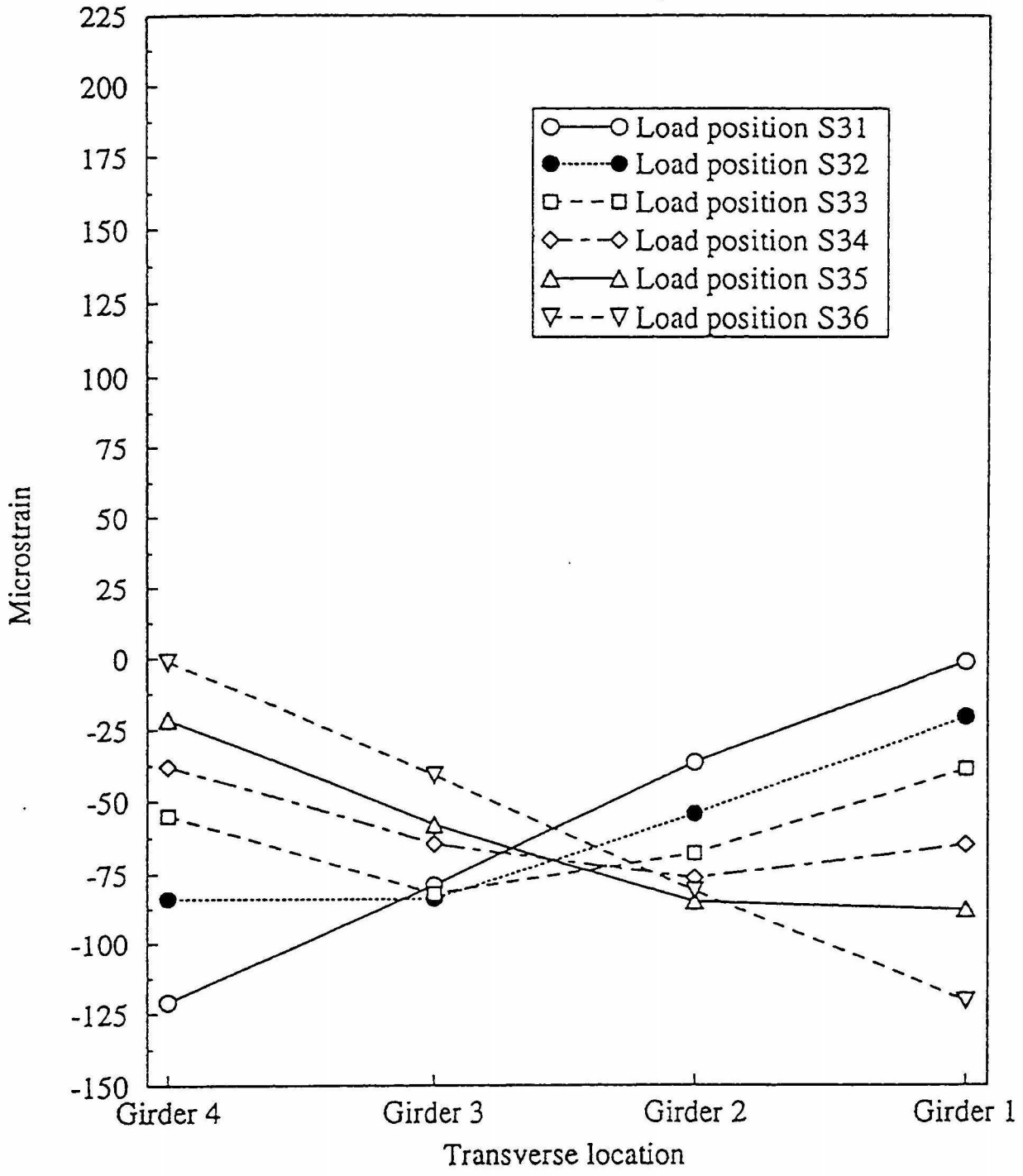

Figure 3.5. Average bottom flange girder strains near pier 1 for various load positions

near the edges of the roadway (lane lines 1 or 6) there was considerable variation in the bending strains between the girders. This asymmetric loading caused the bridge cross section to twist, as evidenced by the measured girder deflections. When the truck was at position S11 the deflections at the middle of Span 1 were 0.000, 0.036, 0.103, and 0.139 in. at girders 1, 2, 3, and 4, respectively. These deflections included the effects of small vertical movements at the girder bearing points on the north abutment. When the truck was traveling along lane lines 3 or 4, which were near the mid-width of the bridge, the interior girders resisted the largest proportion of the load. Figures 3.3 and 3.4 revealed that symmetric bridge response behaviors occurred as evidenced by the symmetric nature of the generated patterns shown.

3.2. Finite Elemental Analyses

3.2.1. ANSYS program

A finite element model of the bridge was developed for the purpose of analyzing the bridge. Several commercial software programs were available at ISU for developing a finite-element model (FEM). The one that was selected for this research is Analysis of Systems (ANSYS). The ANSYS program Version 5.0, which was developed by Swanson Analysis Systems, Inc., was selected for use in the analysis primarily due to its convenient preprocessing (model generation) and postprocessing (retrieving results) algorithms. The ANSYS software contains various types of finite elements that can be used to model and analyze different structures. Moreover, running ANSYS on work stations had the advantages of large memory storage capacity and high speed of execution, thus permitting the development of a large and sophisticated model.

3.2.2. Postprocessing programs

To expedite the postprocessing phase of an finite element analysis a postprocessing program was written in the Fortran 77 language. The postprocessor program was used to retrieve the ANSYS results for the element nodal forces and moments at cross sections which define the finite elements and used these element force and moment values to compute the total axial force and longitudinal bending moment on the composite girder sections. These results were used in the determination of the wheel load distribution factors, which describe the distribution of bending moments throughout the bridge.

3.2.3. Finite element model of the bridge

Figure 3.6 shows the plan view of the deck and a typical cross section of the finite-element model that was analyzed using the software program. The model consisted of plate elements for the bridge deck, bridge curbs, webs of the girders and three-dimensional beam elements for the girder flanges, shear connectors, and diaphragms. The circled numbers shown in the figure refer to element numbers and the other numbers refer to node numbers. All of the elements seen in the plan view are bridge deck elements. The reinforcing bars in the RC slab were not included in the finite-element model of the bridge, and the properties for the slab elements were based on an uncracked concrete section. The circled numbers 2945, 3848, 5289, 4571, and 5051 shown in the typical cross section refer to a girder web, shear connector, diaphragm, girder top flange, and girder bottom flange elements, respectively. The finite-element model contained a total of 4477 nodes and 5335 elements, which consisted of 2880 deck elements, 480 girder elements and 121 shear connector elements for each of the four girders, and a total of 51 diaphragm elements for the 51 diaphragms. The connections between the diaphragms and the girders were modeled as rigid connections, since the

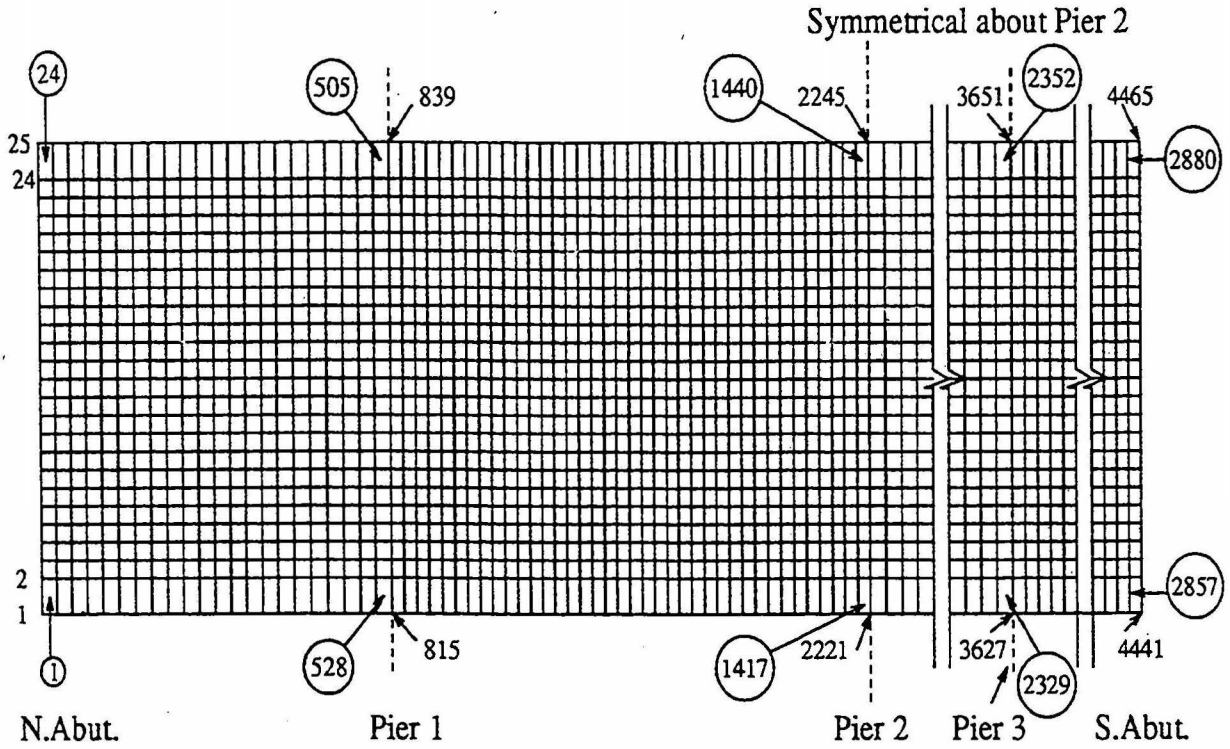

(a)

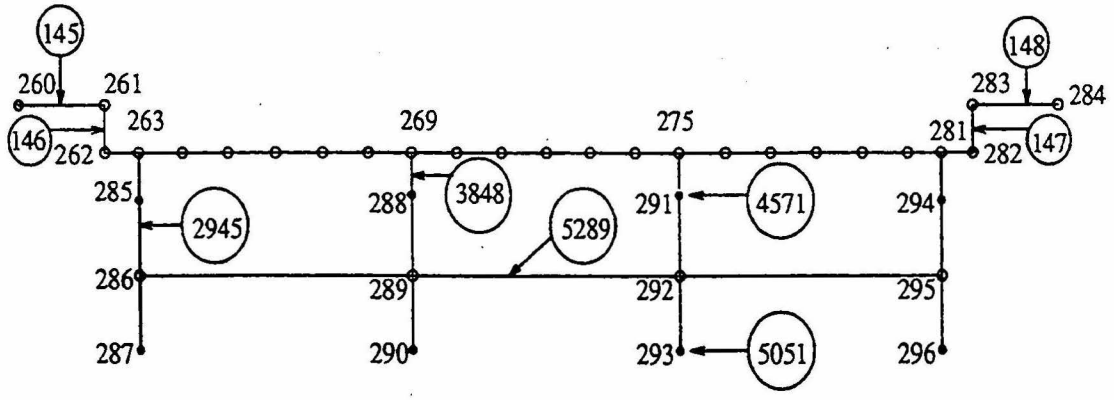

(b)

Figure 3.6. Finite element model: (a) Plan view of deck, (b) Typical cross section

actual bridge joint detail involved a significant amount of rotational restraint between these two members.

The supports at the abutments and at the first and third interior supports of the actual bridge allowed for expansion of the bridge in the longitudinal direction. Therefore, these supports were modeled in the finite-element model as restrained only in the vertical direction. At the center pier, the displacements were restrained in both longitudinal and vertical directions for both the actual bridge and the finite-element model. In addition, the finite-element model had lateral restraint provided at the center pier of one of the exterior girders to prevent transverse displacements of the bridge model.

Several displacements at the end of the shear connector elements were coupled to produce a composite behavior between the modeled RC slab and the aluminum girders. For example, in the cross section seen in Fig. 3.6 the girder node 288 and the corresponding deck node 269 were linked together by constraint equations for the finite-element model. The rotations in all the three orthogonal planes and the vertical displacement for these nodes were forced to be equal. The longitudinal and transverse displacements for both of these nodes were not coupled; therefore, different amounts of movement could occur at these two nodes for these two displacements. The shear stiffness of the shear connector element was established from a separate finite-element model of just the shear connector.

Finite-element models of the bridge were used to establish the distribution of the vertical loads to each of the four aluminum girders. By changing the magnitude of a specific design parameter from the value corresponding to the original Clive Road Bridge, the researchers were able to mathematically evaluate the influence that a particular parameter has on vertical load distribution. The finite-element model of the original Clive Road Bridge involved the geometrical configuration

and dimensional distances for the bridge superstructure that were discussed in Chapter 2. The material properties for this model were the modulus of elasticity and Poisson's ratio of the aluminum, E_a and μ_a, respectively and modulus of elasticity and Poisson's ratio of the concrete, E_c and μ_c, respectively. The values of these properties were E_a = 10,400,000 psi, μ_a = 0.30, E_c = 4300 psi, and μ_c = 0.20. The modulus E_c was obtained from the expression

$$E_c = 33w^{1.5}\sqrt{f'_c} \tag{3.1}$$

where, w = unit concrete weight (150 pcf) and f'_c = 28-day concrete compressive strength (5000 psi) of the slab. A minimum concrete strength f'_c of 3500 psi was specified for the actual bridge construction in 1957. The writers have estimated that the strength f'_c had increased to about 5000 psi when the 1993 field tests were conducted.

The bending moments and the corresponding stresses for the composite sections, the vertical displacements, axial forces, and bending moments in the longitudinal direction for each element were derived from a postprocessor program that used the results obtained from the finite-element analysis. The width of the RC slab used for the composite sections was in accordance with the criteria in the current AASHTO Specification (1).

3.3. Analytical Predictions of the 1993 Field Test Results

The finite-element model was used to establish analytical predictions of the girder bending strains for various positions of the truck. Figures 3.7, 3.8, and 3.9 show the influence lines for the bottom flange average strain in girder 4 at the 0.45 point in span 1 for lane line 1 truck loads, the average bottom flange girder strains at the 0.45 point in span 1 for various transverse load positions corresponding to that location, and the average bottom flange girder strains at 18 in. north of pier

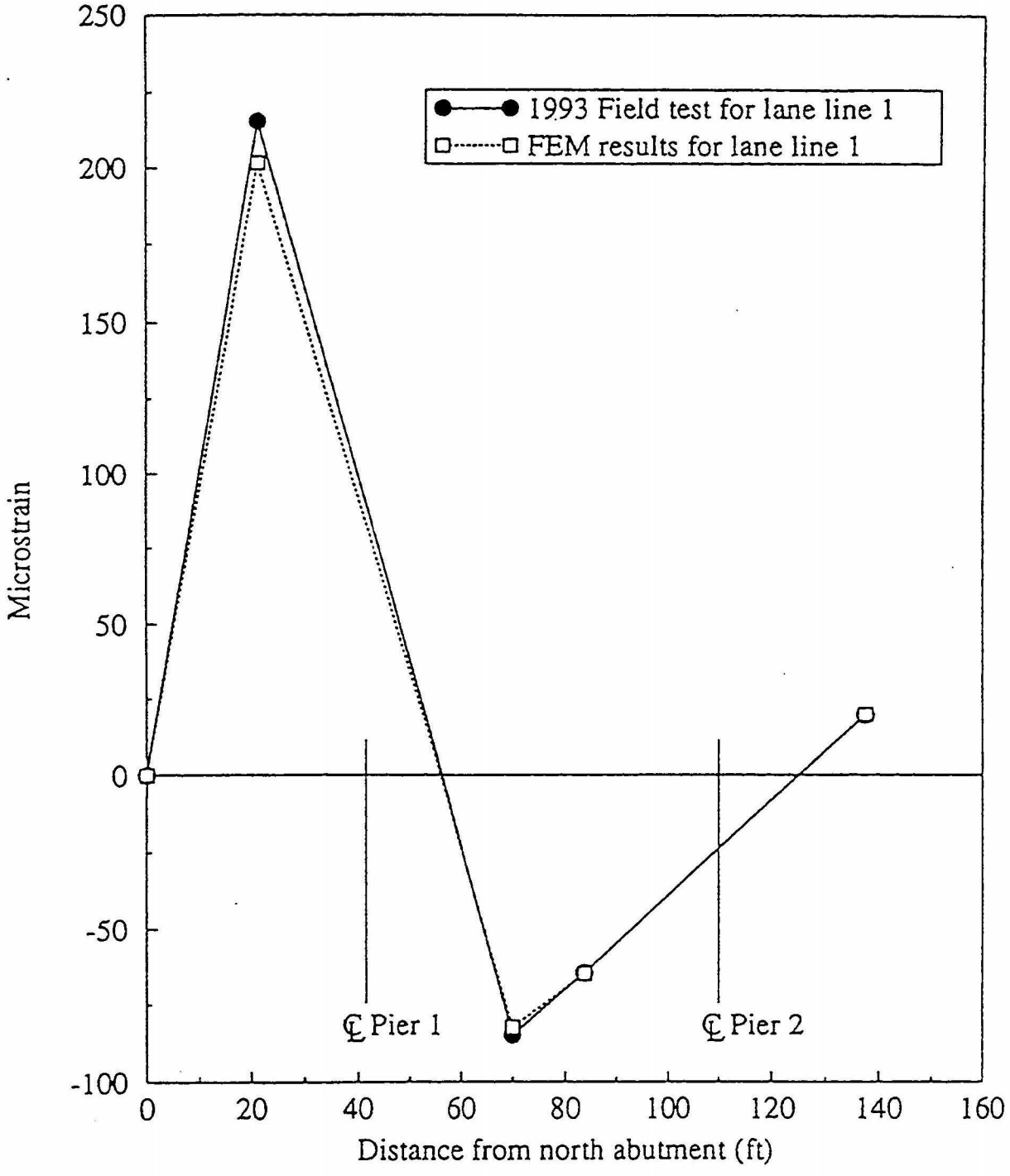

Figure 3.7. Predicted and measured strain influence lines for the bottom flange average strain in girder 4 at the 0.45 point of span 1 for lane line 1

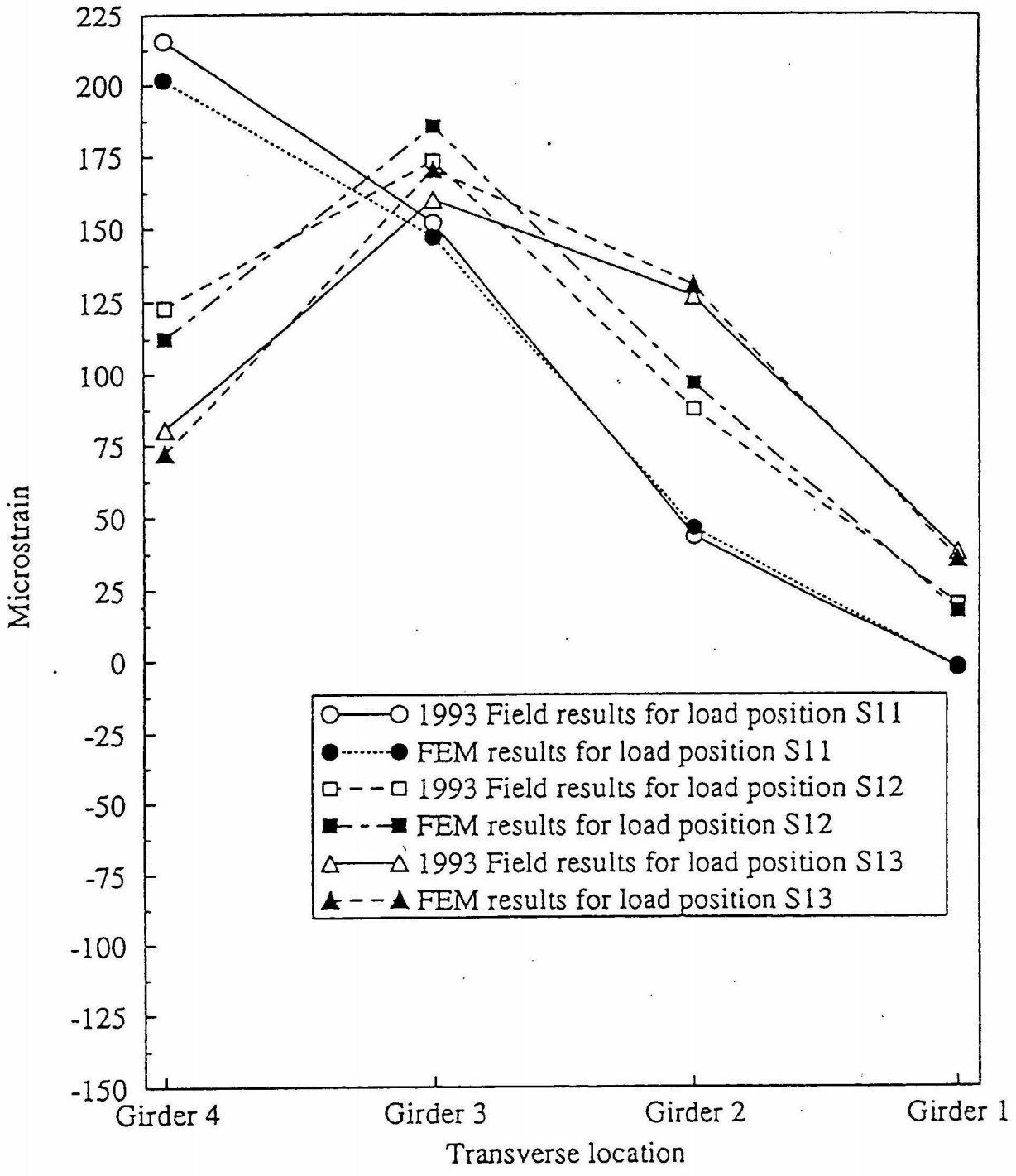

Figure 3.8. Predicted and measured average bottom flange girder strains at the 0.45 point of span 1 for various load positions

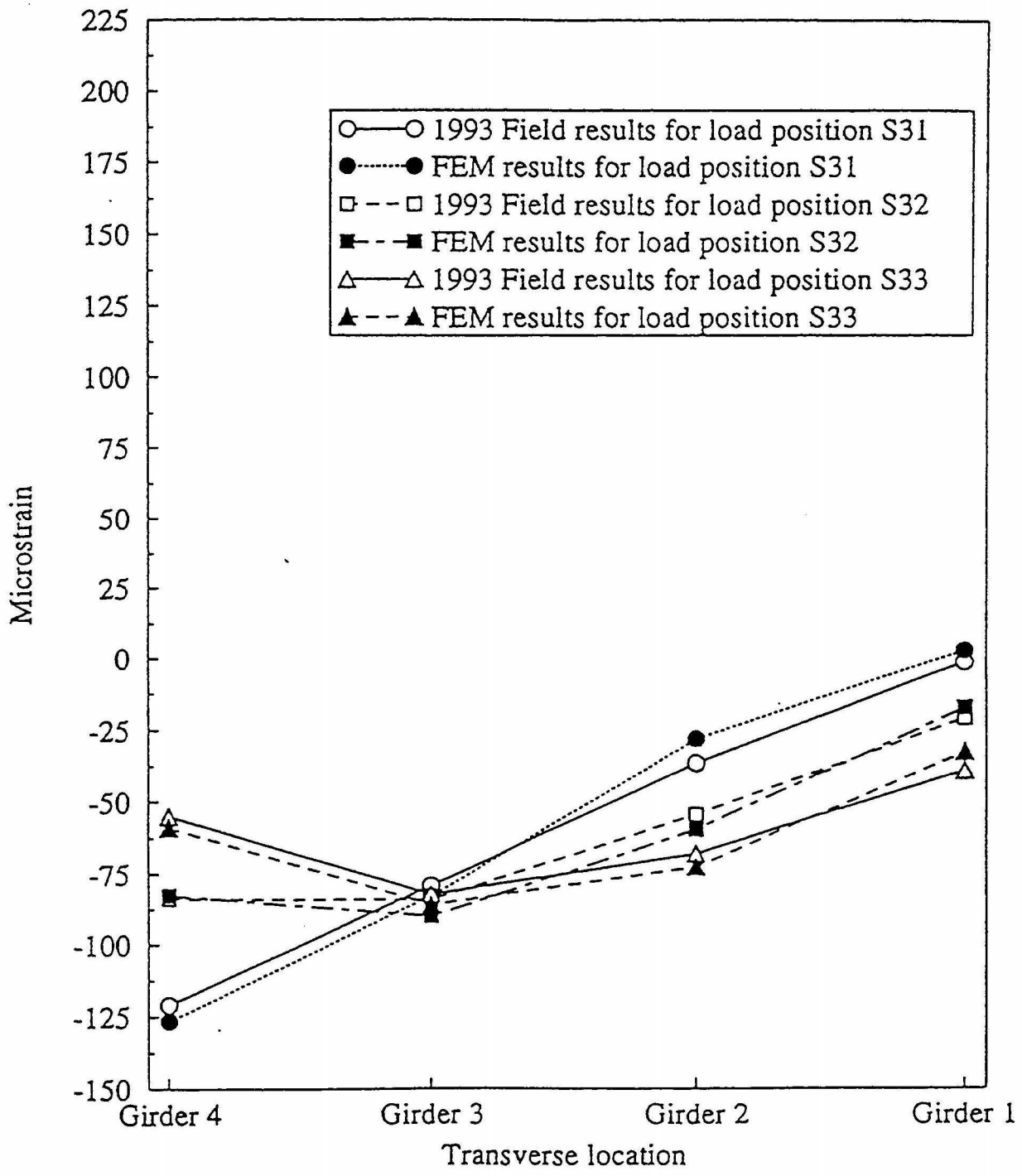

Figure 3.9. Predicted and measured average bottom flange girder strains near pier 1 for various load positions

1 for various transverse load positions corresponding to that location, respectively, that were predicted by analytical investigations using the finite-element model and measured during the 1993 field testing of the bridge. These figures show that excellent correlation occurred between the analytical solutions and the experimental measurements of the girder bending strains.

Girder deflections at the 0.3, 0.5, and 0.7 points within span 1 were measured during the field tests and calculated for the finite element model when the truck was at various positions on the bridge deck. Figures 3.10, 3.11, and 3.12 show the experimentally established and theoretically predicted girder deflections for load positions S11, S12, and S13, respectively, used in the 1993 field testing. The DCDT on girder 2 at the 0.7 point in span 1 did not function properly; therefore, the experimental data at this point was omitted for the field test results. The experimentally measured span deflections were adjusted to account for the measured vertical displacements that were recorded at the girder bearing points on the north abutment. Except for the girder displacements at the 0.7 point of span 1 when the truck load was at positions S12 and S13, the finite element predictions of the girder displacements were good.

Bending strains were experimentally measured in the webs of the intermediate diaphragms at the one-third and two-thirds points of span 1. Diaphragm bending strains at the same locations were also calculated using the finite element model of the bridge and from simplified two-dimensional finite element models of the diaphragms as continuous beams supported by the bridge girders. The supports of each two-dimensional beam model were vertically displaced a distance equal to the measured girder deflections at the diaphragm location. All the supports in the model were considered to be pinned due to the low torsional resistance of the girders. The induced bending strains in the diaphragms at the one-third point of span 1 that were obtained from the two-dimensional finite element model of the diaphragms, finite element model of bridge, and the field

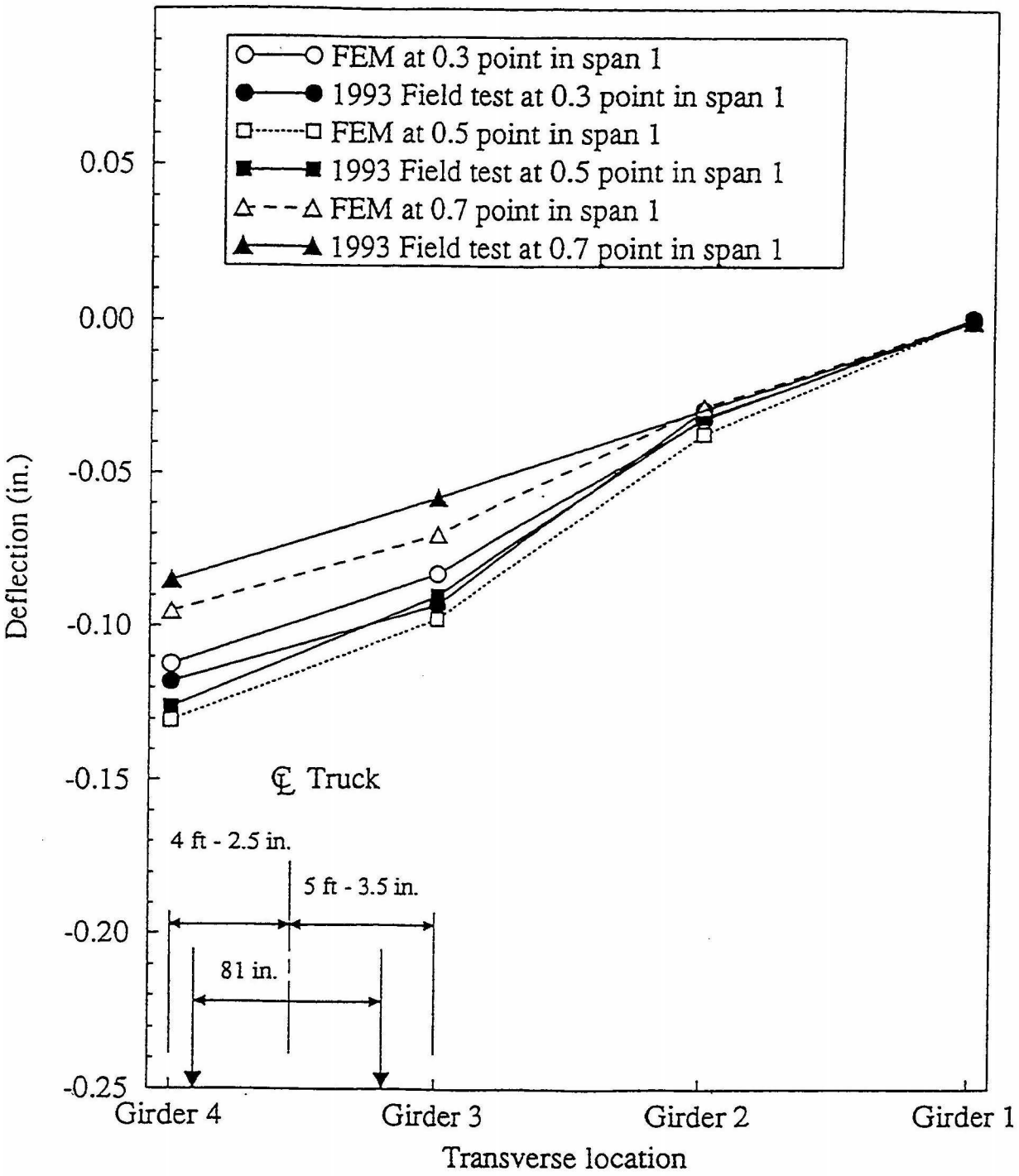

Figure 3.10. Girder deflections in span 1 with the truck at position S11.

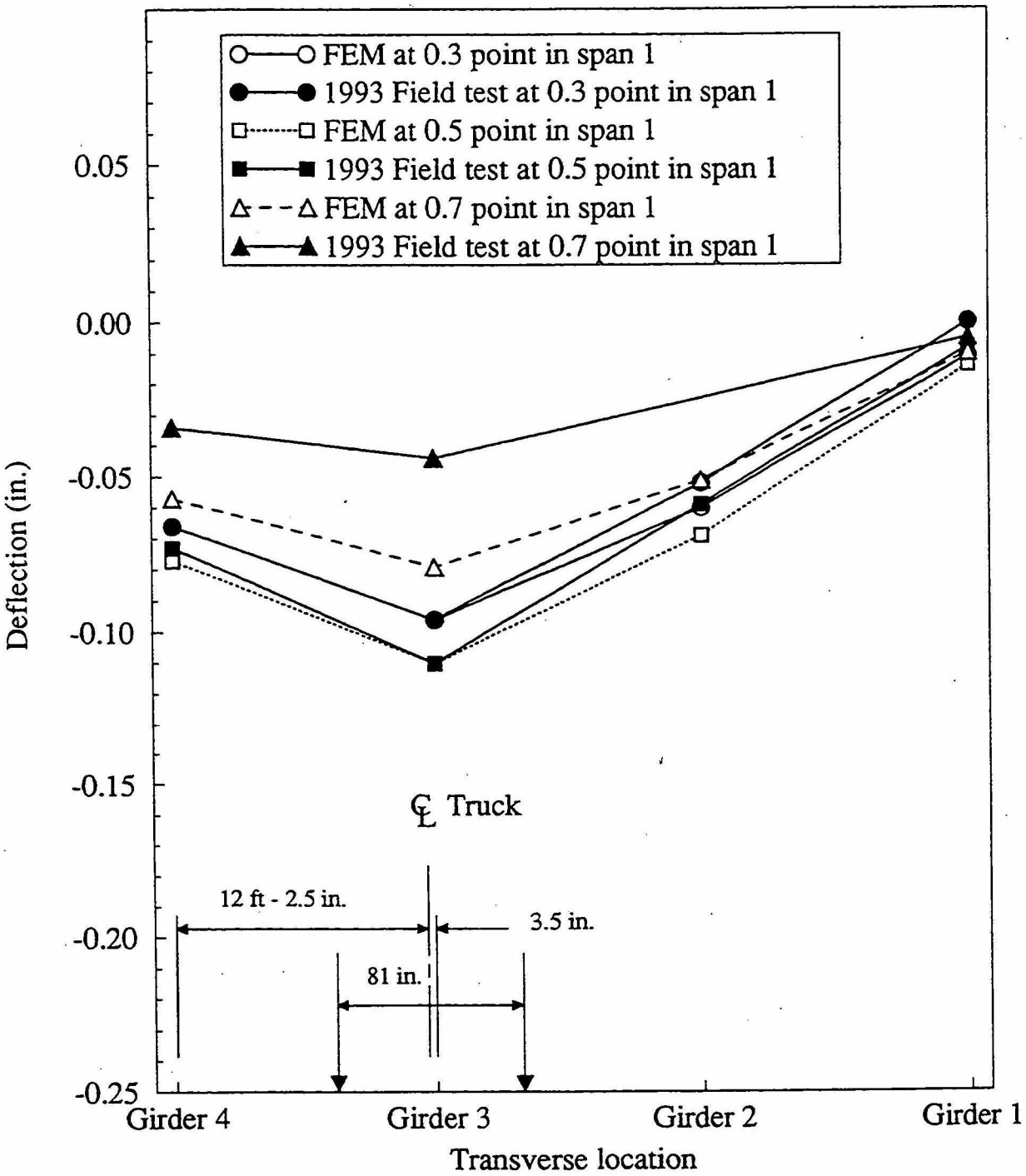

Figure 3.11. Girder deflections in span 1 with the truck at position S12.

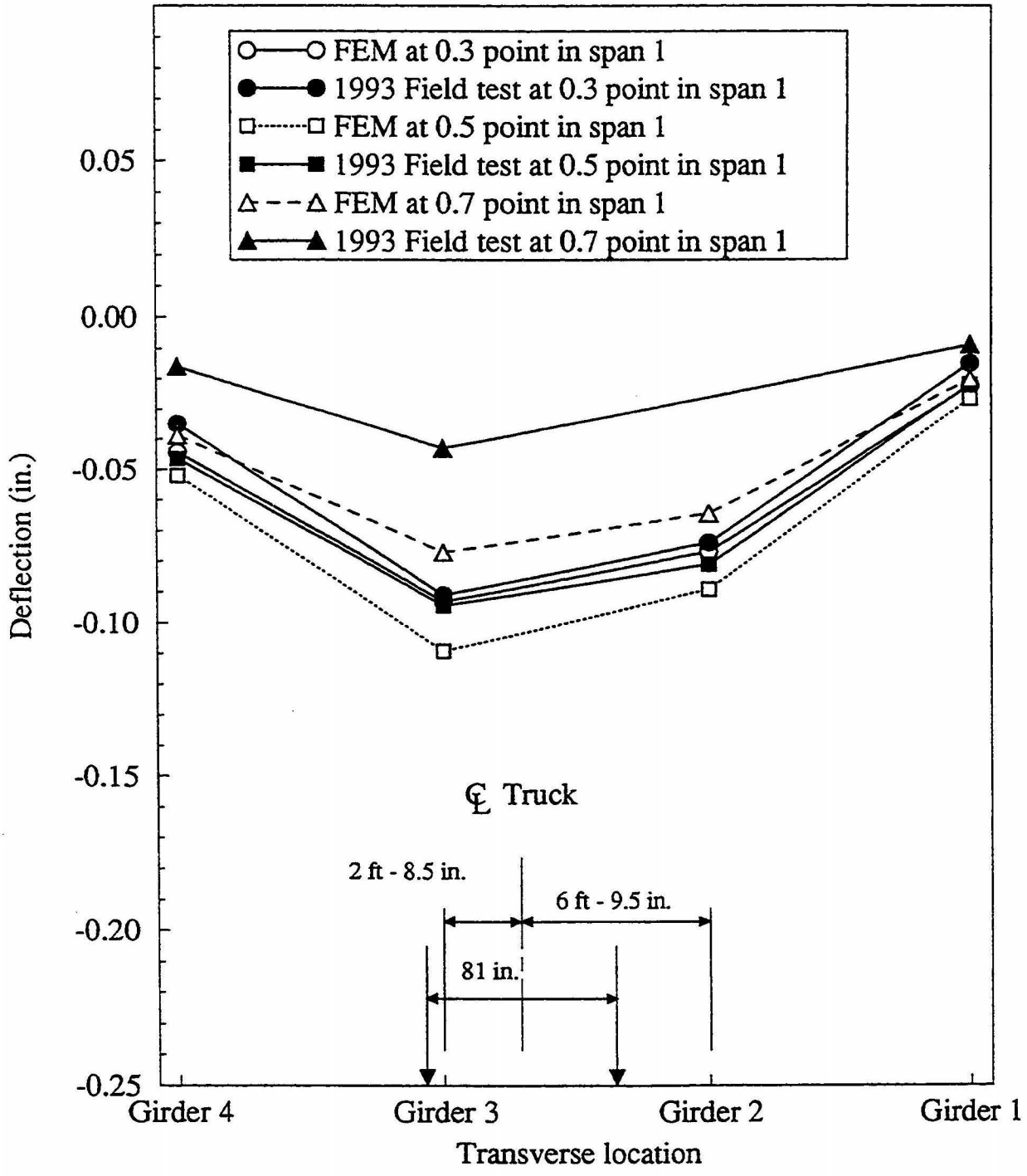

Figure 3.12. Girder deflections in span 1 with the truck at position S13.

test are shown in Figs. 3.13 and 3.14 for load position S11 and S14, and S15 and S16, respectively. For each truck position, the pattern of experimentally and analytically established strains along the diaphragm length is the same, although the strain magnitudes are slightly different. In many instances, the analytically predicted diaphragm bending strains were in close agreement with the measured strains. The symmetric response of the bridge can be observed by comparing Fig. 3.13a with Fig. 3.14b and Fig. 3.13b with Fig. 3.14a. The diaphragm bending strains at the two-thirds point in span 1 can be found in Ref. (11). Since the finite-element model has correctly predicted the behavior of this bridge, parameter studies were conducted on wheel load distribution. These results are discussed in Chapter 4 of this report.

3.4. Comparisons of the 1959 and 1993 Field Test Results

Comparisons were made between the 1959 and 1993 field test results to determine whether changes occurred in the structural behavior of the bridge. Since the AASHTO criteria for the number of lanes and their location on the bridge changed between 1959 and 1993, the test lanes adopted for each field test program were different. Therefore, the comparisons were made only for the load cases for which the truck positions across the width of the bridge in both of the field tests were essentially the same. The truck positions chosen were position 3-W from the 1959 tests (Fig. 2.7) and position 2 from the 1993 tests (Fig. 2.6). To compare these two load cases, the percentage of the total longitudinal moment bending resisted by each girder at similar positions along the length of the bridge were selected. For the 1993 field test, the bending moment in each girder was calculated from the measured longitudinal bending strains. Figures 3.15, 3.16, and 3.17 show the percentage of the total bending moment resisted by each girder for maximum positive moment in

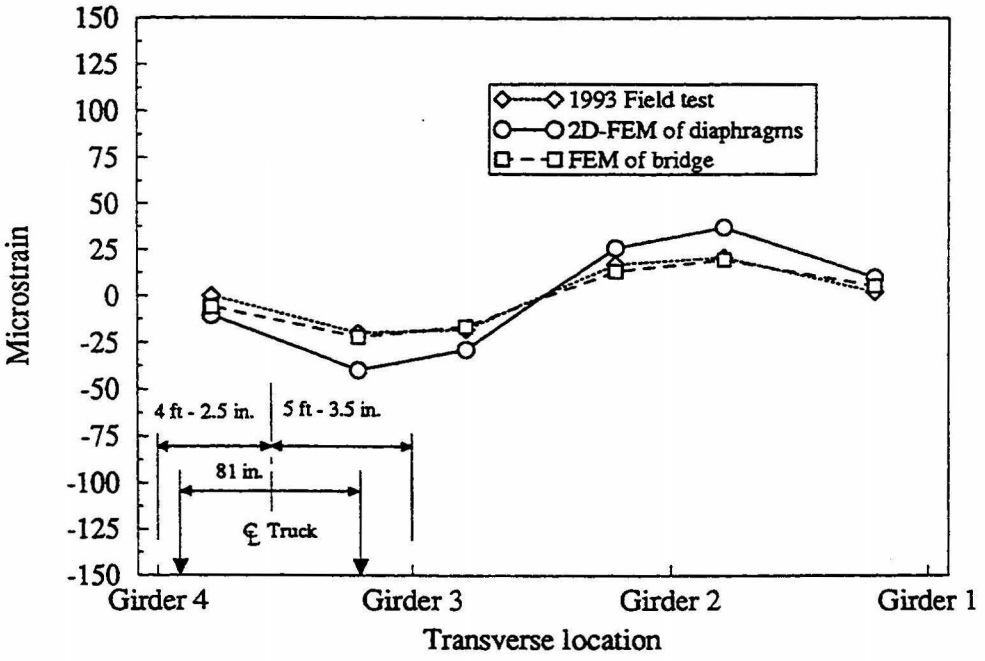

(a)

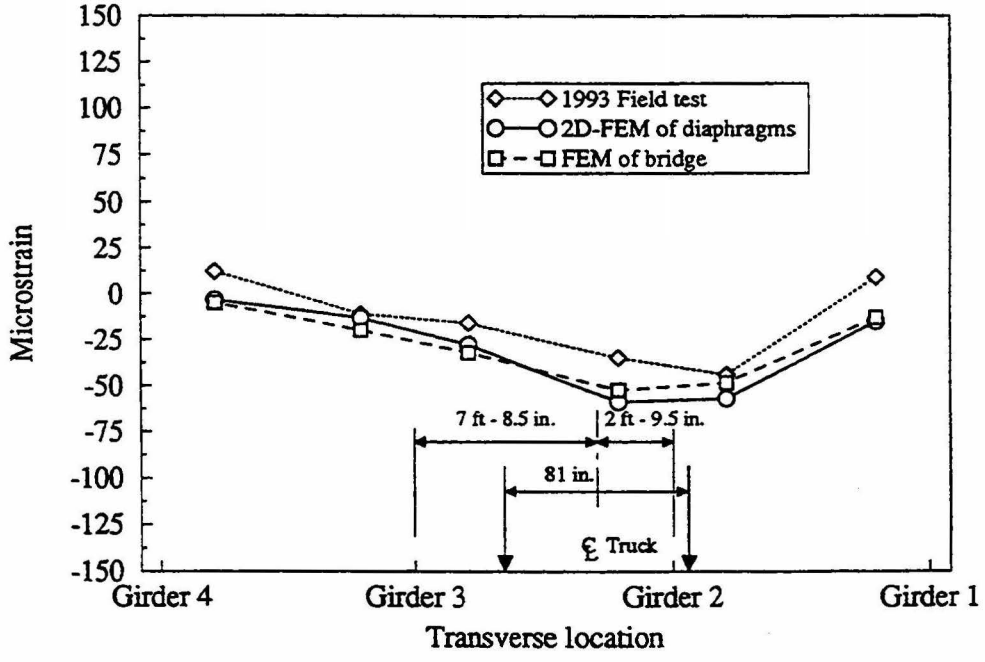

(b)

Figure 3.13. Bending strains in intermediate diaphragms at the one-third point of span 1: (a) Truck at position S11, (b) Truck at position S14

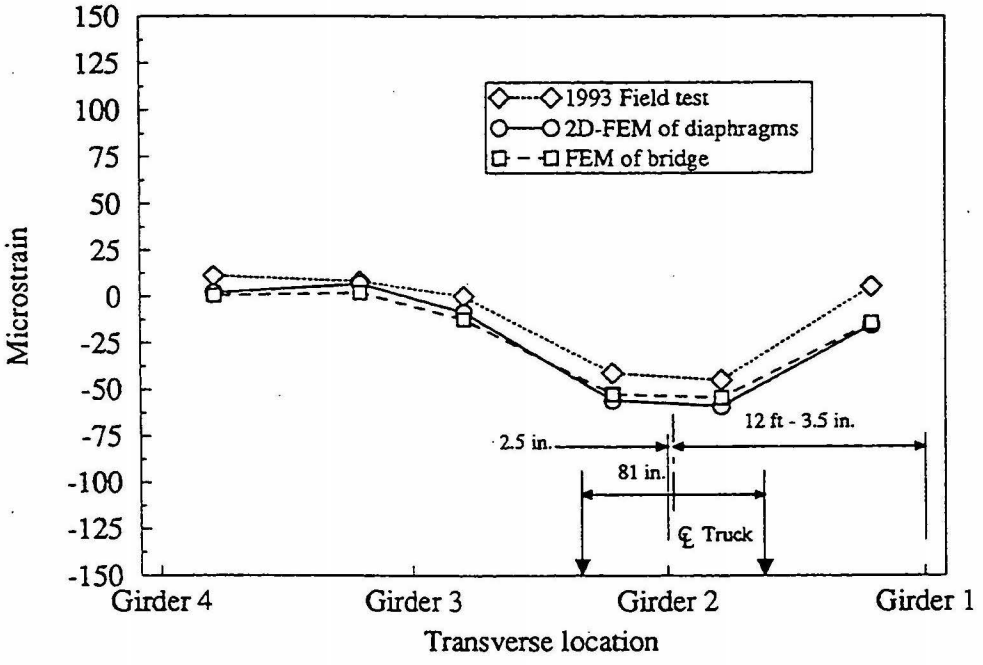

(a)

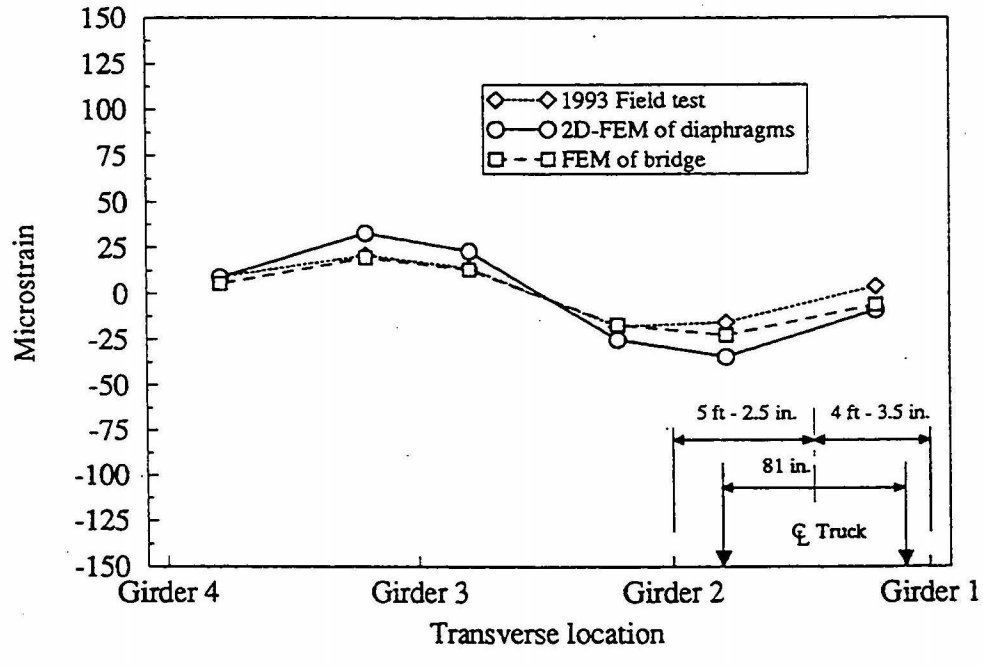

(b)

Figure 3.14. Bending strains in intermediate diaphragms at the one-third point of span 1: (a) Truck at position S15, (b) Truck at position S16

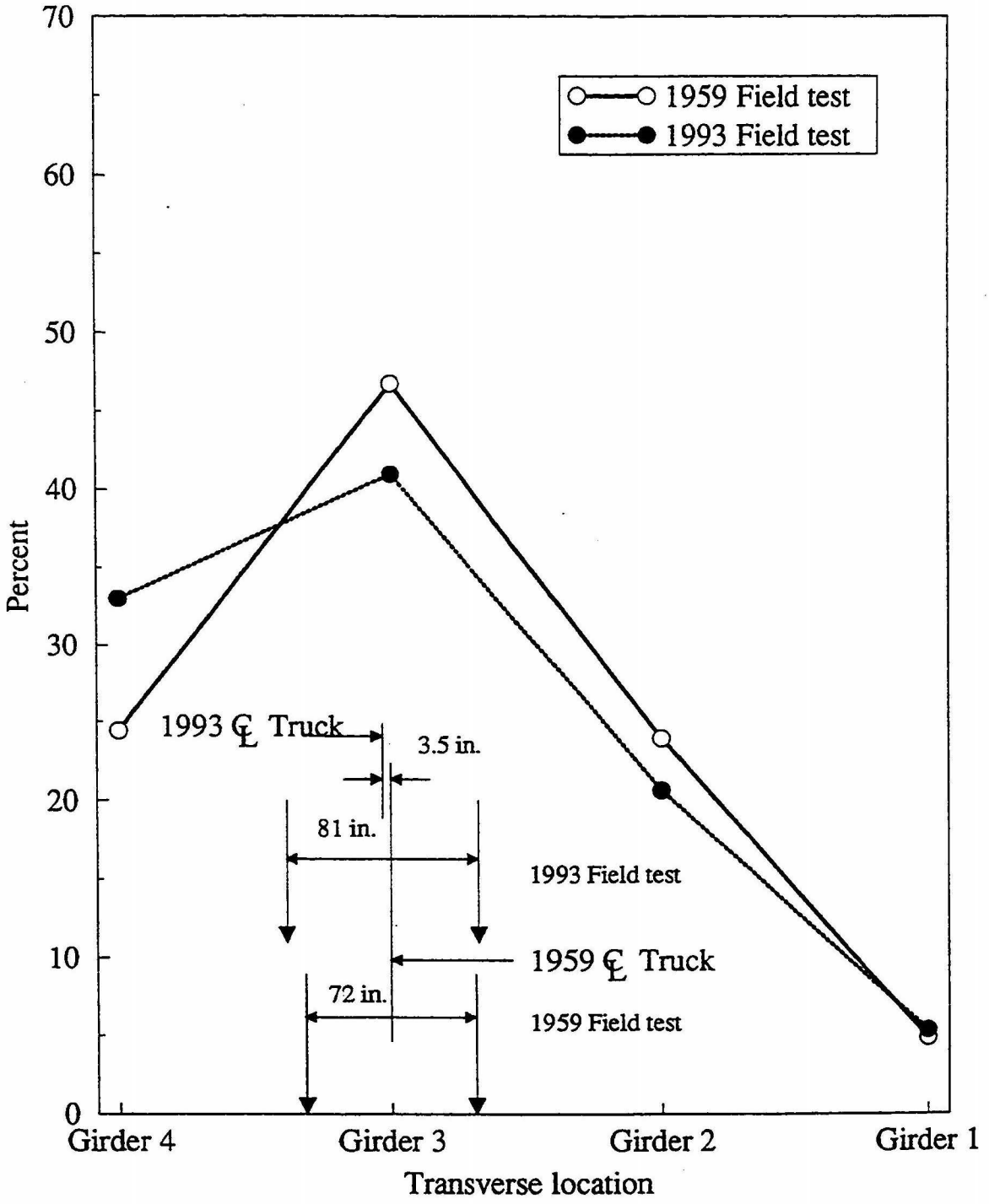

Figure 3.15. Percentage of total moment resisted by each girder for maximum positive moment in span 1 with 1959 truck at position at 3-W and 1993 truck at position S12

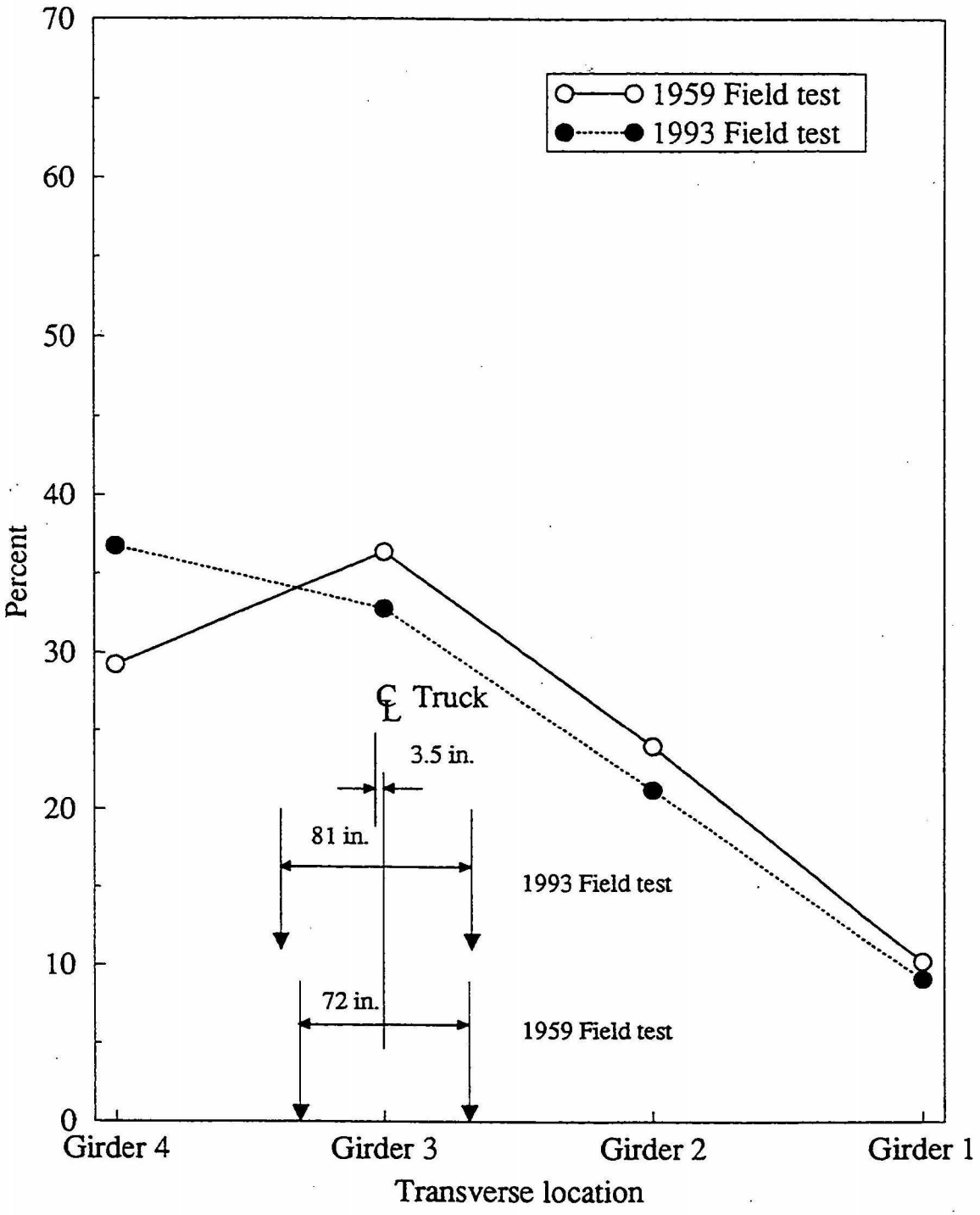

Figure 3.16. Percentage of total moment resisted by each girder for maximum negative moment near pier 1 with 1959 truck at position at 3-W and 1993 truck at position S32

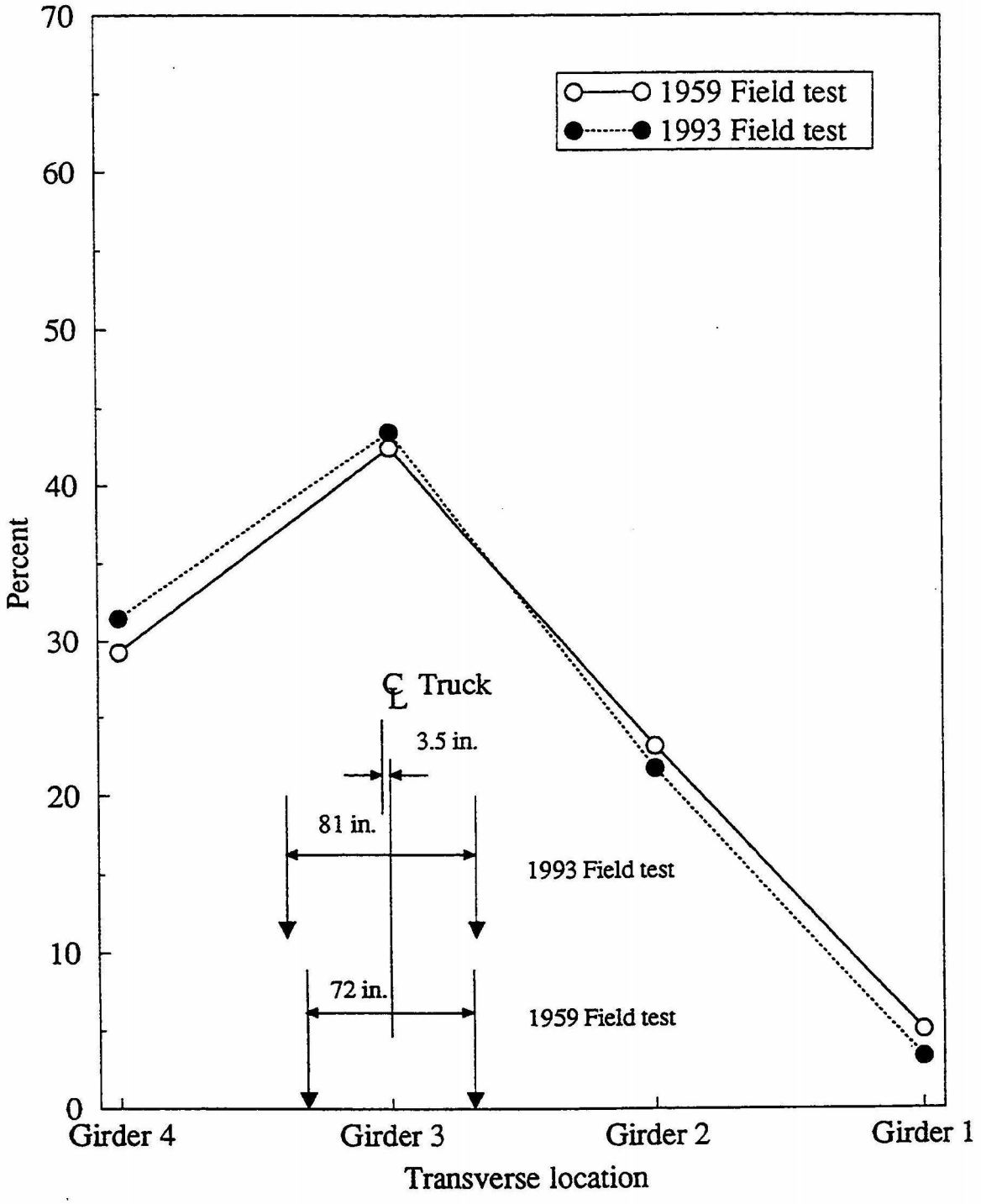

Figure 3.17. Percentage of total moment resisted by each girder for maximum negative moment near pier 2 with 1959 truck at position 3-W and 1993 truck at position S52

span 1 and maximum negative moment near piers 1 and 2, respectively. Girder 3 was selected to investigate the reasons for the different responses between the two field tests. The parameters studied were the truck gage width, lateral truck position, longitudinal truck position, and concrete compressive strength.

3.4.1. Truck gage width

As shown in Fig. 3.15, the percent positive bending resisted by girder 3 in the 1959 field tests was about 5% higher than that for the 1993 field tests. The gage width of the 1993 truck was 9 in. greater than that for the 1959 truck. The 3.5 in. shift in the centroid of the applied wheel loads between the 1993 and 1959 trucks towards girder 4, caused a greater wheel load distribution to girder 4 and a reduced distribution to girder 3 for the 1993 truck. To verify that the difference in the truck gage widths could produce a difference in the wheel load distributions, finite element analyses were performed for two gage spacings of the 1993 truck wheel loads. The locations of the center of gravity for the two trucks were at the same position on the model bridge as that for the actual truck used in the 1993 field tests. For each analysis, the predicted percentage of the total positive bending moment at the 0.45 point in span 1 for each girder is shown in Fig. 3.18. A decrease in the gage width for the 1993 truck produced a 2% increase in the percent moment resisted by girder 3. A comparison of the results given in Figs. 3.15 and 3.18 reveals that the change in the gage spacing of the wheel loads produced a change in the distribution of the bending moment to the four girder that was consistent with the results obtained between the two field tests. Therefore, the difference in gage width of the wheel loads for the trucks used in the 1993 and 1959 field tests provides one explanation for the differences in the moment percentage resisted by each girder.

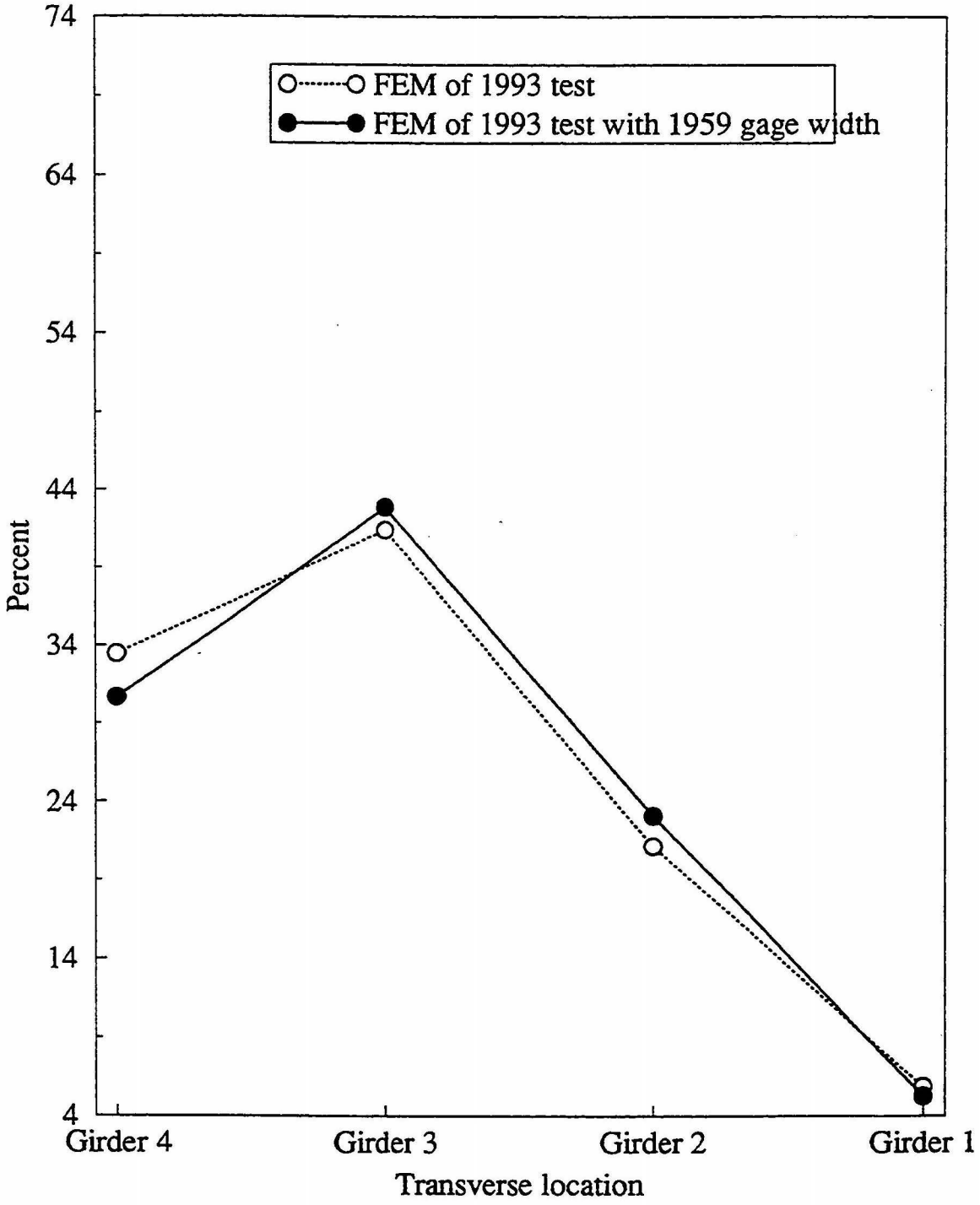

Figure 3.18. Percentage of total moment resisted by each girder at the 0.45 point of span 1 with truck at position at S12

3.4.2. Truck lateral position

The lateral truck positions on the bridge were slightly different in the 1959 and 1993 field tests. As shown in Fig. 3.15, the center of gravity for the 1993 truck was 3.5 in. to the left of the center of gravity for the 1959 truck and center line of girder 3. Therefore, the percentage of the total bridge cross-sectional moment induced in girder 3 was larger in the 1959 field test than it was in the 1993 field test, while for girder 4, the 1993 field test produced the larger moment percentage. To establish the effect of the lateral position of the truck on wheel load distribution, a finite element analysis was performed with the 1959 truck shifted laterally away from girder 3 to match the 1993 truck position. The moment percentage (not shown) resisted by girder 4 and girder 3 was about 1% higher and essentially unchanged, respectively.

3.4.3. Truck longitudinal position

The selected positive moment location were at the 0.40 and 0.45 points of span 1, and for the 1959 and 1993 tests, respectively. To establish whether the approximately 2 ft difference in the locations for the longitudinal sections would cause the difference in the load distribution between the 1959 and 1993 field tests, a finite element analysis was performed when the 1959 truck was repositioned to cause maximum positive moment at the 0.45 point of span 1. Figure 3.19 shows the moment percentage at the 0.45 point of span 1 for each girder when the 1959 truck was repositioned. Similar results are also shown for the 0.40 point of span 1 to correspond with the truck load position used in the 1959 field test. The moment percentage resisted by girder 3 decreased by approximately 3 percent when the 1959 truck loads were moved to the same longitudinal location that was used in the 1993 field test. Therefore, the difference in the longitudinal load positions between the 1959 and 1993 trucks account for some of the differences in the load distribution factors associated with the two field tests.

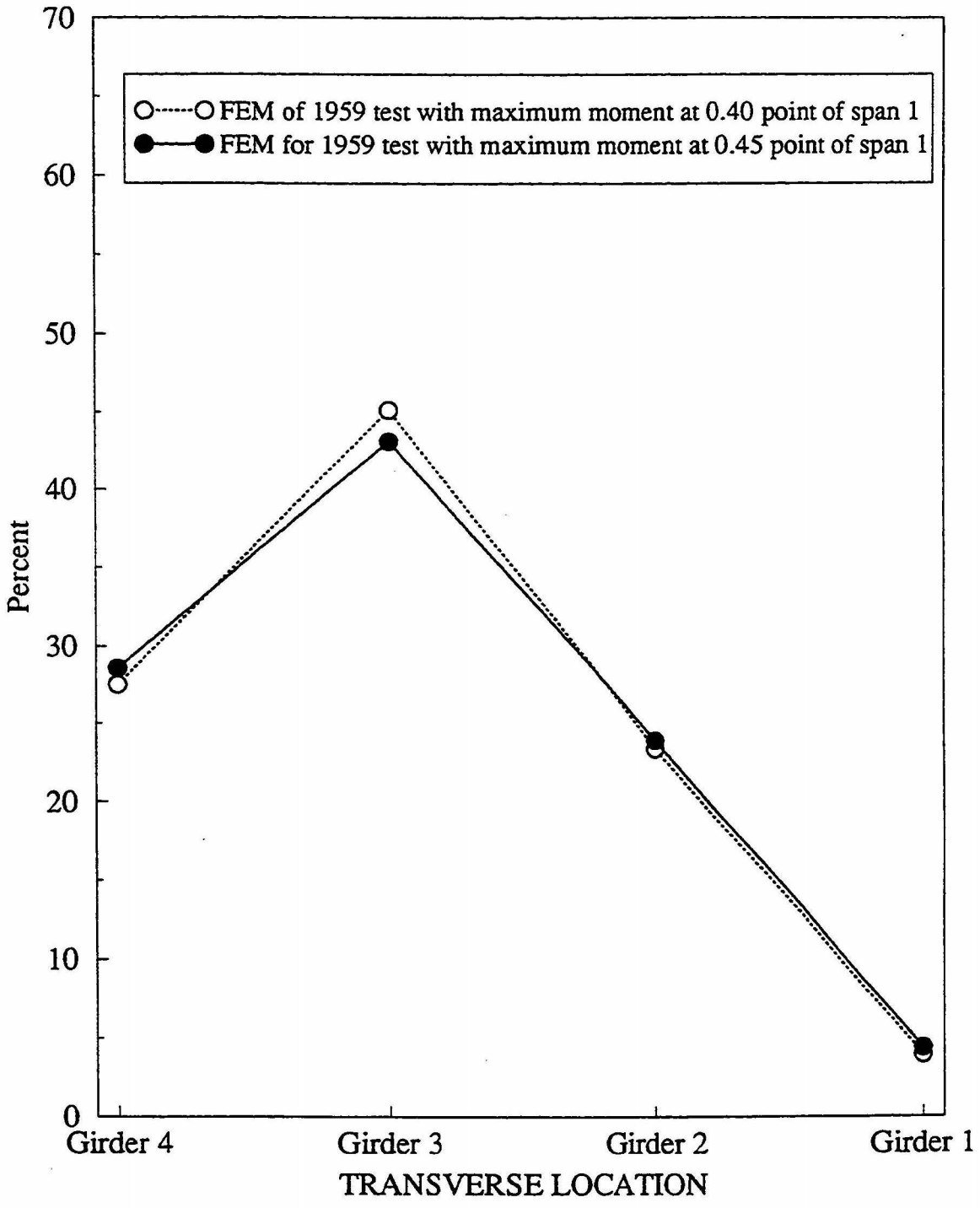

Figure 3.19. Percentage of total moment resisted by each girder for positive moment at span 1 with truck at position 3-W

3.4.4. Concrete compressive strength

The flexural stiffness of the bridge deck is a function of the modulus of elasticity of the concrete, moment of inertia of the slab, and span length. The modulus of elasticity of the concrete is approximately proportional to the square root of its compressive strength. Since the bridge was constructed in 1959, the concrete strength would have been higher in 1993 than it was in 1959. An increase in the concrete strength would increase the deck stiffness and cause better load distribution. To establish the effect of the concrete compressive strength on load distribution, analyses were performed for strengths of 3500 and 7000 psi for a particular truck load position. As shown in Fig. 3.20, an increase in the concrete strength produced better load distribution. The percentage of the bridge cross-sectional moment resisted for girder 3 decreased by approximately 2 percent, when the concrete strength was doubled. The better load distribution for the 1993 field test as compared to that for the 1959 field tests was partly due to an increase in the concrete strength for the bridge deck over time.

3.5. Assessment of the Bridge Superstructure

The truck gage width, lateral truck position, longitudinal truck position, and concrete compressive strength have some affect on the wheel load distribution. When each of these parameters are considered individually, they do not account for the total difference in the computed load distribution factors between the 1959 and 1993 field tests. When several of these parameters are considered simultaneously, their interaction effect may account for the total difference in the values of the moment percentage for the girders between the two field tests.

The analytical studies of the parameter variations have provided explanations for the small differences in the load distribution between the 1959 and 1993 field tests. Therefore, the response

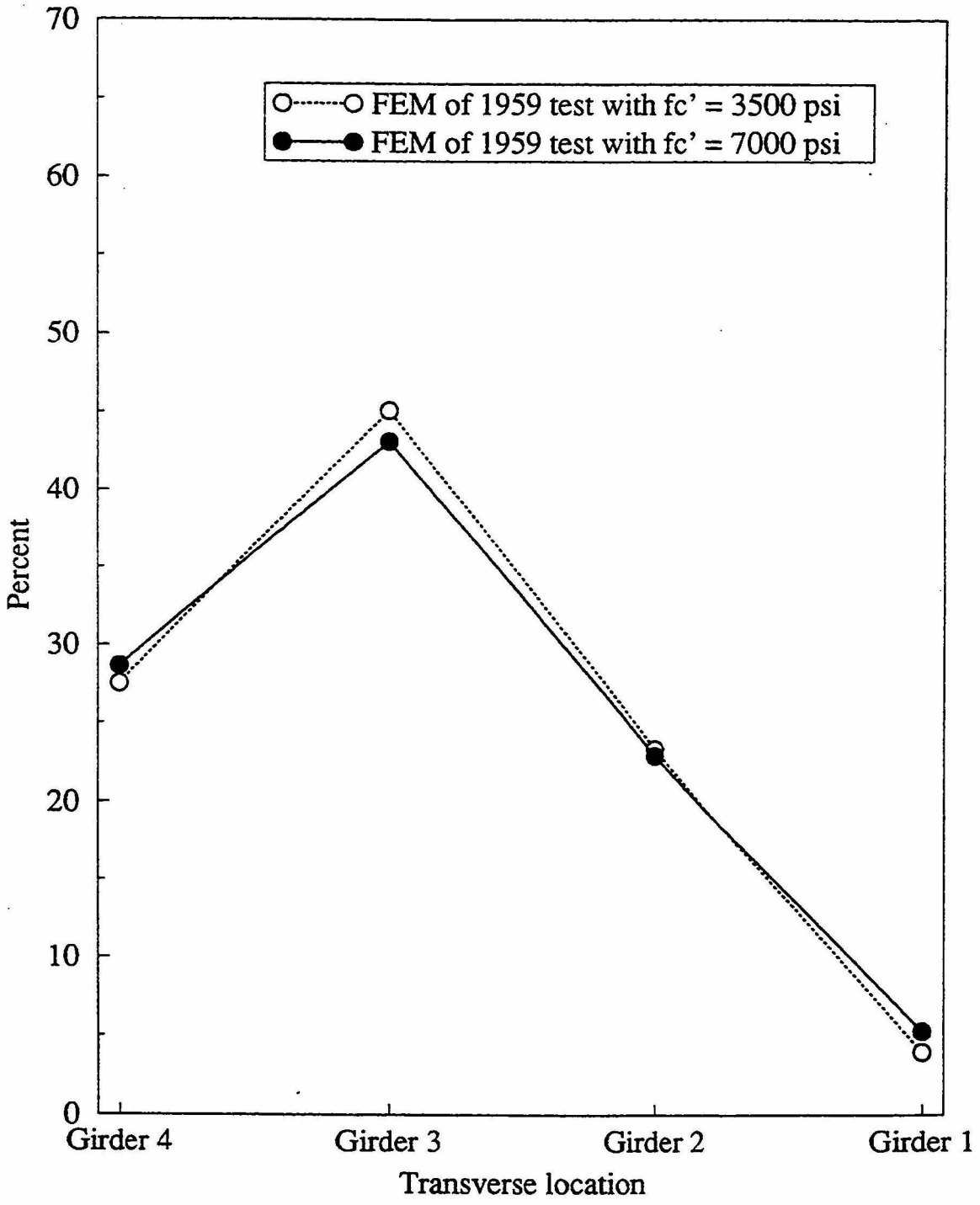

Figure 3.20. Percentage of total moment resisted by each girder at the 0.40 point of span 1 with truck at position 3-W for different concrete compressive strength

of the bridge to static truck loads did not appear to have changed over the 34 years between the two field tests. Except for the need of a possible deck overlay, the performance of the composite, welded, I-shaped, aluminum-girder bridge had not deteriorated to any measurable extent.

Additional studies that address evaluation of the 1959 field tests can be found in Refs. (10) and (11).

CHAPTER 4. LOAD DISTRIBUTION STUDIES

The effects of several design parameters on the load distribution for the welded-aluminum, composite-girder, highway bridge was investigated. The parameters considered were the flexural stiffness of the intermediate diaphragms, torsional stiffness of the girders, flexural stiffness of the slab, flexural stiffness of the girders, and lateral spacing of the girders. This chapter presents mathematical models for load distribution and summarizes the parametric studies that were undertaken regarding load distribution.

4.1. Standard and LRFD Bridge Specifications

In the United States, two specifications exist for the design of highway bridges. They are the AASHTO Standard Specifications for Highway Bridges (17), which will be referred to as the Standard Specifications; and the AASHTO Load Resistance and Factor Design (LRFD) Bridge Design Specifications (1), which will be referred to as the LRFD Specifications. Standard practice in highway bridge design has emphasized approaches which idealize a deck and multiple-girder structure as a series of isolated girders. A convenient method to establish girder bending moments that are induced by wheel loads is to proportion the total longitudinal bending moment that is produced by a single line of wheel loads or a single lane of trucks at an entire transverse cross section of the bridge to the interior or exterior girders. The proportionality factor is the load distribution factor.

The wheel load distribution factors for multi-girder, concrete-slab (girder-slab) bridges were developed by idealizing the bridge deck as an orthotropic plate. Both the Standard and LRFD Specifications address load distribution for the exterior and interior girders of steel and concrete girder-slab bridges. These specifications do not directly address load distribution factors for

aluminum girder, concrete-slab bridges. For this discussion, the writers have assumed that the load distribution criteria for steel and concrete girder-slab bridges are valid for aluminum and concrete girder-slab bridges. The live load to be resisted by a girder is represented as the number of single-line of wheel loads in the Standard Specifications and by the number of lanes of trucks in the LRFD Specifications. In the Standard Specifications, the fraction of the wheel loads, defined as the Load Distribution Factor (LDF), are functions of the girder spacing, S. For an interior, steel I-beam stringer (interior girder) in a concrete-deck bridge that can accommodate two or more traffic lanes, the LDF is given by

$$LDF_i = \frac{S}{5.5} \tag{4.1}$$

when $S \leq 14$ ft. If $S > 14$ ft, the LDF for an interior girder is the reaction of the wheel loads on the girder assuming that the concrete deck behaves as a simple span between the girders. For an outside steel I-beam stringer (exterior girder) in a concrete-deck bridge that has four or more steel stringers, the LDF is given by Eq. (4.1) when the spacing, S, between the exterior girder and the adjacent interior girder is less than or equal to six feet. When $6 \text{ ft} < S < 14$ ft, the LDF for an exterior girder is expressed by

$$LDF_e = \frac{S}{4.0 + 0.25S} \tag{4.2}$$

When $S \geq 14$ ft, the LDF for an exterior girder is the reaction of the wheel loads on the girder assuming that the concrete deck behaves as a simple span between the exterior and adjacent interior girder. These expressions do not directly involve the parameters associated with the flexural stiffnesses of the bridge deck and intermediate diaphragms, torsional resistance of the girders, and longitudinal distribution of the load along the girders.

The LRFD Specifications present more complex expressions for the load distribution factors that directly account for several design parameters that influence load distribution. When a concrete bridge deck has two or more loaded design lanes and steel girders support the deck, the LDF per lane for bending moment in an interior girder of a non-skewed bridge is given by

$$LDF_i = 0.075 + \left(\frac{S}{9.5}\right)^{0.6}\left(\frac{S}{L}\right)^{0.2}\left(\frac{K_g}{12.0\ Lt_s^3}\right)^{0.1} \tag{4.3}$$

with the girder longitudinal stiffness parameter K_g expressed as

$$K_g = n(I + Ae_g^2) \tag{4.4}$$

where, I = non-composite girder moment of inertia, t_s = slab thickness, L = span length, A = non-composite cross-sectional area of girder, e_g = eccentricity of a girder with respect to the slab that is calculated as the distance between the centroid of a girder and mid-depth of the slab, S = spacing of girders, and n = modular ratio that is calculated as the ratio of the elastic modulus of girder to that of the slab. The design parameters S, t_s, L, and number of girders N_b must satisfy the following ranges when Eq. 4.3 is applied to establish the LDF: 3.5 ft $\leq$ S $\leq$ 16.0 ft, 4.5 in. $\leq t_s \leq$ 12.0 in., 20 ft $\leq$ L $\leq$ 240 ft, and $N_b \geq 4$. Equation 4.3 includes the effects of the slab and girder stiffnesses and the length of the bridge on LDF. Recall that the LDF in the LRFD Specification is the proportion of the lane loading that is to be applied in the flexural design of a particular girder.

When a concrete bridge deck has two or more loaded design lanes and steel girders support the deck, the LDF per lane for the bending moment in an exterior girder of a non-skewed bridge is given by

$$LDF_e = e * LDF_i \tag{4.5}$$

where, the factor e that relates the LDF for an exterior girder to that for an interior girder is expressed as

$$e = 0.77 + \left(\frac{d_e}{9.1}\right) \geq 1.0 \tag{4.6}$$

where, d_e = distance between the center of the outside roadway girder web and the edge of the exterior lane, with the range limitation that -1.0 ft $\leq d_e \leq$ 5.5 ft.

Both the Standard and LRFD Specifications specify that an exterior girder shall be designed to have a strength equal to or greater than that of an interior girder. From preliminary analyses of the Clive Road Bridge with only one traffic lane, LDF_i and LDF_e were calculated from other LDF expressions given in Standard and LRFD Specifications for a single traffic lane. These LDF values were not as large as the LDF values for two or more traffic lanes. Since only two traffic lanes would fit across the width of the Clive Road Bridge, all of the subsequent analyses were done for two traffic lanes using the LDF obtained from Eqs. 4.1 and 4.3 when the Standard and LRFD Specifications, respectively, were applied.

4.2. AASHTO Standard HS-20 Truck

The wheel load for the AASHTO Standard HS-20 truck, shown in Fig. 4.1, were used in the finite element analyses of the Clive Road Bridge to investigate the parameters that affect the load distribution. The front axle load of the truck is 8,000 lbs and the front rear and back rear axle loads are 32,000 lbs each. The spacing between the front axle and front rear axle is fixed at 14 ft, while

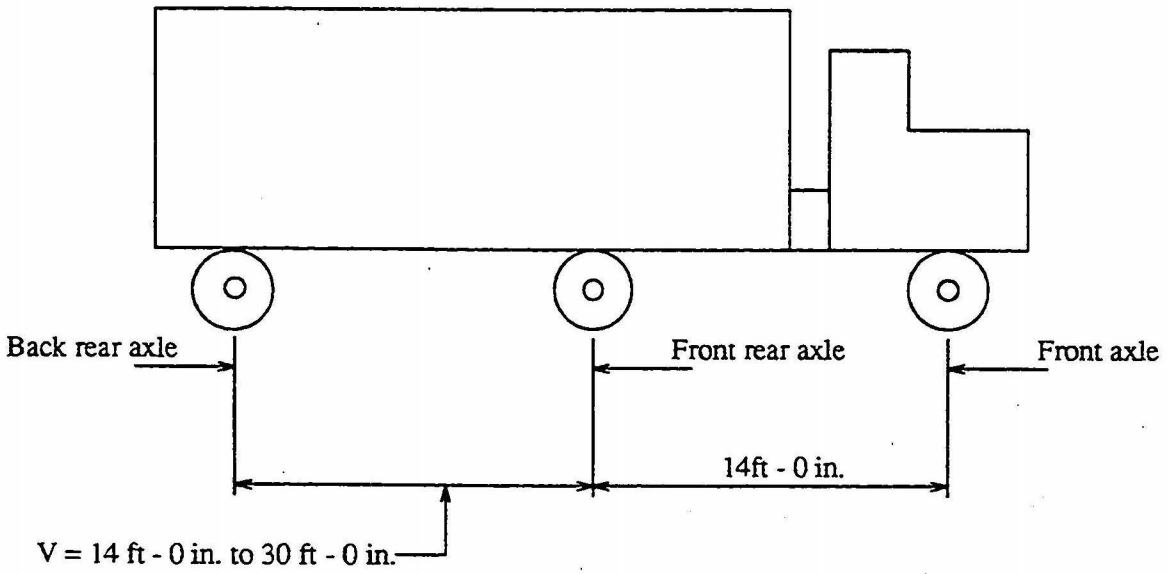

(a)

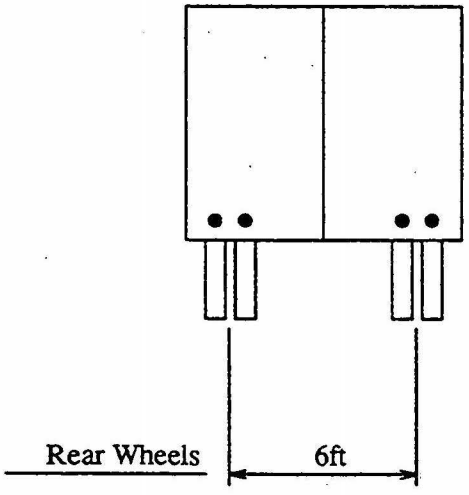

(b)

Figure 4.1. AASHTO Standard HS-20 Truck: (a) Side view, (b) Rear view

the spacing V, between the rear axles is variable and can be between 14 ft and 30 ft. The spacing V to be used is the dimension that produces the maximum value of the function under consideration (shear or moment). The gage width of the vehicle is 6 ft.

4.3. Load Positions for Interior and Exterior Girders

The truck load positions selected were in accordance with the Standard Specifications (17). Referring to Fig. 2.6, the truck load positions that would cause maximum positive bending moment in an exterior girder in span 1 would involve two HS-20 trucks, one truck at position 1 and another truck at position 4 across the width of the bridge. Similarly, the critical load position for the interior girder could either be same as that for the exterior girder or when two trucks are simultaneously placed at positions 2 and 5 across the width of the bridge. From analyses of the finite-element model of Clive Road bridge, the load position that was critical for an exterior girder was found to be critical for an interior girder.

4.4. Calculation of Load Distribution Factor

To mathematically establish the LDF for the interior and exterior girders in the Clive Road bridge, finite-element analyses of the bridge model presented in Section 3.2.3 were performed for two HS-20 trucks located simultaneously at positions 1 and 4 across the width of the bridge. The moments in the composite section were calculated using the ANSYS post-processor program as discussed in Section 3.2.2) at the element nodal sections along the length of the bridge. The load distribution factor, as defined by the Standard Specification (17), was calculated at the point of maximum positive moment by applying the concept discussed in next paragraph.

In Fig. 4.2, a single line of wheel loads P, acts directly on top of a single girder. Let the maximum bending moment caused by the load P be M_{max}. Now, consider a generalized bridge cross

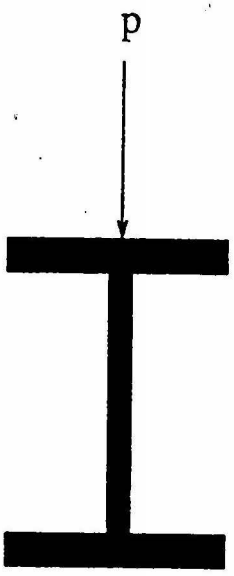

Figure 4.2. A single line of wheel loads acting directly on a girder.

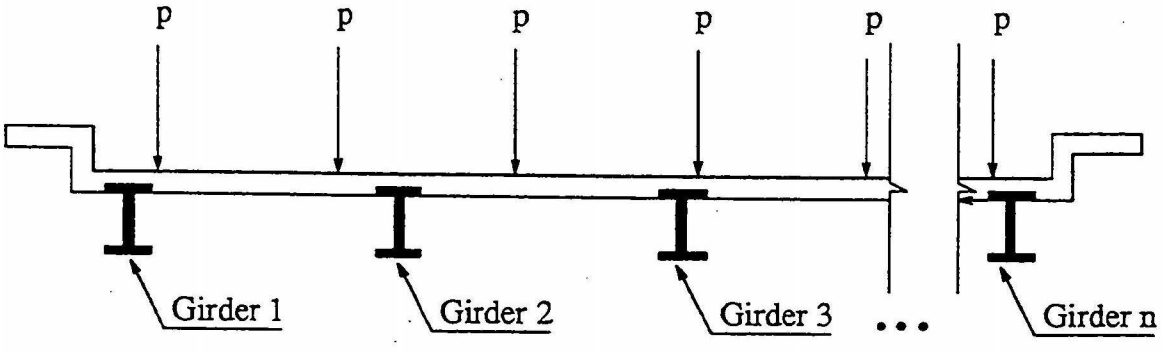

Figure 4.3. Many single lines of wheel loads on the bridge.

section shown in Fig. 4.3 that has a span length which is the same as that of the single girder in Fig. 4.2. This bridge has a number of evenly spaced girders and is loaded by a number of single lines of wheel loads, such that they cause a critical moment at either one of the interior or exterior girders. The bending moment resisted by each girder at the region of maximum moment in this bridge is M_1, M_2, ..., M_n such that

$$M_1 + M_2 + M_3 + \ldots + M_n = M_T \tag{4.7}$$

where, n = number of girders and M_T = maximum bending moment at a particular transverse cross section in the bridge. Since the longitudinal position of the wheel loads is same in both the single girder and multiple-girder system, the moments M_T and M_{max} are related to each other by

$$M_T = N_s M_{max} \tag{4.8}$$

where, N_s = number of single lines of wheel loads. For the general case, consider the jth girder to be critical. Girder j has to be designed for a moment M_j that is given by

$$M_j = (LDF_j) M_{max} \tag{4.9}$$

where, LDF_j = LDF for girder j. From Eqs. 4.8 and 4.9, LDF_j is expressed as

$$LDF_j = N_s \left(\frac{M_j}{M_T} \right) \tag{4.10}$$

For the Clive Road Bridge, four girders were present; therefore, N_s in Eq. 4.10 would equal 4. A similar development was also performed to establish the LDF, as defined by the LRFD Specifications (1). The results of that development gave

$$LDF_j = N_\ell \left(\frac{M_j}{M_T} \right)$$

where, N_ℓ = number of traffic lanes. For the Clive Road Bridge, two traffic lanes were present; therefore, N_ℓ in Eq. 4.11 would equal 2.

4.5. Parameters that affect Load Distribution

To establish the effect that changes in a particular design parameters has on the load distribution, structural analyses were performed for the finite-element model of the bridge. For the finite-element analyses, HS-20 truck loads were positioned simultaneously at positions 1 and 4 across the width of the bridge, as shown in Fig. 2.7, to cause maximum moment in girder 1, (an exterior girder) and at positions 2 and 5 to cause maximum moment in girder 2 (an interior girder). As previously mentioned, transverse load positions 1 and 4 on the Clive Road Bridge induced the maximum moments in girders 1 and 2. Both the Standard and LRFD Specifications state that an exterior girder shall not be designed for a capacity less than that of an interior girder. If an exterior girder is subjected to a larger bending moment than that for an interior girder, different LDFs are used for exterior and interior girders. However, if an interior girder is subjected to a larger bending moment than that for an exterior girder, the LDF for the interior girder is applied to both the interior and exterior girders. This latter condition occurred for most of the analyses associated with the parametric studies for load distribution with the Clive Road Bridge.

To properly determine the influence that a change in a design variable has on the distribution of the bending moments to the bridge girders, the percentage of the total transverse cross-sectional bending moment that each girder must resist, rather than the load distribution factor, was evaluated.

The percentage of total moment does not involve the minimum strength criteria for an exterior girder. For all the parameter studies, the positive bending moment was calculated at the 0.45 point in span 1 when HS-20 truck loads were simultaneously located at positions 1 and 4 across the width of the bridge. The following design parameters were investigated:

- Flexural stiffness of the intermediate diaphragms,
- Torsional stiffness of the girders,
- Flexural stiffness of the slab,
- Flexural stiffness of the girders as affected by the length and width of the bridge and spacing of the girders.

4.5.1. Flexural stiffness of the intermediate diaphragms

To establish the effect that the intermediate diaphragms have on the load distribution, analyses were performed with different flexural stiffness for the intermediate diaphragms, including the case without intermediate diaphragms. The flexural stiffness of the intermediate diaphragms was modified by changing the flexural rigidity, EI, of the diaphragms. Figure 4.4 shows the percentage of the total positive bending moment that is induced in each girder by the two HS-20 trucks for four diaphragm stiffness conditions. When the intermediate diaphragms were omitted from the finite-element model, the maximum positive bending moment in girder 3 (one of the interior girders) was only 3% greater than the maximum bending moment in that same girder, when the diaphragms for the actual bridge were modeled in the finite-element model. Even for a 150% increase in the intermediate diaphragm stiffness, the maximum bending moment in girder 3 was reduced only by 3% with respect to the value for the actual bridge. Moreover, a 150% increase in the stiffness of the intermediate diaphragms requires that their size would become comparable to that of the girders. Since the maximum interior girder moments changed by only about $\pm$ 3% for the full range in

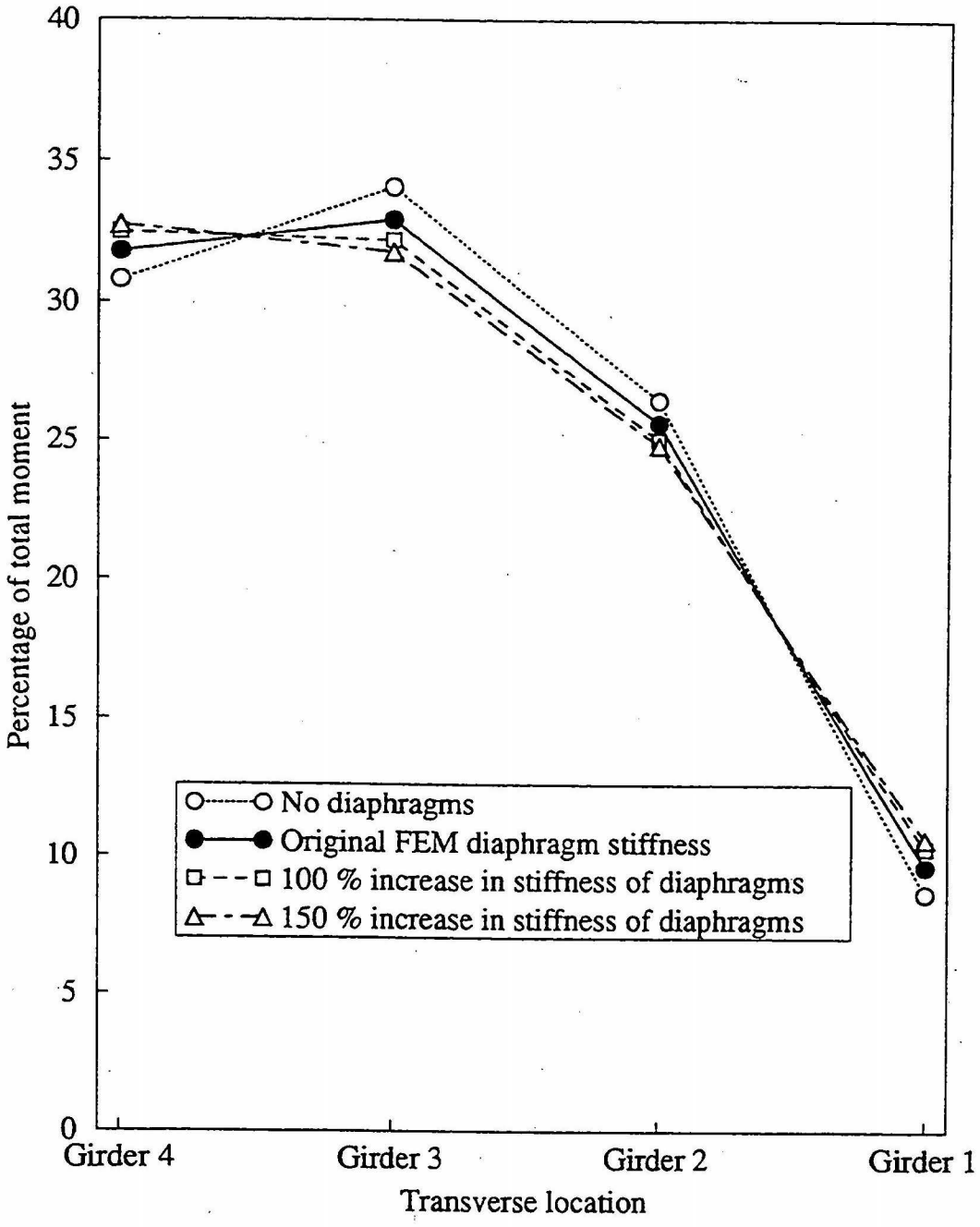

Figure 4.4. Intermediate diaphragm flexural stiffness effects on load distribution

diaphragm stiffness with respect to that for the actual diaphragms, the intermediate diaphragms only have a minor effect on load distribution. The same conclusion was reached by Hisham (7) and Walker (21).

4.5.2. Torsional stiffness of the girders

The torsional stiffness of an I-shaped girder is a function of the torsional rigidity, GJ, and the warping rigidity, EC_w. The shear modulus of elasticity, G, and flexural modulus of elasticity, E, were held constant throughout the parameter studies. The torsional constant J and warpage constant C_w were effectively changed by changing the flange thickness for the modeled girders. Two torsional stiffnesses were considered for the finite-element analyses. The original bridge girders were initially modeled using element thicknesses for the flanges that matched those in the actual bridge. An increased torsional stiffness for the girders was accomplished by doubling the flange thicknesses for the elements that modeled the girder flanges. A review of the finite-element analyses revealed that the torsional stiffness of the girders did not have a significant effect on the load distribution factor.

4.5.3. Flexural stiffness of the slab

The flexural stiffness of a bridge deck is a function of the gross moment of inertia I_c of the slab, modulus of elasticity E_c of the concrete, and girder spacings. For the parameter study of slab stiffness, the girder spacing was held constant and equal to the girder spacing for the actual bridge. Since E_c can be assumed to be proportional to the square root of the 28-day compressive concrete strength, f'_c and I_c is proportional to the cube of the slab thickness, changes in the slab stiffness were accomplished through changes in the slab thickness and concrete compressive strength.

Figure 4.5 shows the percentage of the total positive bending moment that is induced in each girder by the two HS-20 trucks when five different thicknesses are considered for the bridge deck.

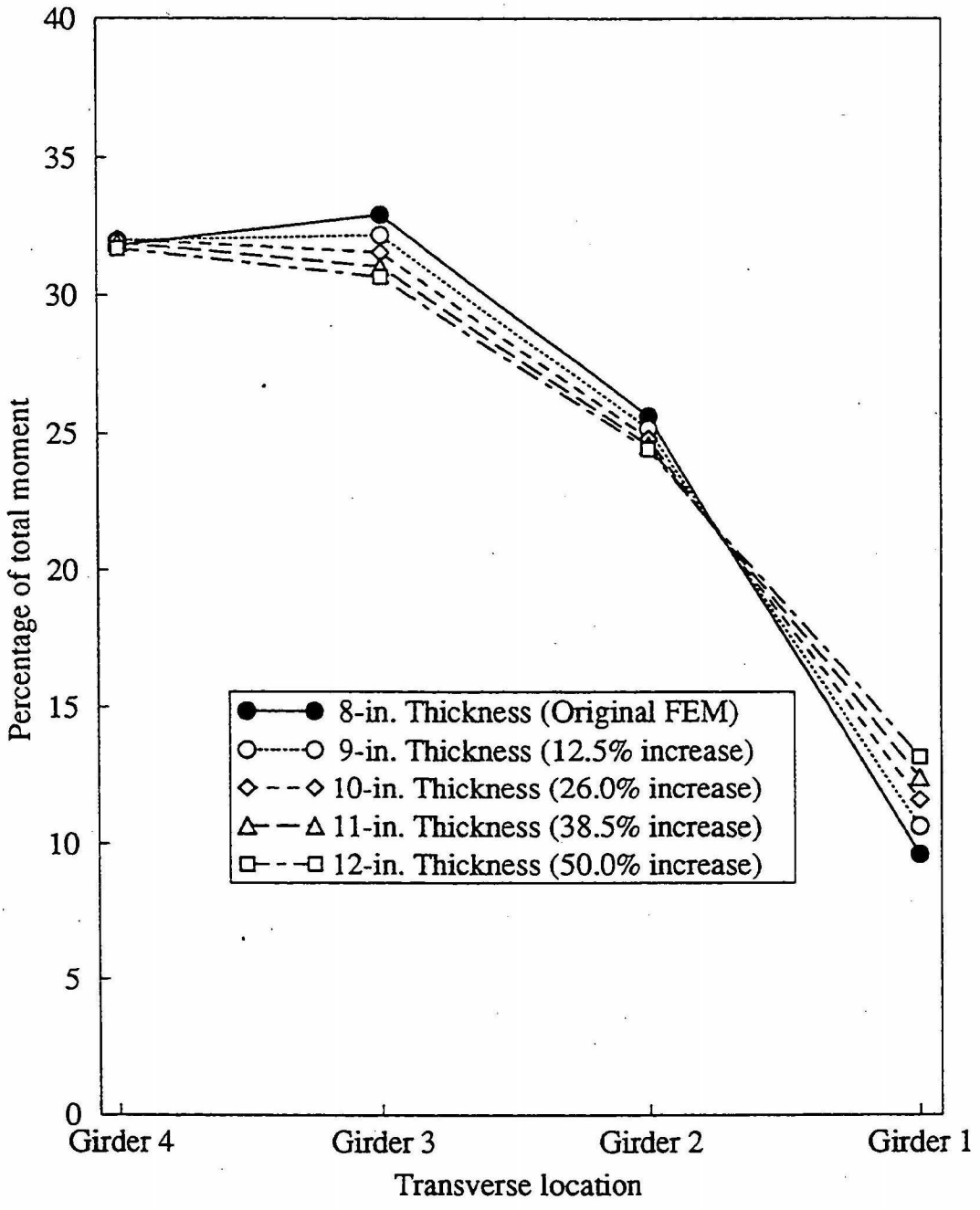

Figure 4.5. Slab thickness effects on load distribution

As expected, there was a decrease in required bending moment strength for the critical girder (girder 2) when the thickness of the slab was increased. A 12-in. thick slab, which represents a 238% increase in the slab stiffness when compared to that for the original 8-in. thick slab thickness, produced only a 7% decrease in the required moment strength for girder 2. Since such a large increase in the slab stiffness produced a very small decrease in the required girder strength, thickness of the slab was not considered to have a significant effect on load distribution. An 8-in. minimum bridge deck thickness, which is required by the Iowa DOT, has substantial flexural stiffness. Further increases in the slab thickness beyond the 8-in. thickness do not produce a significant change in the required moment strength for the critical girder.

The flexural stiffness of the slab was also modified by changing the modulus of elasticity of the concrete. Calculated E_c values were obtained by applying Eq. (3.1) for selected concrete compressive strengths. Recall that the strength f'_c was estimated to be equal to 5000 psi when the 1993 field tests were conducted. When the strength f'_c was increased by 40% to 7000 psi, the required maximum bending moment in critical interior bridge girder decreased by only about 2%, and when the concrete strength was reduced by 40% to 3000 psi, the required maximum bending moment in that same girder increased by only about 3%. Therefore, considering the practical range in concrete compressive strength that were considered, significant changes in the required girder bending moments did not occur. This result indicates that the flexural stiffness of a nominal 8-in. thick reinforced concrete deck with $f'_c \geq 3000$ psi is sufficient to produce adequate load distribution for designing the bridge girders.

4.5.4. Flexural stiffness of the girders

The flexural stiffness of the girders affects the load distribution (15). Since the Clive Road Bridge girders were designed for a particular stress level, the stiffness of an individual girder was

not arbitrarily changed to evaluate the load distribution characteristics of the bridge. However, the flexural stiffness of the girders was addressed during the parameter studies that involved the width and length of the bridge. For these studies, which are discussed in the following sections of this report, the size of the girders was changed to maintain the particular flexural stress level in the girders that was predicted by the finite-element model of the original bridge.

4.5.4.1. Length of the bridge. The length of the bridge affects the distribution of the wheel loads to the bridge girders. Bridge lengths of 220, 242 and 264 ft were investigated using finite element models. The two longest lengths represent a 10% and 20% increase in the length of the original Clive Road Bridge. To maintain the same geometric proportions for the modeled bridges, each of the four span lengths were increased by the same percentage. Since the girders in the original bridge were designed for a particular longitudinal stress level, the girder stress predicted for each of the model bridges should be the same for similar loading conditions so that a proper comparison of the load distribution can be made. Therefore, when the length of the model bridge was increased, the girder size was increased in the finite element model by increasing the area of the girder flanges to essentially maintain the same maximum flexural bending stress. The size of the girder flanges were determined by an iterative process. The effects of changes in the bridge length on the percentage of the total maximum positive transverse bending moment in span 1 that is resisted by each of the four bridge girders are shown in Fig. 4.6. There was a very slight difference in the induced moment in the critical girder (girder 2) when the length of the bridge was increased by 10%, but there was essentially no change in the induced girder moment when the bridge length was increased from 10% to 20%. The reason for the minimal change in the girder moments is that the longitudinal flexural stiffness of the girders was almost identical for each of the finite element models. Figure 4.6 also shows the distribution of the induced girder moments that occur due to a

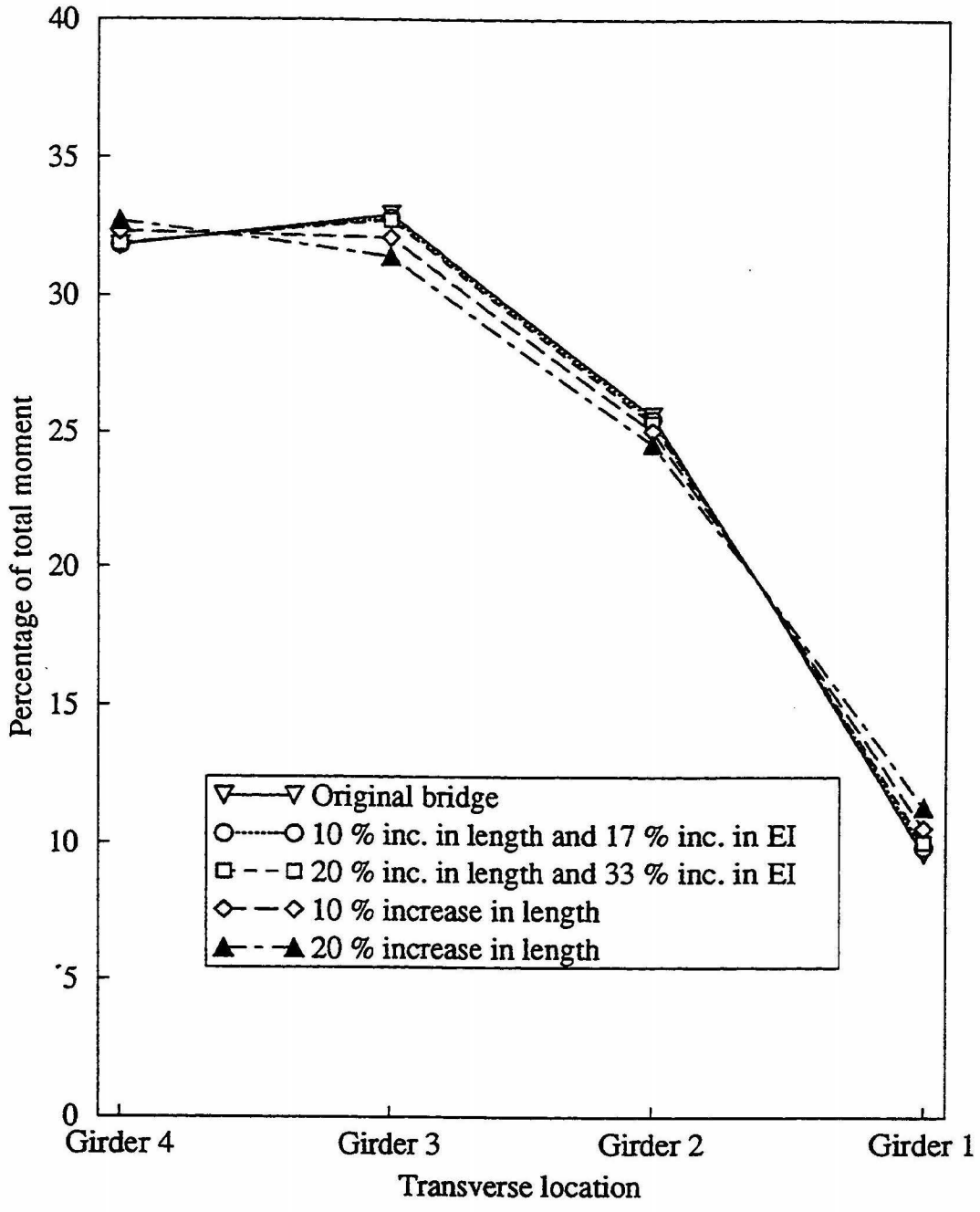

Figure 4.6. Bridge length effects on load distribution

10% and 20% increase in the bridge length without an increase in the girder sizes. Since the girder sizes were not modified in these analyses, the longitudinal stiffness of the girders decreased which caused a better load distribution amongst the girders.

4.5.4.2. Width of the bridge and spacing of the girders. The width of the bridge and the spacing of girders were studied simultaneously. When the roadway width of a modeled bridge was changed, the spacing of the girders was also changed to maintain the same number of girders and the same distance between the edge of the curbs and the centerline of the exterior girders. The same edge distance was necessary to properly compare the girder moments predicted by the finite element models. As discussed in the previous section, the final sizes of the girders were obtained by an iterative process to essentially maintain the same maximum girder bending stress as that for the original bridge model. As the tributary width of each girder changed, the girder size was changed by either increasing or decreasing the area of the flanges to accommodate larger or smaller loads, respectively. To establish the effect of width of the bridge and spacing of the girders on load distribution, three bridge widths, and related girder spacings were analyzed. In the first model, the roadway width of the bridge was reduced from the original 30 ft to 27 ft and correspondingly, the girder spacing was reduced from the original 9 ft-6 in. to 8 ft-6 in. on center. The second model was finite element model of the original Clive Road Bridge. The third model had a roadway width of 33 ft and girder spacings of 10 ft-6 in. The percentages of the total maximum positive moment in Span 1 that is induced in each girder for the three bridge roadway widths and corresponding girder spacings are shown in Fig. 4.7. When the width of the bridge and the spacing of girders in the original bridge were reduced, the distribution of the total bending moment amongst the four girders improved. This improved behavior occurred because the reduced spacing of the girders caused the wheels of a truck to be closer to the girders adjacent to the critical girder (girder 2). Figure 4.7 also

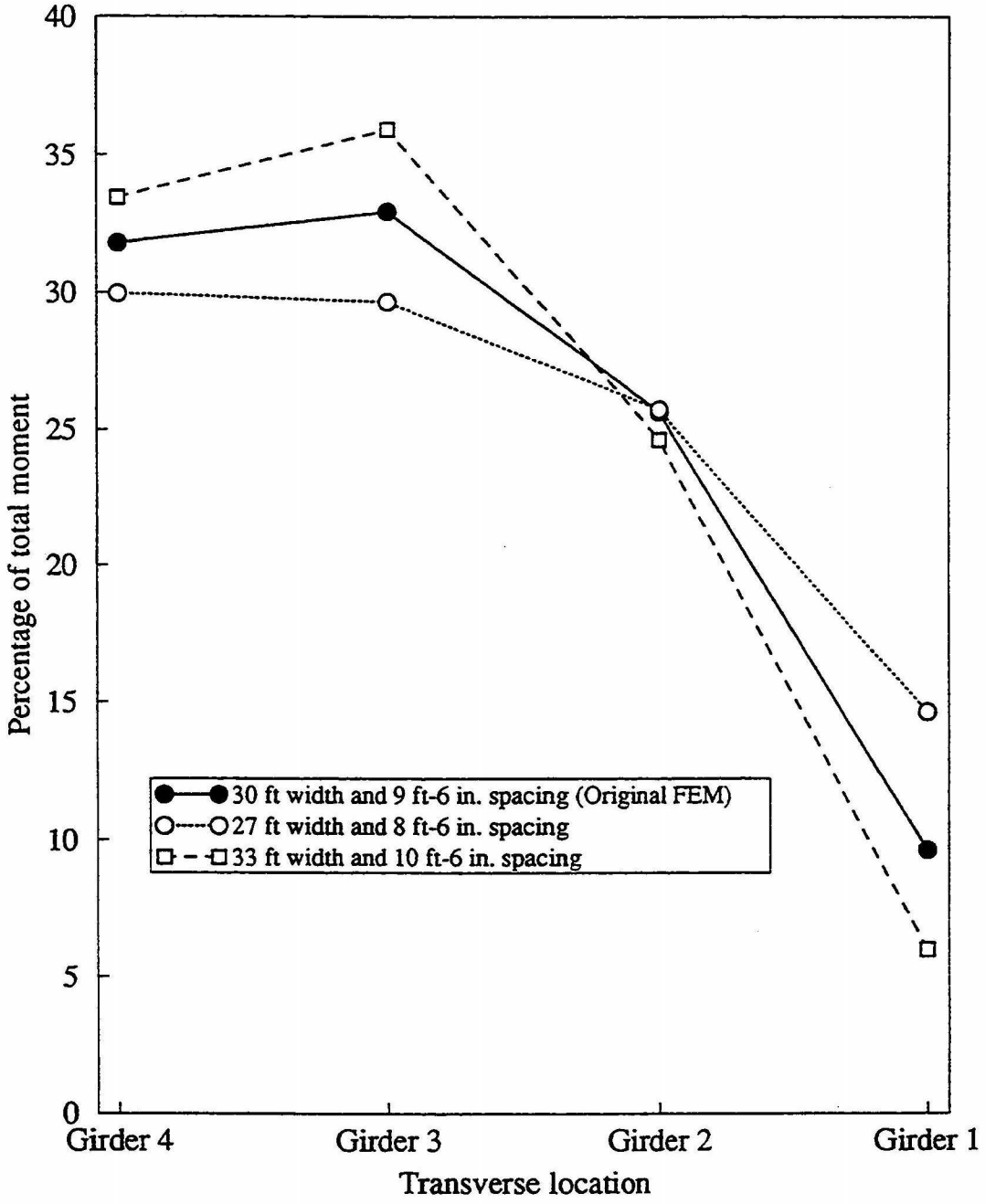

Fig. 4.7. Bridge width and girder spacing effects on load distribution

shows that the distribution of the total bending moment was reduced when the bridge width and girder spacing were increased.

4.6. Comparison of LDF with the Standard and LRFD Specifications

The Standard Specifications (17) load distribution expression has the girder spacing as the only design parameter in the equation for a given bridge type. The LRFD Specification (1) load distribution equation accounts for the length of the bridge, moment of inertia of the girder, spacing of the girders, and modulus of elasticity of the beam material and the concrete slab. However, as previously mentioned, there are other design parameters which neither specification directly considers, that affect load distribution. A comparison of the LDF-values for an interior girder that were predicted by the finite-element models and obtained by applying the LDF criteria given by Eqs. 4.1 and 4.3 for the Standard and LRFD Specifications, respectively, are presented in the following sections.

4.6.1. Flexural stiffness of the intermediate diaphragms

The load distribution expressions in the Standard Specifications (17) and LRFD Specifications (1) do not directly account for the stiffness of the intermediate diaphragms. The finite element and Specification results for the LDF for an interior girder in span 1 are shown in Fig. 4.8. The abscissa scale in the figure is the percent increase in diaphragm flexural stiffness with respect to the stiffness of the diaphragms in the finite-element model of the original bridge. For the load distribution factor given by Eq. (4.3), the modular ratio was set equal to 3. The result obtained from Eq. (4.3) was multiplied by 2 to account for two wheel lines per lane. As seen from the finite element results, the diaphragms do not significantly affect the load distribution. Both Specifications give a conservative value for load distribution factor, but the LRFD Specification expression predicts

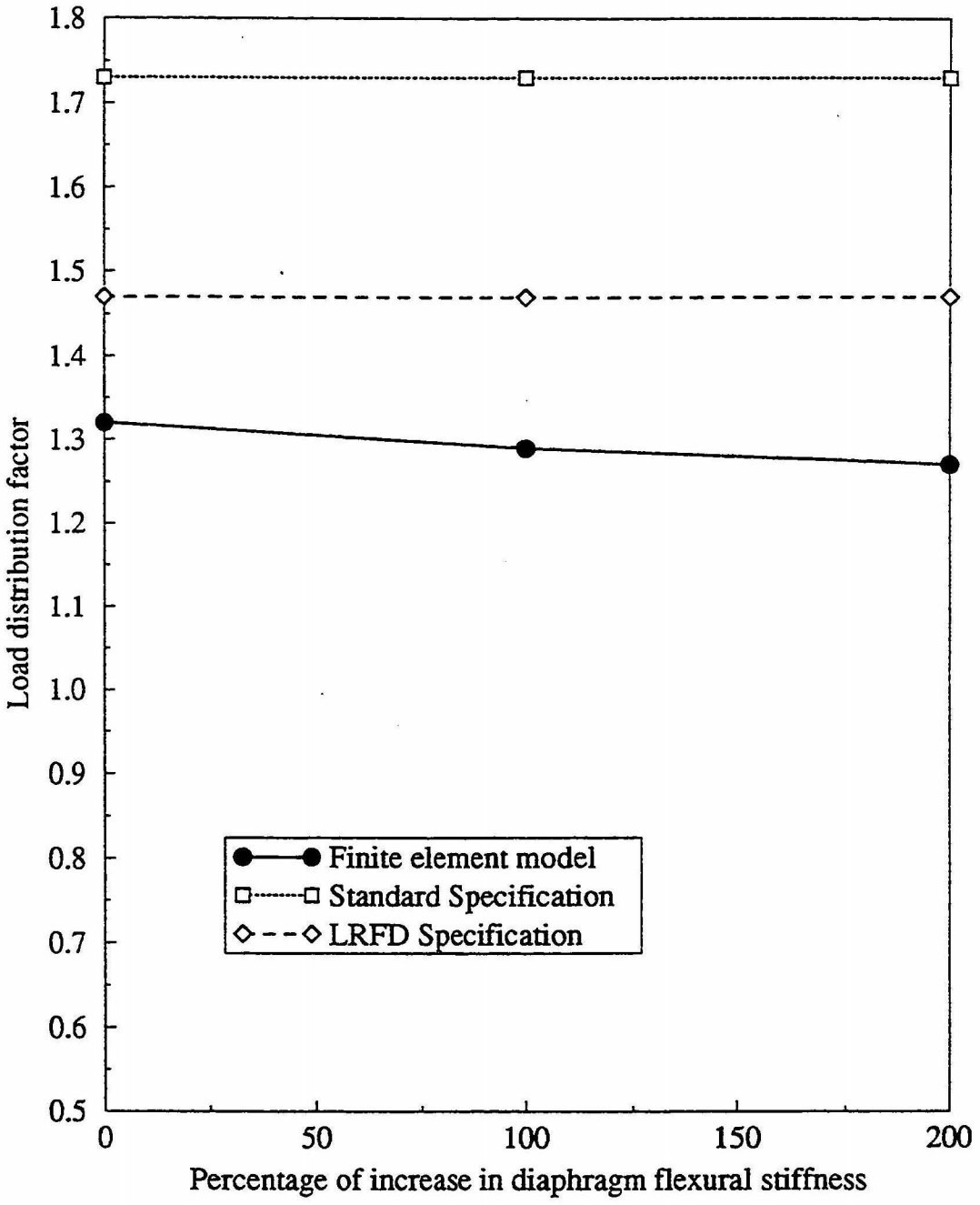

Fig. 4.8. Load distribution factor for an interior girder in span 1 versus flexural stiffness of the intermediate diaphragms

a load distribution factor closer to that predicted by the finite-element model.

4.6.2. Torsional stiffness of the girders

The LDF expressions given by Eqs. 4.1 and 4.3 do not directly include the torsional stiffness of the girders as a design parameter in determining the load distribution. The results (not shown) from the finite element analyses indicate that the torsional stiffness of the girders does not significantly affect the load distribution factor.

4.6.3. Flexural stiffness of the slab

4.6.3.1. Thickness of the slab. Figure 4.9 shows the load distribution factors for an interior girder in span 1 for bridges with different slab thicknesses. The pattern of variation of the LDF obtained from the LRFD Specifications (1) closely matches the pattern predicted by the finite element mode; however, application of the LRFD Specification expression produced conservative results. The Standard Specification expression for LDF does not directly account for the slab thickness; therefore, the LDF become increasingly conservative as the thickness of the slab is increased. For the entire range of slab thicknesses, the Standard Specifications produce more conservative results than those obtained from the LRFD Specifications.

4.6.3.2. Concrete compressive strength of the slab. The load distribution factors for an interior girder for different concrete compressive strengths of the slab are shown in Fig. 4.10. The pattern of variation of LDF obtained by applying the LRFD Specification closely matched that predicted by the finite-element model. The Standard Specification expression for LDF does not directly account for the concrete compressive strength; therefore, the graphs for the LDF obtained from this specification shows no change in LDF for different concrete strengths. Application of the LRFD and Standard Specifications for LDF produced conservative results; however, the results predicted by the Standard Specifications are more conservative than those predicted by the LRFD Specifications.

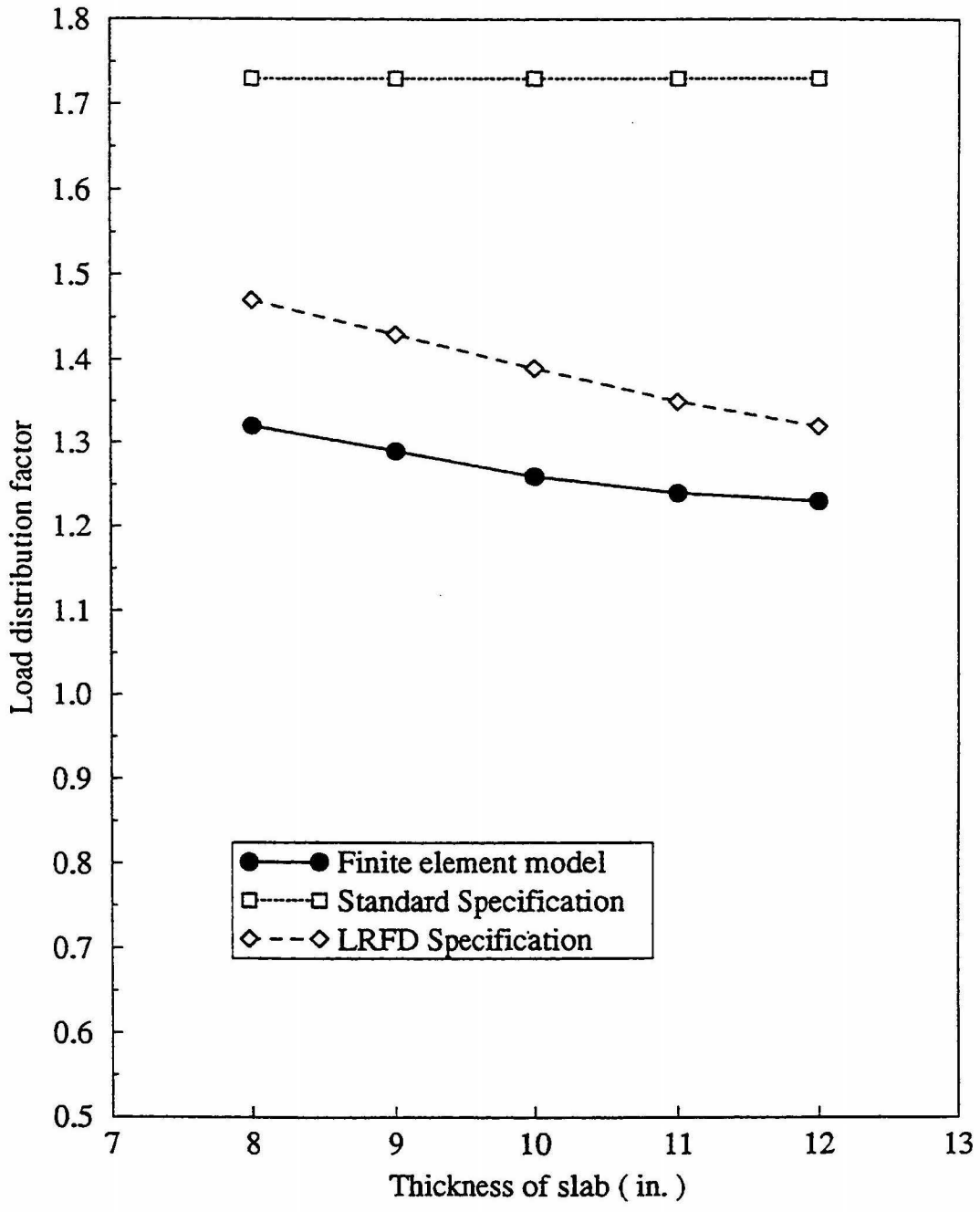

Figure 4.9. Load distribution factor for an interior girder in span 1 versus slab thickness

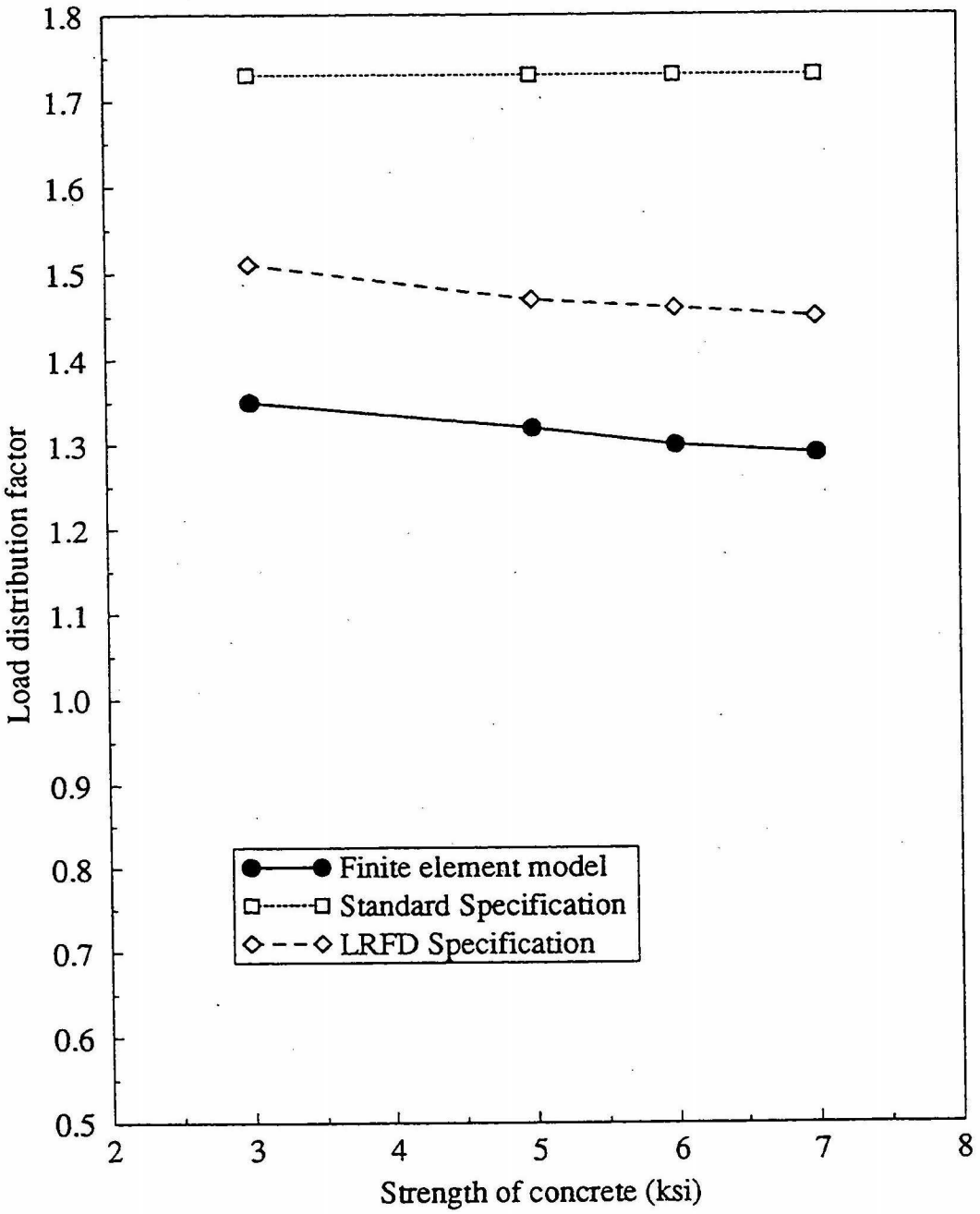

Fig. 4.10. Load distribution factor for an interior girder in span 1 versus concrete compressive strength

4.6.4. Length of the bridge

Figure 4.11 shows the load distribution factors for an interior girder of different length bridges. The Standard Specification gives the same values for LDF regardless of the length of the bridge, since this specification does not directly account for the bridge length. The LRFD Specification equations for LDF has the span length of the bridge as one of the parameters affecting the load distribution. The LDF values predicted by the LRFD Specifications are closer to those predicted by the finite-element model than are those predicted by the Standard Specifications.

4.6.5. Width of the bridge and girder spacing

As mentioned earlier, changes in the width of the bridge and the girder spacing had to be considered simultaneously. Figure 4.12 shows the load distribution factors for an interior girder in span 1 for bridges with different girder spacings and corresponding changes in the width of the bridge. The pattern of variation in the LDF values is the same in the Standard and LRFD Specifications and the finite element results, but the magnitudes differ. The width of the bridge is not a parameter considered in either the Standard and LRFD Specification expressions. Both the LRFD and Standard Specifications equation for LDF produce conservative results; however, the Standard Specifications approach to evaluate LDF is more conservative than that for the LRFD Specifications.

4.7. Comparison with Specifications

A comparison was made of the LDF results that were obtained from the 1959 and 1993 field tests and from the load distribution criteria in the Standard and LRFD Specifications (17,1). The LDF values are shown in Table 4.1.

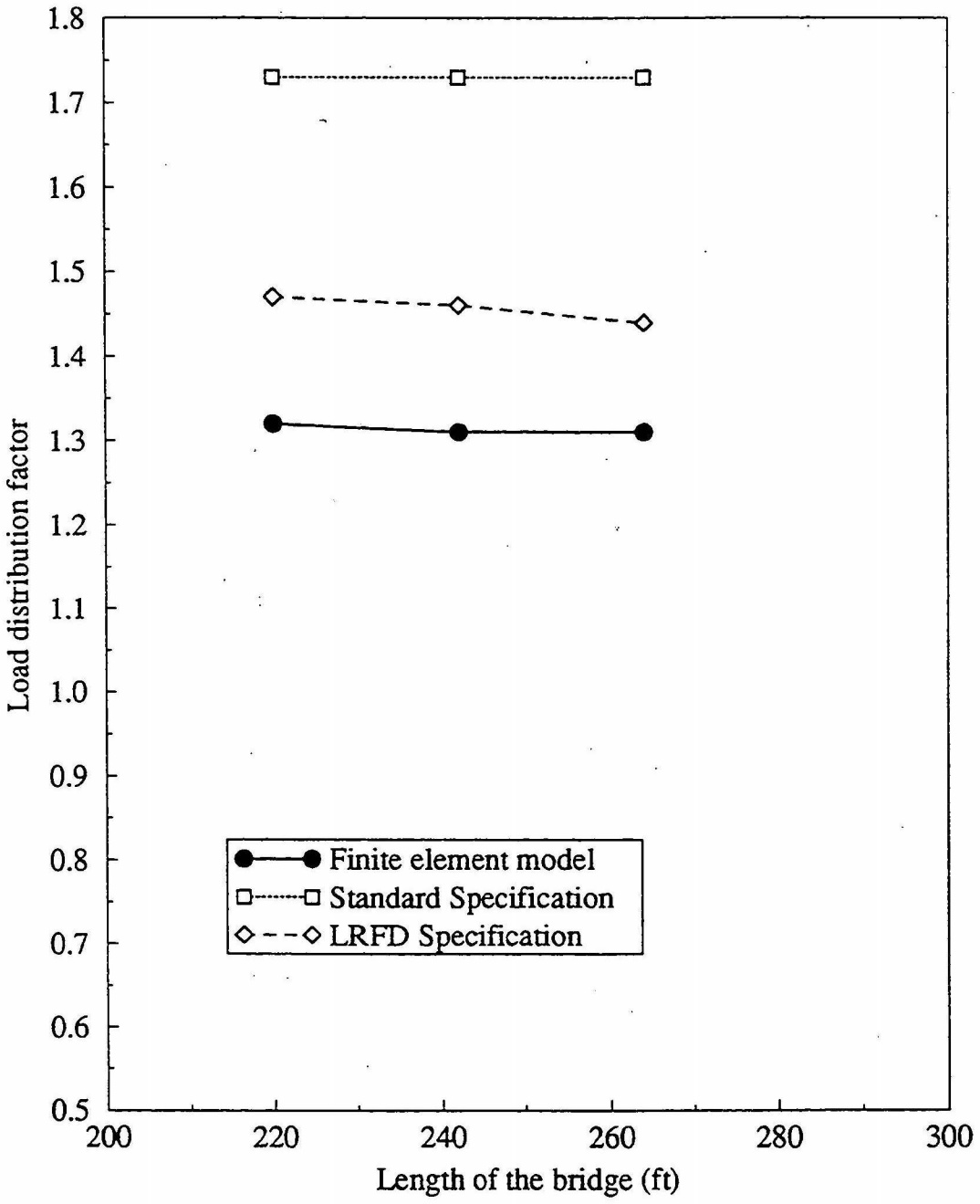

Figure 4.11. Load distribution factor for an interior girder in span 1 versus bridge length

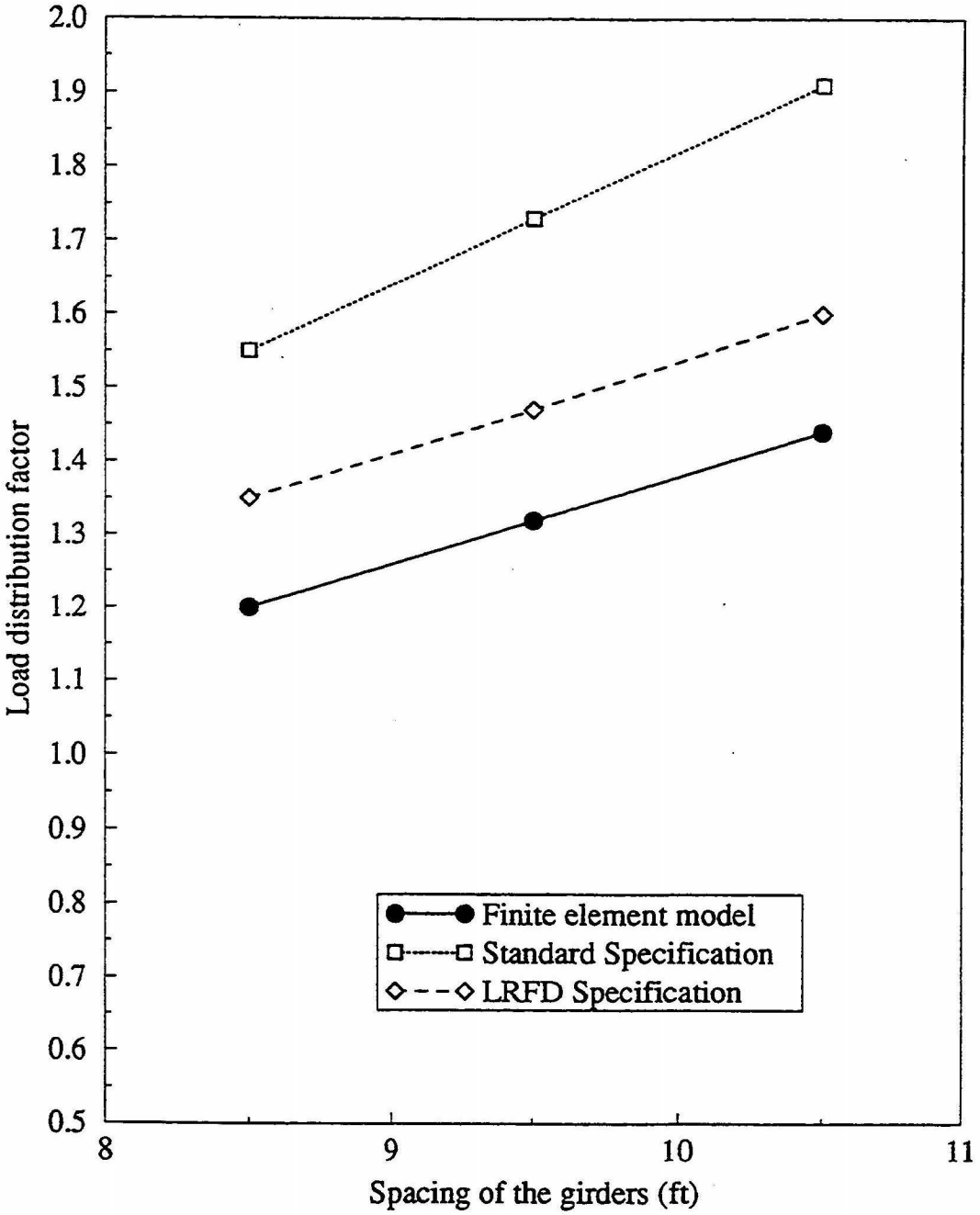

Fig. 4.12. Load distribution factor for an interior girder in span 1 versus bridge width and girder spacing

Table 4.1. Load distribution factors from the 1959 and 1993 field tests and from the AASHTO Specifications

Girder	1959 Tests	1993 Tests	AASHTO 1993 (17)	AASHTO LRFD (1)[a]
Interior	1.41	1.38	1.73	1.47
Exterior[b]	1.15	1.24[c]	1.49	1.29[c]

(a) Modular Ratio = 3
(b) Neglecting requirement that exterior girders have capacity at least that of interior girders.
(c) Based on lane positions that place truck in lane 3 ft closer to exterior girder.

The criteria in both specifications that requires an exterior girder to have at least the same moment strength as an interior girder has not been applied, since this criteria is based on potential future widening of a bridge that would cause an existing exterior girder in the original bridge to become an interior girder in the altered bridge.

The analytical results for the load distribution factors listed in Table 4.1 show that LDF values predicted by the Standard Specifications (17) are rather conservative when compared to the 1959 and 1993 test results and when compared with the predictions on LDF obtained by applying the LRFD Specifications (1). The LRFD Specification LDF expression (Eq. (4.3)) predicts more precise LDF values because of the inclusion of the modular ratio and other design parameters. The predicted LDF values obtained from the LRFD Specifications provides an excellent correlation with the field test results, especially for those from the 1993 tests.

The difference between the LDF results for the 1959 and 1993 tests is assumed to be due primarily to the difference in lane placements in the bridge deck for the two tests. The lane placement in the 1993 tests was based on the criteria given in the LRFD Specifications (1).

CHAPTER 5. SUMMARY AND CONCLUSIONS

5.1. Summary

Design specifications for aluminum girder highway bridges have been available for a number of years. In many instances, specific design criteria have been taken directly from or modified from those of steel girder bridges. The load distribution criteria for aluminum girder bridges is based on tests of steel-girder concrete-deck bridges. Specific studies are needed to establish if the load distribution expressions for steel girder bridges are applicable to aluminum girder bridges. Several years ago, representatives from the Iowa Department of Transportation (Iowa DOT) and Polk County Engineering Office determined that the Clive Road (NW 86th street) overpass above Interstate 80 would be redesigned as a full interchange. The removal of the bridge provided a unique opportunity to investigate the static load behavior of an aluminum girder bridge and to obtain aluminum girders for laboratory fatigue tests.

The research program involved field inspection and static load tests; finite-element bridge analyses; and laboratory, constant-amplitude, fatigue tests. This part of the Final Report addresses the field studies and finite-element investigations of the aluminum girder bridge. Part 2 of the Final Report addresses the laboratory fatigue tests. The inspection of the bridge superstructure, was performed by a team consisting of Iowa State University (ISU) staff, Lehigh University staff, and personnel from the Iowa DOT. Field testing of the bridge was conducted in September of 1993 by researchers at ISU. Instrumentation consisted of electrical resistance strain gages that were attached to the girder flanges at the 0.45 point in span 1 and near piers 1 and 2, direct current displacement transducers that were placed on the girders in the north end-span, and dial gages that were positioned at the girders supports at the north abutment. The monitored strains and displacements provided data on the general static load behavior of the bridge.

Analytical studies of the bridge were performed using finite-element techniques. Three-dimensional beam elements were used to model the aluminum shear connectors, diaphragms, and the top and bottom flanges of the girders. Plate elements were used to model the reinforced concrete deck and curb and webs of aluminum girders. Separate finite-element models of the shear connectors were developed to calculate the shear stiffness of the shear connectors that was used in the complete bridge model. After the finite-element model was determined to provide accurate analytical predictions of the bridge response to static loads, the model was used for parametric studies of load distribution.

To evaluate the long-term performance of the bridge, a comparative study of the 1959 and 1993 field test results was conducted. The comparison of the bridge behavior to applied static truck wheel loads was based on the percentage of the total longitudinal bending moment resisted by each girder at a particular cross section of the bridge. Small differences in these girder moment percentages occurred for the two field tests. To provide an explanation for the differences, finite element analyses of the bridge were conducted. Since the trucks used in the two field tests were not identical and their location on the bridge deck were not the same and since the concrete age was greater for the 1993 field test, effects of changes in the truck load, gage width of truck, lateral and longitudinal truck load positions, and concrete compressive strength on the load distribution were investigated. These studies provided possible reasons for the difference between the two field test results.

Theoretical investigations of wheel load distribution were performed using a finite-element model of the bridge. Standard HS-20 truck wheel loads were positioned in the design traffic lanes that are specified by American Association of State Highway and Transportation Officials (AASHTO) Standard Specifications for Highway Bridges (17) (Standard Specifications). The

parameters investigated were the flexural stiffness of the intermediate diaphragms, torsional stiffness of the girders, flexural stiffness of the slab, flexural stiffness of the girders, and spacing of the girders. Load distribution factors were calculated from the percentage of the total longitudinal bending moment that is resisted by each girder at a particular cross section of the bridge. The load distribution factors predicted by the finite-element model were compared with those obtained by applying the appropriate expressions in the Standard Specifications and in the AASHTO Load Resistance and Factor Design (LRFD) Bridge Design Specifications (1) (LRFD Specifications).

5.2. Conclusions

The following conclusions were based on the results obtained from the 1959 and 1993 field tests and from the finite-element analyses of the bridge.

1. The analytical predictions of the girder bending strains and deflections were in close agreement with the measured values obtained from the 1993 tests.
2. The finite-element analyses of the bridge of the different load cases for the 1959 and 1993 field tests revealed that there was no significant difference in the wheel load distribution for the two field tests. The theoretical predictions of the load distribution were quite accurate when compared to the load distribution associated with the 1959 and 1993 field tests. Since the concrete was assumed to be uncracked in the finite-element model of the bridge and since the mathematical model accurately predicted the bridge response to the truck loads, the conclusion was reached that the bridge deck had not significantly cracked during its thirty-five years of service.
3. The intermediate diaphragms and the torsional stiffness of the I-shaped aluminum girders in the Clive Road Bridge did not significantly affect load distribution.

4. Since an 8-in. thick reinforced concrete bridge deck has substantial flexural stiffness, a moderate increase in the slab thickness or concrete compressive strength will not produce a significant change in the load distribution.
5. An increase in the bridge length, accompanied by an increase in the sizes of the girders to maintain essentially the same maximum girder bending stress level as that in the original bridge, caused a minimal change in the load distribution. This result occurred because the longitudinal flexural stiffness of the girders for the longer bridge spans remained almost the same as that for the original bridge.
6. An increase in the width of the bridge, accompanied by an increase in the girder spacing to maintain essentially the same position of an exterior girder with respect to the roadway curb, caused a decrease in the distribution of the wheel load among the girder. Therefore, the distribution factor for the critical girder increased.
7. The applicable load distribution factor expression in the Standard Specifications predicted larger distribution factors than those obtained by applying the governing LRFD Specification expression. The evaluation of the appropriate wheel load distribution criteria from both specifications produced conservative results in comparison with the predicted distribution factors obtained from the finite element model. The load distribution expression in the LRFD Specification was more accurate than that in the Standard Specification.
8. The load distribution equations in the Standard and LRFD Specifications were assumed to be valid for a composite, I-shaped, welded-aluminum girder bridge. The load distribution studies conducted during this research have shown that the LRFD

Specification criteria for load distribution is applicable for a composite, I-shaped, welded-aluminum girder bridge.

5.3. Recommendation

The descriptions for the kind of floor and type of beams associated with load distribution in the Standard Specifications (17) and LRFD Specifications (1), respectively, should be revised for bridges that have a concrete deck on steel beams to include aluminum, I-shaped girders. The research on load distribution presented in this report has shown that the Standard Specifications (17) will provide conservative design values for the wheel load distribution factors and that the LRFD Specifications (1) that incorporates the modular ratio, which relates the girder and deck materials, will provide reasonable and slightly conservative design values for the wheel load distribution factors in bridges construction with I-shaped, welded-aluminum girders and a concrete deck.

REFERENCES

1. "AASHTO LRFD Bridge Design Specifications," First edition, *American Association of State Highway and Transportation* Officials, Washington, D.C., 1994.
2. Abendroth, R. E., Sanders, W. W., and Mahadevan, V., "Field Testing of a Continuous Aluminum Girder Highway Bridge," *Proceedings of Structural Faults and Repairs Conference, Vol. 1*, London, England, pp. 257-266, July 1995.
3. Alison, Gordan A., "Evaluation of Seven Aluminum Highway Bridges After Two to Three Decades of Service," *Transportation Research Record*, No. 950, 1984, pp. 123-129.
4. Ashton, N. L., "First Welded Aluminum Girder Bridge Spans Interstate Highway in Iowa," *Civil Engineering*, October 1958, pp. 78-80.
5. Ashton, N. L., "Iowa Tries a Welded Aluminum Bridge," *Engineering News Record*, February 20, 1958, pp. 30-32.
6. Bishara, Alfred G. Liu, Chuan, Maria, and El-Ali, Nasser D., "Wheel Load Distribution on Simply Supported Skew I-beam Composite Bridges," *Journal of Structural Engineering*, ASCE, 119, February, 1993, pp. 399-419.
7. El-Arabaty, Hisham Ahmed, *Strengthening of Continuous-Span Composite Bridges Using Post-tensioning and Superimposed Trusses*, Ph.D. Dissertation, Iowa State University, Ames, Iowa, 1993.
8. "Guide Specifications for Aluminum Highway Bridges," American Association of State Highway and Transportation Officials, Washington, D.C., 1992.
9. Kosteas, D. and Sanders, W., "Redesigning an Aluminum-Concrete Composite Bridge," *Proceedings of the Sixth International Conference on Aluminum Weldments*, Cleveland, Ohio, pp. 125-130, April 1995.

10. Linger, D. A. and Hulsbos, C. L., "Dynamics of Highway Bridges," *Iowa Engineering Experiment Station, Joint Publication: Bulletin No., 188 and Iowa Highway Research Board, Bulletin No. 17*, Ames, Iowa, December 1960.

11. Mahadevan, Vaidyanathan, "Analysis of the Behavior of a Continuous Span Concrete Deck Aluminum Bridge," M.S. Thesis, Iowa State University, Ames, Iowa, 1995.

12. "Moments, Shears and Reactions, for Continuous Highway Bridges,", *American Institute of Steel Construction*, Chicago, Illinois, 1966.

13. Prentzas, E. G., "Experimental Structural Behavior of Iowa's Aluminum Bridge," *The Central Constructor*, October 1958, pp. 15.

14. Sanders, W. W. and Abendroth, R. E., "Construction and Evaluation of a Continuous Aluminum Girder Highway Bridge," *Proceedings of Sixth International Conference on Aluminum Weldments*, Cleveland, Ohio, pp. 115-124, April 1995.

15. Sanders, W. W., Jr. and Elleby, H. A., "Distribution of Wheel Loads on Highway Bridges," NCHRP Report 83, Engineering Research, Iowa State University, Ames, Iowa, 1970.

16. Sanders, W. W., Jr., "Distribution of Wheel Loads on Highway Bridges," *NCHRP Synthesis of Highway Practice 111*, Transportation Research Board, Washington, D.C., 1984.

17. "Standard Specifications for Highway Bridges," Fifteenth edition, *American Association of State Highway and Transportation* Officials, Washington, D.C., 1992.

18. "Structural Welding Code - Aluminum", (D1.2-90), American Welding Society, Miami, Florida, 1990.

19. Tarhini, Kassim M. and Frederick, Gerald R., "Wheel Load Distribution in I-girder Highway Bridges," *Journal of Structural Engineering*, ASCE, No. 118, May, 1992, pp. 1285-1294.

20. Trinidad, A. A. Jr., "Aluminum Highway Bridges in the USA," *Bridge Management 2*, New York, Bettigole Andrews & Clark Inc.

21. Walker, William H., "Lateral Load Distribution in Multi-girder Bridges," *Engineering Journal*, No. 24, 1987, pp. 21-28.

22. Zokaie, T., Osterkamp, T. A., and Imbsen, R. A., "Distribution of Wheel Loads on Highway Bridges," NCHRP 12-2611, Washington, D.C., Transportation Research Board.

ACKNOWLEDGMENTS

The research discussed in this report was conducted by the Bridge Engineering Center under the auspices of the Engineering Research Institute of Iowa State University. This investigation was funded through the Center for Transportation Research and Education (then the Iowa Transportation Center) at Iowa State University by the Iowa Department of Transportation in cooperation with the Federal Highway Administration. The authors would like to thank William A. Lundquist, Bridge Engineer, and John P. Harkin, Chief Structural Engineer, with the Iowa Department of Transportation for their support of the research effort. The assistance and cooperation given by Mark Wandro, Assistant County Engineer with the Polk County Engineering Office; representatives from the Lehigh University Center for Large Structural Systems (ATLSS); and personnel from the Iowa State Department of Transportation Maintenance Office and Jensen Construction Company from Des Moines, Iowa, the contractor for the new interchange, were greatly appreciated. We would particularly like to acknowledge Douglas L. Wood, Structures Laboratory Supervisor and Russell A. Stuart and Donghui Yuan, two recent graduate research assistants, for their expertise during all aspects of the field tests.